# Computer simulation of ground coupled heat pump systems

Tarnawski, V.R.; Leong, W.H.



https://doi.org/10.4224/21275328

SAINT MARY'S UNIVERSITY
Division of Engineering

# COMPUTER SIMULATION OF GROUND COUPLED HEAT PUMP SYSTEMS *

V.R. Tamawski and W.H. Leong

HALIFAX 1990

*Performed under contract to the National Research Council, Ottawa, Canada

SAINT MARY'S UNIVERSITY
Division of Engineering

# COMPUTER SIMULATION OF GROUND COUPLED HEAT PUMP SYSTEMS *

V.R. Tamawski and W.H. Leong

HALIFAX March 30, 1990

*Performed under contract to the National Research Council, Ottawa, Canada

TABLE OF CONTENTS

## ABSTRACT

The main objective of this work was to develop a detailed, physically based two-dimensional model simulating the operation of a ground coupled heat pump system.

The coupled, nonlinear partial differential equations governing heat and mass flow in soils, developed by Philip - de Vries, were used in the model. Freezing/thawing of soil moisture was modelled as an isothermal process, and below the freezing point only heat transfer by conduction was allowed.

The Galerkin finite element method was used for the development of the numerical algorithm for the solution of the governing equations. The numerical and heat pump design procedure was coded in Fortran 77 for computer simulation and a computer package G-HEADS (Ground Heat Exchanger Analysis, Design and Simulation) was developed.

The model considered twelve soil types from sand to clay. The thermal conductivity of the soils was evaluated, as a function of soil dry bulk density and soil water content, using Kersten's equations. The soil moisture transport characteristics were obtained from the Philip - de Vries and Campbell equations. Soil strata, the presence of a ground water table, and the site topography were also considered.

Comprehensive climatological data, such as: ambient temperature, solar radiation, wind velocity, rainfall, snowfall, snow properties, and water vapor pressure, was used to simulate boundary conditions over a whole year.

The model is able to simulate two cases: natural site condition (no heat pump operation), and ground heat storage conditions (heat pump operation). Three modes of the model are available for each case:

1. Domain with soil layers and fixed values of moisture content:
   Pure Heat Conduction Mode (PHCM)
2. Apparent uniform soil domain : Pure Heat Conduction Mode (PHCM)
3. Apparent uniform soil domain : Coupled Heat and Moisture Mode (CHMM)

The model was designed for the heating and the cooling operation of ground heat pump systems.

Nine different horizontal ground heat exchanger systems are available for design purposes (e.g. single-layer, double-layer, threeply-layer, fourfold-layer).

Technical data for sixteen plastic pipes for ground coils is also available in G-HEADS.

As far as ground coil fluids are concerned, water and six other secondary refrigerants, having a concentration of 10 and 20%, are also covered by G-HEADS. The user is able to modify data entered into a computer in order to obtain the best flow regime in the ground heat exchanger.

The characteristics of seven heat pump models manufactured by Water Furnace International are available for design and simulation purposes.

The length of the ground heat exchanger can be obtained either by: using the line source theory, which is also implemented into the package, or just from the site dimensions.

Preliminary simulation runs for the natural site conditions show a close agreement between field data and numerical results. The results obtained show a clear advantage for the CHMM approach over the PHCM with respect to the accuracy of soil moisture and temperature predictions for the natural site conditions. This problem may become even more noticeable when heat deposition to the ground takes place. Therefore the coupled heat and moisture approach shall be tested intensively for ground heat pump applications and site conditions. Unfortunately, the model verification for the case of ground heat pump operation was not carried out due to a lack of experimental data regarding soil moisture and thermal regime in the ground.

G-HEADS is user friendly and menu driven (see User Manual for details).The executable version of this package is available for the VAX 11/780 mainframe computer, Apple Macintosh, and IBM PC microcomputers.

LIST OF SYMBOLS

| *Symbol* | *Description* |
|---|---|
| A | area |
| $A_c$ | conversion factor in Eq. (4 - 48) |
| a | albedo |
| $a_f$ | fluid thermal diffusivity |
| $a_p$ | pipe thermal diffusivity |
| Bv | van Bavel transport function |
| b | empirical power of soil moisture characteristic function |
| C | volumetric heat capacity of soil |
| $C_a$ | apparent heat capacity, $(C_{pf} + L_f \frac{\partial \theta_l}{\partial T})$ |
| c | specific heat of dry soil |
| $c_f$ | specific heat of ground coil fluid |
| $c_w$ | specific heat of water |
| $COP_c$ | coefficient of performance (cooling mode) |
| $COP_h$ | coefficient of performance (heating mode) |
| COPc(1...3) | COP constants of heat pump unit model (cooling mode) |
| COPh(1...3) | COP constants of heat pump unit model (heating mode) |
| $C_{pf}$ | volumetric heat capacity of soil-water-ice mixture |
| $\mathbf{C}_K$ | global capacitance matrix in heat flow equation |
| $\mathbf{C}_\theta$ | global capacitance matrix in moisture flow equation |
| D | diffusion coefficient of water vapor in air |
| $D_\varepsilon$ | $= L\varepsilon\rho_l D_\theta$ |
| $D_\varepsilon^*$ | $= L_v\varepsilon\rho_l D_\theta^*$ |
| $D_{pi}$ | inside pipe diameter |
| $D_{po}$ | outside pipe diameter |

| | |
|---|---|
| $D_s$ | effective soil diameter |
| $D_{ts}$ | apparent diameter of the contact resistance annulus |
| $D_\theta$ | isothermal moisture diffusivity in soil, $D_\theta = D_{\theta l} + D_{\theta v}$ |
| $D_\theta^*$ | $= D_\theta 10^{-I\theta_I}$ |
| $D_{\theta l}$ | isothermal liquid diffusivity in soil |
| $D_{\theta v}$ | isothermal vapor diffusivity in soil |
| $D_{\theta pf}$ | isothermal diffusivity of partially frozen soil |
| $D_T$ | thermal moisture diffusivity, $D_T = D_{Tl} + D_{Tv}$ |
| $D_T^*$ | $= D_T 10^{-I\theta_I}$ |
| $D_{Tl}$ | thermal liquid diffusivity in soil |
| $D_{Tv}$ | thermal vapor diffusivity in soil |
| $\mathbf{D}_K$ | global conductance (stiffness) matrix in heat flow equation |
| $\mathbf{D}_T$ | global mass-heat diffusion matrix in moisture flow equation |
| $\mathbf{D}_\varepsilon$ | global mass-heat diffusion matrix in heat flow equation |
| $\mathbf{D}_\theta$ | global diffusion matrix in moisture flow equation |
| $d_g$ | geometric mean diameter of soil particle |
| E | source or sink of water as liquid is transferred into vapor and vice versa |
| EWT | entering water temperature |
| $e_a$ | water vapor pressure in air |
| $e_s$ | saturated vapor pressure in air |
| $\mathbf{F}_K$ | global forcing vector matrix in heat flow equation |
| $\mathbf{F}_\theta$ | global forcing vector matrix in moisture flow equation |
| f | friction factor |
| g | acceleration due to gravity |
| h | convection heat transfer coefficient |
| $h_f$ | film heat transfer coefficient (coil fluid-pipe wall) |
| HE(1…3) | QH constants of heat pump unit model (heating mode) |

| | |
|---|---|
| HR(1...3) | QC constants of heat pump unit model (cooling mode) |
| I | calibration factor |
| K | thermal conductivity of soil |
| $K_a$ | thermal conductivity of air |
| $K_f$ | thermal conductivity of frozen soil |
| $K_{pf}$ | thermal conductivity of partially frozen soil |
| $K_u$ | thermal conductivity of unfrozen soil |
| $K^*$ | apparent thermal conductivity of soil , $K + L\varepsilon\rho_l D_T$ |
| $K^*$ | $= K_{pf} + L_v\varepsilon\rho_l D_T^*$ |
| $K_{hs}$ | saturated hydraulic conductivity of soil |
| $K_h$ | unsaturated hydraulic conductivity of soil |
| $K_h^*$ | $= K_h 10^{-I\,\theta_I}$ |
| $K_{ds}$ | thermal conductivity of dry soil |
| $K_I$ | thermal conductivity of ice |
| $K_p$ | thermal conductivity of pipe wall |
| $K_s$ | thermal conductivity of soil near the ground coil |
| $K_{sn}$ | thermal conductivity of snow |
| $K_{tc}$ | thermal conductivity of the contact zone (pipe-soil) |
| $K_w$ | thermal conductivity of water |
| L | latent heat of vaporization of water |
| $L_{GHE}$ | length of the ground heat exchanger |
| $L_f$ | volumetric latent heat of fusion of water |
| $L_{sub}$ | latent heat of sublimation of ice |
| $m_{cl}$ | mass fraction of clay |
| $m_{si}$ | mass fraction of silt |
| $m_{sa}$ | mass fraction of sand |
| $m_f$ | mass flow rate of ground coil fluid |

| | |
|---|---|
| $m_r$ | mass of rainfall |
| $m_w$ | mass flow rate of water |
| N | relative amount of cloudiness |
| $N_s$ | shape function |
| $Nu_D$ | Nusselt number |
| PLF | partial load factor |
| PO | soil porosity |
| Pr | Prandtl number |
| p | total gas pressure |
| $p_d$ | vapor pressure deficit ($e_s - e_a$) |
| $p_v$ | partial pressure of water vapor |
| $Q_B$ | heating or cooling load requirement |
| $Q_c$ | cooling load |
| $Q_h$ | heating load |
| $Q_{HP}$ | heat pump nominal capacity |
| $Q_L$ | effective heat |
| Q* | rate of heat generation |
| $QH_{HE}$ | heating capacity of a heat pump unit |
| $QC_{HE}$ | cooling capacity of a heat pump unit |
| $Q_{gen}$ | rate of heat source/sink |
| $Q_{loss}$ | house heat losses (heating load), $QH_{HE}$ |
| $Q_{RWHE}$ | $= QH_{HE} = QC_{HE}$ |
| $q_l$ | liquid flux density |
| $q_{li}$ | longwave radiation incoming from the cloudy sky |
| $q_h$ | convective heat transfer of sensible heat from air |
| $q_{lr}$ | longwave radiation from the ground |
| $q_m$ | total moisture flux density |

| | |
|---|---|
| $q_e$ | latent heat flux by evaporation, evapotranspiration, melting snow or sublimation |
| $q_{gs}$ | penetration of solar radiation through the snowpack |
| $q_n$ | conduction of heat from underground |
| $q_{si}$ | incident shortwave radiation |
| $q_{sn}$ | = qsi - qsr |
| $q_{lo}$ | = qli - qlr |
| $q_{sr}$ | reflected shortwave radiation |
| $q_{adv}$ | advection of heat by precipitation |
| $q_v$ | vapor flux density |
| Re | Reynolds number |
| Rf | rainfall flux |
| $R_T$' | total thermal resistance |
| $R_c$' | internal convective resistance |
| $R_p$' | thermal resistance of a pipe wall |
| $R_{th}$' | thermal contact resistance |
| $R_v$ | water vapor gas constant |
| r | relative time of compressor operation |
| $r_1$ | inner pipe diameter |
| $r_2$ | outer pipe diameter |
| S | $= \frac{\rho_I \, \partial\theta_I}{\rho_w \, \partial t}$ |
| s1 | empirical constnt |
| s2 | empirical constant |
| T | temperature |
| TC | total cooling capacity |
| TH | total heating capacity |
| $T_{air}$ | air temperature |

| | |
|---|---|
| $T_{ka}$ | absolute ambient air temperature |
| $T_{DB}$ | dry bulb temperature |
| $T_{WB}$ | wet bulb temperature |
| $T_{con}$ | condensing temperature in a heat pump unit |
| $T_{evp}$ | evaporating temperature in a heat pump unit |
| $T_{d1}$ | domestic water temperature (exit from desuperheater) |
| $T_{d2}$ | domestic water temperature (inlet to desuperheater) |
| $T_a$ | ambient temperature. |
| $T_f$ | ground coil fluid temperature |
| $T_{f1}$ | temperature of ground coil fluid entering heat pump unit |
| $T_{f2}$ | temperature of ground coil fluid leaving heat pump unit |
| $T_o$ | initial temperature of the system |
| $T_p$ | pipe wall temperature |
| $T_r$ | standard room temperature in winter ( for Ottawa: $T_r = 22°C$) |
| $T_{rain}$ | temperature of rain |
| $T_{sur}$ | temperature of the ground surface |
| $T_s$ | temperature of soil adjacent to the ground coil |
| $T_{s1}$ | mean soil temperature at exit from the GHE and for the effective soil diameter Ds |
| $T_{s2}$ | mean soil temperature at inlet to the GHE and for the effective soil diameter Ds |
| $T_{sp}$ | temperature at the pipe-soil interface |
| $\Delta T_m$ | mean logarithmic temperature difference |
| $\Delta T_1$ | $= T_{f1} - T_{s1}$ |
| $\Delta T_2$ | $= T_{f2} - T_{s2}$ |
| $T_{sn}$ | temperature of snow surface |
| t | time |
| $\Delta t$ | time increment |
| $t_{off}$ | *off-cycle* theoretical compressor time |

| | |
|---|---|
| $t_{on}$ | *on-cycle* theoretical compressor time |
| $t_{ona}$ | *on-cycle* actual compressor time |
| U | overall heat transfer coefficient, per unit length of pipe |
| $V_a$ | volumetric air flow rate |
| $V_f$ | volumetric ground coil fluid flow rate |
| v | wind velocity |
| $v_f$ | ground coil fluid velocity |
| $W_c$ | power input to the compressor |
| $W_p$ | power input to the circulation pump |
| w | soil water content based on the dry mass of the soil ($w_u$+ $w_I$) |
| $w_u$ | unfrozen water content in soil based on the dry mass of the soil |
| $w_I$ | ice content based on the dry mass of the soil |
| y | elevation |
| z | distance along the ground coil |

*Greek Symbols*

| | |
|---|---|
| $\beta$ | $= \frac{d(\rho_l \theta_l)_{pc}}{d(\rho_l \theta_l)_m}$ |
| $\kappa$ | constant coefficient |
| $\eta_a$ | dynamic viscosity of air |
| $\varepsilon$ | phase conversion factor |
| $\delta_c$ | degradation coefficient, given by manufacturer or taken as 0.25 |
| $\theta$ | total volumetric content of soil-moisture , $\theta = \theta_l + \theta_v$ |
| $\theta_a$ | volumetric content of air |
| $\theta_I$ | volumetric content of ice |
| $\theta_l$ | volumetric content of liquid |

| | |
|---|---|
| $\theta_{lk}$ | critical volumetric moisture content at which liquid continuity fails |
| $\theta_v$ | volumetric content of vapor |
| $\theta_s$ | volumetic water content in saturated soil |
| $\theta^*$ | initial soil moisture content in freezing process |
| $\rho_b$ | bulk density of soil |
| $\rho_I$ | density of ice |
| $\rho_l$ | density of liquid water |
| $\rho_{bs}$ | bulk density of snow |
| $\upsilon_{et}$ | flux of evapotranspiration |
| $\upsilon_{ex}$ | flux of moisture exfiltration from the underground |
| $\upsilon_m$ | flux of snowmelt |
| $\upsilon_r$ | flux of rainfall |
| $\Omega$ | total area of the domain of interest |
| $\xi$ | volume fraction of unfrozen soil, ratio of thermal gradient |
| $\psi$ | matric potential |
| $\phi$ | total potential of soil water ($\psi + y$) |
| $\gamma$ | psychrometric constant |
| $\Delta/\gamma$ | weighting factor in Eq.(4-48) |
| $\sigma$ | surface tension of water against air |
| $\sigma_g$ | geometric standard deviation of particle diameter, mm |

*Subscripts*

| | |
|---|---|
| c | Celsius scale |
| m | total number of elements |
| n | number of soil components, time step level |
| o | reference value |
| pc | phase change |

| | |
|---|---|
| b | bulk |
| l | liquid |
| v | vapor |
| s | finite element number (1...m), saturation |
| e | number of elements associated with node "i" |
| i | node number |
| f | fusion, freezing |
| w | water, wall |

# 1. INTRODUCTION

Our future depends very much on the availability of energy resources which are limited. Therefore, there is a great need to conserve energy in everyday life, at home, in offices, and in industry. Ground heat pump technology plays an important role in energy conservation and its contribution to this sector has a growing influence. This technology is applied mainly to the heating and/or cooling of residential and commercial buildings. When a heating mode is applied, a low grade ground thermal energy is absorbed by a ground coil and then upgraded by a heat pump to a level sufficient to maintain a comfortable temperature in a living space. In summer, when cooling of indoor air is necessary, excesses of thermal energy in the building are extracted by the same heat pump unit operating in the reverse mode, and dumped to the ground by use of the ground coil.

There is a lot of evidence gathered over last 40 years that the ground can be a very good heat source/sink for residential or commercial heat pumps. The ground is readily available as a source or sink of thermal energy for a heat pump and has a number of very useful characteristics, viz. high heat capacity, stable temperature, and high thermal conductivity, which in general offer good thermodynamic performance. Water would be an excellent source or sink of thermal energy but is not universally available and there are serious restrictions regarding the disposal of the used water. Air as a source or sink of thermal energy is universally available but it has a low density and hence a low heat capacity per unit mass compared with water or the ground. It is subject also to large temperature and humidity fluctuations which lead to frost formation on evaporators and poor performance during the coldest days.

In general the lowest ground storage temperature is significantly higher than the minimum temperature of ambient air. Another advantage of ground heat pump technology is the elimination of all outdoor air-conditioning and/or refrigeration heat exchangers, as well as annoying noise from air fans. Many maintenance problems related to corrosion, dirt, vandalism, theft, and freeze are eliminated. The lack of roof top units on large residential/commercial buildings is certainly very attractive to owners and architects. Besides that, ground heat pumps considerably reduce the

demand for electrical energy during critical power utility peak periods. This benefit does not take place when air-source heat pumps are used. The benefits provided by this technology to the consumer and its power utility offset the high cost of installing ground heat exchangers.

In spite of a large research effort on ground heat pumps no sufficiently reliable design methods or guidelines have yet been developed in order to predict ground heat pump performance and the dimensioning of ground heat exchangers. There are still major discrepancies between analytically and numerically designed ground coils and those suggested by practical experience. The reason for this situation is the very complex phenomena taking place in the ground during heat extraction and/or heat deposition. Soil itself is a very complex composition of many different constituents. In practice soil is not homogeneous and its composition can vary drastically even over the relatively small area proposed for ground heat storage. This leads to a great variation in ground physical properties such as, density, diffusivity of moisture, specific heat, and thermal conductivity. Moreover, the type of soil and its moisture content, depth of the ground water table, ground water velocity, and boundary conditions at the ground surface, as well as at the ground coil-soil interface, have an additional strong influence on the ground heat pumps performance. Therefore a desirable mathematical model of the ground heat exchanger shall consider all of the above problems in great detail.

It is well known that heat transfer in any soil is strongly influenced by the presence of moisture. This phenomenon becomes even more evident when artificial heat extraction or deposition to the ground takes place. Operation of a ground heat exchanger (GHE) can result in a number of undesirable problems such as, frost heave, freezing/thawing soil integrity, soil dry out in the vicinity of the ground coil and ground surface, and significant thermal contact resistance on the soil-pipe interface. Therefore, the movement of soil-moisture under a temperature gradient is a challenging problem of considerable interest for ground heat pump technology. Other fields of engineering which are also involved in solving similar problems are listed below:

| | |
|---|---|
| - Energy Engineering | * underground pipes of district heating systems |
| | * underground high voltage power cables |
| | * long-term storage of high-level radioactive waste from nuclear reactors |
| - Agriculture Engineering | * pre-conditioning of ambient air for greenhouses and livestock shelters |
| | * warming of soil by utilization of waste heat from power plants |
| - Civil Engineering | * roads, airfields and buildings in northern climates |
| | * gas and oil pipe lines |
| | * heat losses from solar ponds and buried buildings |
| | * soil shrinkage problems |
| | * artificial ground freezing |
| - Mining Engineering | * artificial ground freezing |

It is worthwhile stressing that the foundations and the development of a general theory of simultaneous heat and moisture transport in soils, including determination of thermal and mass transport characteristics for various soils, were laid first by scholars representing soil physics.

## 1.1 Review of Literature

In general, there are two theories describing simultaneous heat and mass transfer in soils. The first is based on the principle of irreversible thermodynamics and was developed Cary and Taylor (1962) and Luikov (1966). The second theory is based on the mechanistic approach, developed by Philip and de Vries (1957), de Vries (1958). The Philip - de Vries approach has gained most recognition in almost all branches of engineering. In the majority of cases, comparisons between

the theory and experiments or field data are within reasonable limits [de Vries (1987)]. A large number of researchers have effectively used the mechanistic equations of Philip and de Vries in their studies: Gee(1966), Cassel et al.(1969), Sepaskhah (1974), Schroeder (1974), Slegel (1975), Shapiro and Moran (1978), Sophocleous (1978), Dempsey (1978), Ahmed(1983), Thomas et al.(1980, 1986), Baladi et al.(1981), Dakshanamurthy et al. (1981), Hartley et al.(1981), Walker et al. (1981), Schieldge et al. (1982), Milly (1982), Puri (1984), Radhakrishana et al. (1984), Geraminegad et al. (1986), Shen (1986). An excellent review of all existing mathematical models (up to 1982) of heat and moisture flow in soils above the freezing point was published by Fisher (1983). He concluded that Slegel's and Schroeder's models, after necessary modifications, could well simulate ground source heat pump operation.

In northern climates a rate of heat extraction from the ground can be so high that it will cause freezing of soil moisture around the ground heat exchanger and this in turn will significantly influence heat and mass transport characteristics of soil. Fundamental phenomena associated with soil moisture freezing were studied by Dirksen (1964) and Hoekstra (1966). They pointed out that the soil-moisture of unfrozen soil has a tendency to migrate towards the freezing zone and then freeze. In other words, migration of soil-moisture and heat transfer are highly interrelated phenomena. For fine grained soils and close presence of ground water, the freezing of soil may lead to accumulation of ice exceeding the porosity of the soil and thus cause vertical movement and destruction of the soil and any structure in contact with the soil (so called frost heave). The magnitude of frost heave depends strongly on the surface load applied to the soil. In general, two different types of mathematical models describing heat and moisture transfer in partly frozen non-heaving soils exist.

The first type of model was published by Harlan (1971) who formulated the coupled heat and mass transfer equations with partial derivatives for freezing a column of soil. This formulation is based on the analogy between mechanisms of moisture flows in unsaturated and in partially frozen soils. This formulation became known as the hydrodynamic model and it was successfully applied to

predict the rate of extraction of water from soil below the frozen zone (Sheppard et al., 1978). This model assumes that ice is accumulating in the frozen zone and if it amounts to more than soil porosity, the frozen zone is supposed to expand wherever the extra space is needed. The hydraulic model does not take into account the effect of surface load on the rate of frost heave. The hydrodynamic model was further developed by Taylor and Luthin (1978), Guymon et al. (1980), and Hromadka et al. (1981). In their models, moisture content and hydraulic conductivity in the freezing zone are independent of temperature, being a function of liquid pressure head alone. The latent heat of the fusion of water per unit volume of soil is proportional to ice content and there is no moisture flow in the frozen zone.

The second type of model was developed by Kay and Groenevelt (1974) and was based on the thermodynamics theory of irreversible processes. This model is very general and includes simultaneous transport of vapor, liquid moisture, and heat under the gradients of temperature, ice, water and vapor. This model is limited to non-heaving conditions. It was tested by Kung et al.(1986) and simulated results agreed rather well with experimentally obtained values.

From a large number of available mathematical models on freezing soil, it is worth mentioning a new approach made by Karvonen (1988). He derived a freezing characteristic curve and the relationship between soil temperature and soil water potential in the frozen soil from the soil water retention curve. The hydrodynamic model, however, was simplified by neglecting the vapor flux terms. He proposed both iterative and explicit techniques to calculate unknown unfrozen and frozen water content and soil temperature.

A physically based one-dimensional mathematical model of the freezing soil-residue-snowpack system was presented by Flerchinger and Saxton (1989). It simulates a coupled flow of heat and water through snow, residue and soil and includes the effects of tillage and residue on soil freezing. The model predicts hourly values of ground freezing depths, snow depth, evaporation, soil temperature, and contents of water and ice. Simulated soil temperatures, frost depth, and soil-water profiles were in very good or good agreement with measured values.

From the above review of literature it becomes obvious that simultaneous heat and moisture movement in the vicinity of the GHE is an important factor which may have a weighty impact on the summer and/or winter operation of ground coupled heat pump systems. Therefore a mathematical model of ground heat storage should be a dynamic one and include a coupled movement of heat and soil-moisture in the entire domain over a period of at least one year.

Design methods for GHE's were discussed in detail by Bose et al. (1985), and generally can be divided into three categories:

- empirical design standards (rules of thumb)
- steady-state and transient models with analytical solutions
- transient models with numerical solutions.

Rules of thumb based on the data obtained from prototype installations appear to be successful in a locality similar to that where prototype couplings were developed. Therefore there is a great need for more information to properly assess effects of climatic changes and any design innovations.

Analytically based design methods use mainly a line source theory to determine the soil temperature as a function of location and time. In general this method does not consider complex boundary conditions at the soil/snow-air interface and the nonuniform heating and cooling load of the ground couple heat pump system. Therefore it offers little practical value in predicting the transient ground temperature due to heat extraction and/or deposition. In general this method leads to a serious overdesign of the GHE. However, its simplicity and a lack of other competitive methods still makes it a popular design tool.

A number of various transient mathematical models, based on the finite difference and finite element approach, simulating mainly heat extraction from the ground, have been developed over the last ten years. Among them the only model which accounts for heat and soil moisture in ground

heat storage was developed by Tarnawski (1982) for northern climate ground heat pumps. This one-dimensional model, developed for a heating mode, includes freezing of soil moisture and soil-water flow due to a gradient of moisture content. The remaining models, developed to date, have completely disregarded soil-moisture migration and only a few considered soil freezing. The literature on this subject is quite extensive and some review publications have been reported by Bose and Parker (1983), Bose et.al. (1985), and Svec (1987). Here a brief overview of the more important mathematical models, developed after 1983, will be given.

Mei and Fischer (1983) developed a mathematical model for the analysis of the ground coupled vertical heat exchanger. The model is based on energy balances and consists of five differential equations describing temperature distribution in the water, the pipes, and the ground in terms of time, depth, and the distance from the heat exchanger. Constant input values are used for the thermal properties of the fluid, piping material and soil. Heat rejection or extraction is simulated by imposing a temperature change using steady-state heat pump data. The cycling behavior of the ground coil was modelled by specifying operating time as a function of time of day and portion of each hour for a typical day of the month. The program uses an explicit method to solve the governing differential equations. Because the nodal geometry includes fluid and inner piping nodes, a time step of less than a second is required for stable calculations. Experimental validation of this model for both continuous and cyclic operation was conducted in 1981 - 1983 by comparison with data from a deep vertical coil installed at ORNL. The parametric study showed that high thermal-conductivity pipe material will increase the amount of energy exchange between the heat exchanger and the ground. This improvement becomes negligible when the thermal conductivity of casing is close to, or higher than, that of the ground. The parametric study also shows several possible ways of designing a higher capacity heat exchanger such as by the increased flow rate of the working fluid, diameter of the outer casing, and length of the heat exchanger.

Edwards and Vitta (1985) developed the two-dimensional transient model predicting the interaction of the ground coupled heat exchanger with the surrounding ground. The model used a finite difference method for a non-steady heat exchange process, and included the interaction of the horizontal heat exchanger with the surrounding ground, the solar flux upon and reradiation from the ground surface, and the convective interaction between the surface of the earth and the ambient air. Euler's explicit method was used and the derivatives were approximated by central differences. The daily variations of ambient temperature were represented by a sinusoidal function of time.The incident solar radiation flux on the ground surface was treated in the same manner. The thermal conductivity was allowed to vary with moisture content. The thermal diffusivity of soil was taken as a constant. The free convection heat transfer coefficient at the earth-air interface was assigned as a constant value. The results obtained from the numerical model showed close agreement with the experimental data in predicting the temperature of the earth in the vicinity of the ground-coupled heat exchanger.

Lund and Östman (1985) developed a three-dimensional numerical model for seasonal heat storage in rock using vertical heat exchangers. The model accounts for convective heat flow, in the vicinity of the heat exchanger pipes, which perforate the storage region. Ground water flows were also considered. The storage was employed in a district heating system with a heat pump. On the top of the storage region insulation was applied. It was assumed that in winter months, the ground would be covered by snow. The energy equation of the heat carrier fluid flowing upwards in the duct was described in cylindrical geometry. The temperature of the ground near the hole was modelled by a simple heat conduction equation written in cylindrical coordinates. The global thermal processes within the ground storage were modelled by the energy equation which included the coupling of the holes into the global active storage region, the flux of water in the ground caused by a hydraulic gradient and the buoyancy force in water saturated soil. The equations describing the storage were solved numerically using the finite difference method. The numerical expressions for the

mathematical model of ground storage were based on the explicit method. Economic optimization of the storage and collector installation was also briefly discussed.

Mei (1986) presented three horizontal ground coil models, i.e. a single coil with a radially symmetrical temperature profile and soil moisture freezing effect; a single coil with nonsymmetrical soil temperatures around it; double layer coils with nonsymmetrical soil temperatures around them and with thermal interference effects. The first model revealed that the inlet temperature of the fluid to the GHE must be much below the freezing point of soil moisture in order to utilize effectively the potential of latent heat released due to freezing.The second model enables simulation of the effect of ground surface heat transfer with the ambient air. The third model is used to study the effect of two coils being buried in the same trench. All three models were validated with the field experimental data. It is worth noting that in order to simulate the GHE operation a lot of computer time is required. Time increment used in the computer simulation is in the order of seconds, this requires a very fast mainframe computer in order to simulate full winter and summer operations.

Franck (1986) developed a two-dimensional model simulating an integrated heating system consisting of an electrically driven heat pump, a low temperature seasonal heat storage in clay with vertical pipes, a heat/solar collector, and a heat sink. Local thermal processes around single pipes were considered first and then were coupled to a global temperature field describing the whole storage region. Clay freezing was assumed to occur between 0° and -10°C. Soil thermal properties were assumed to be constant but different values were assigned to frozen and unfrozen clay. The heat flow from ambient air to the ground surface was due to convection only. The finite difference method with an explicit Euler forward difference scheme was used to solve numerically the heat conduction equation describing heat flow in clay. The computer program was verified by comparison of computed and measured results. A satisfactory agreement was found. Based on the technical performance, an economical optimization of the system was carried out for various cost assumptions.

Schulz et al.(1988) presented some data on heat and mass transfer phenomena in ground-coupled heat pumps with vertical heat exchangers. Flexible polypropylene plastic tubes of 25mm diameter were inserted into vertical holes of 100mm diameter and the annulus was filled with a sodium-betonite-water mixture to give a tight thermal contact between the tube and the ground. Two years experience showed that the system worked well. The two dimensional computer program based on heat flow only was developed to simulate an operation of ground heat storage. The development of a mathematical model of coupled heat and moisture flow in an unsaturated medium is under way.

The first book about designing GCHPS (ASHRAE Design Data Manual) was published by Bose et al. (1985) and more recently the installation guide by OSU (1988) appeared. This book contains a wide variety of literature related to soil properties, ground coil materials, circulating fluids, mathematical models, and practical experience. The ground-coupling concept is introduced and explained, and the earth's temperature variations are described. These two books are very useful to those who wish to commit themselves to the design of ground-coupling heat pump systems.

From the above review of literature the following comments can be made:

- there is no two-dimensional model of ground coupled heat pump system which accounts for simultaneous heat and moisture transfer in soils due to heat extraction or deposition to the ground
- freezing of soil is greatly simplified by all models and does not account for moisture migration
- none of the existing models consider the problem of thermal contact resistance between the ground coil and surrounding soil
- the majority of models assume very simple outer (ground surface), and inner (GHE-surrounding soil) boundary conditions
- with a few exceptions only a very simple steady-state model of a heat pump unit is used
- space-conditioning load data is also very elementary in the majority of models

- geological and hydrogeological factors as well as a site topography are in most of cases neglected
- none of the general models of ground coupled heat pump as applied to various loads, geographical locations, and geological and hydrogeological conditions has been fully verified yet
- there is a lack of a computer package, based on the detailed mathematical model, which could be design oriented with a possibility of selecting the optimum alternatives, and is versatile, and user friendly
- there is still a lack of design guidelines leading to the optimum solution of the entire ground coupled heat pump system (GCHPS).

Modern-day research and development efforts have utilized plastic tubing, spiral ground heat exchangers [Svec, 1983, Svec and Palmer, 1989], and computerized techniques. It is a reality of our time that only a computerized approach to the design of a ground heat pump system, based on transient mathematical models, can successfully cope with high requirements regarding appropriate selection hardware and its installation. In the GHE design, every attempt should be made to use soil characteristics applicable to the actual site conditions. The most difficult obstacle to this approach is still a lack of accurate data regarding soil physical properties and experimental data on temperature and soil moisture profiles needed to verify mathematical models for various geological and climatological conditions. Without this reliable information, even the most detailed mathematical model will be unable to accurately predict the ground heat pumps performance and the length of the ground heat exchanger. Therefore, is advisable to carry out extensive sampling of the ground storage medium throughout the year, before any mathematical modeling approach is made.

## 1.2 Scope of the Project

The main objective of this project is to develop a two-dimensional mathematical model of ground heat storage with the horizontal GHE, which accounts for the following:

- heat and moisture flow in ground heat storage
- different soil types and layers , depth of ground water table
- soil freezing-thawing and/or drying-rewetting due to heat extraction and heat deposition;
- dynamic ground-surface effects (ambient temperature, solar radiation, rainfall, snowfall, evapotranspiration, wind speed etc.)
- transient changes of heating and cooling load
- ground coil dimensioning and arrangement (material, size and shape)
- steady-state liquid source heat pump model used for simulation purposes of the entire heat pump system (house-heat pump unit- ground heat exchanger)

Moreover the entire computer program is written in FORTRAN 77 and suitable for execution on a wide range of mainframe and micro-computers including VAX 11/780, IBM PC in MS-DOS format, and Apple-Macintosh system. The program is user friendly, interactive and contains an easy to follow design procedure.

# 2. OVERVIEW OF A GROUND COUPLED HEAT PUMP SYSTEM

## 2.1 Ground Source Heat Pumps

A schematic arrangement of the entire ground heat pump system (GHPS) operating in the heating or cooling cycle is shown in Fig. 2.1. The system can be divided into three sub-systems: a heat pump unit, ground storage, and a building.

The heat pump is a typical commercial water source unit designed for operation throughout the whole year i.e., in heating and cooling modes. Presently, packaged water-to-air heat pumps are the most common in commercial/residential applications. These units are able to handle a wide range of ground coil fluid temperatures which can range from -9° to 45° C. In its standard design version, the heat pump contains five components i.e., a compressor, a refrigerant-air heat exchanger, an expansion valve, a refrigerant-ground coil fluid heat exchanger, and a reversing valve.

The compressor is a hermetic type, reciprocal or screw, compact in size, with a low noise level. Two-speed compressors are also available on the market and may be very helpful in accommodating the oversizing problem of the heat pump operating in the heating and cooling mode.

The refrigerant-air heat exchanger is a device whose purpose is to transfer heat from the unit into the building during the heating mode and extract heat during the cooling cycle. Therefore in the winter it will function as a condenser and in the summer as an evaporator. The hot/cold air is circulated through the duct distribution system in the building by the use of an additional fan.

The refrigerant-ground coil fluid heat exchanger is linked permanently with the ground heat exchanger (GHE) and absorbs heat delivered by the ground coil fluid during heating while rejecting it during the cooling mode.

There are two basic configurations for ground heat exchangers i.e. horizontal and vertical. The horizontal configuration is more common in residential areas, where there is enough land for

ground heat storage. The horizontal GHE can be designed in a series or parallel arrangement and be single-, double-, or multiple-layer.

GENERAL ARRANGEMENT

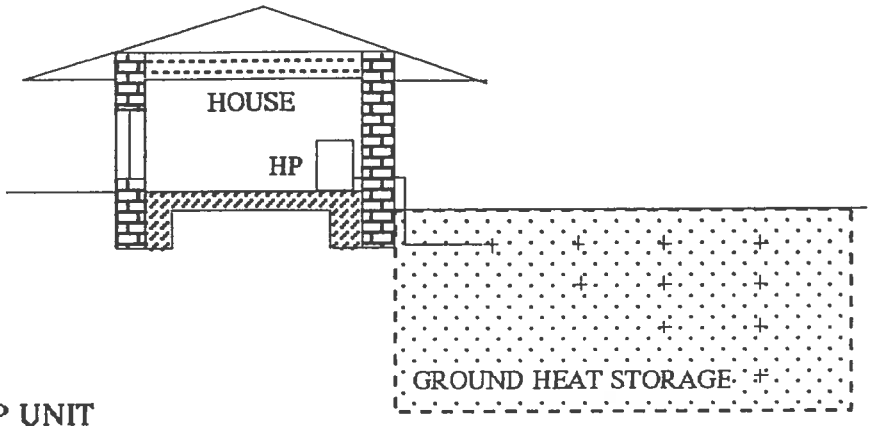


HEAT PUMP UNIT

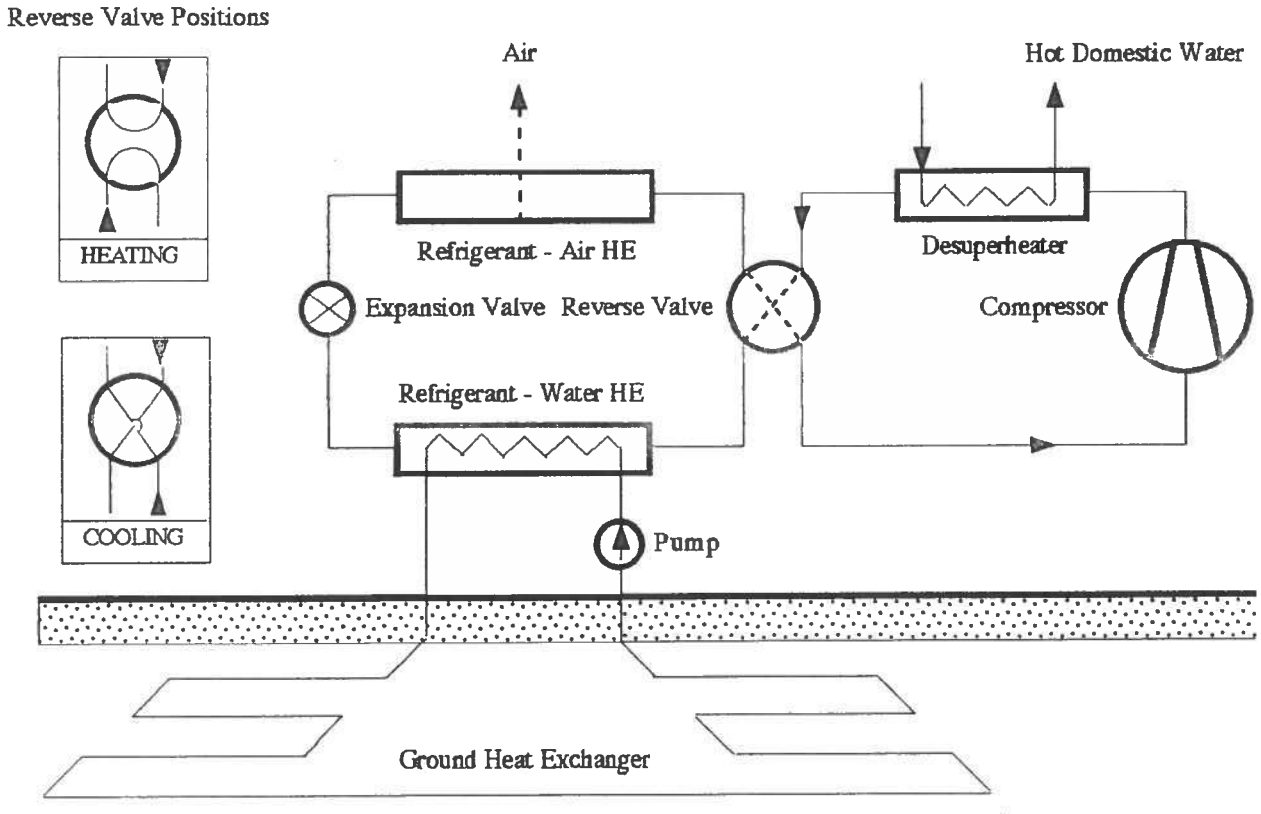


Fig. 2.1 Schematic of the Ground-Coupled Heat Pump System

Two design types of vertical ground heat exchanger are available on today's market, viz., tube-in-shell, and coaxial tube-in-tube. Both have extended heat transfer surfaces from the refrigerant side to reduce their lower film heat transfer coefficient. In both cases the ground coil fluid flows inside the inner tube. Again vertical tubes can be linked in a series or parallel arrangement.

Residential heat pumps normally have used capillary tubes as a refrigerant flow control device due to their low cost and simplicity. Recently, however, thermostatic expansion valves have been used more often as they produce better results in view of the widely varying refrigerant temperatures and loading conditions encountered during the operation of the ground coil.

The reversing valve function changes the flow direction of the refrigerant when the heating cycle is switching into the cooling one and vice versa.

Residential heat pumps are also available in an upgraded version containing a domestic hot water option. In this case the unit is equipped with an additional heat exchanger, a so called desuperheater, which is installed between the compressor and the reversing valve. The desuperheater removes the high grade superheat from compressed refrigerant vapor thus providing a source of heat for the domestic water. The water between the hot water tank and the desuperheater is circulated through a low power pump.

## 2.2 Thermodynamic Analysis of a Ground Heat Pump System

Fig. 2.2 shows a basic schematic of a heat pump system linked to a ground heat exchanger

Applying the first principle of thermodynamics to the above schematic the following heat balances for heating and cooling mode are obtained:

Heating Mode

Amount of heat extracted from the ground

$$QH_{HE} = F_1 (T_{f1}, T_{f2}, T_{s1}, T_{s2}, L_{GHE}, D_{pi}, U) \qquad (2 - 1h)$$

More information about the method used to calculate $QH_{HE}$ can be found in Section 2.7

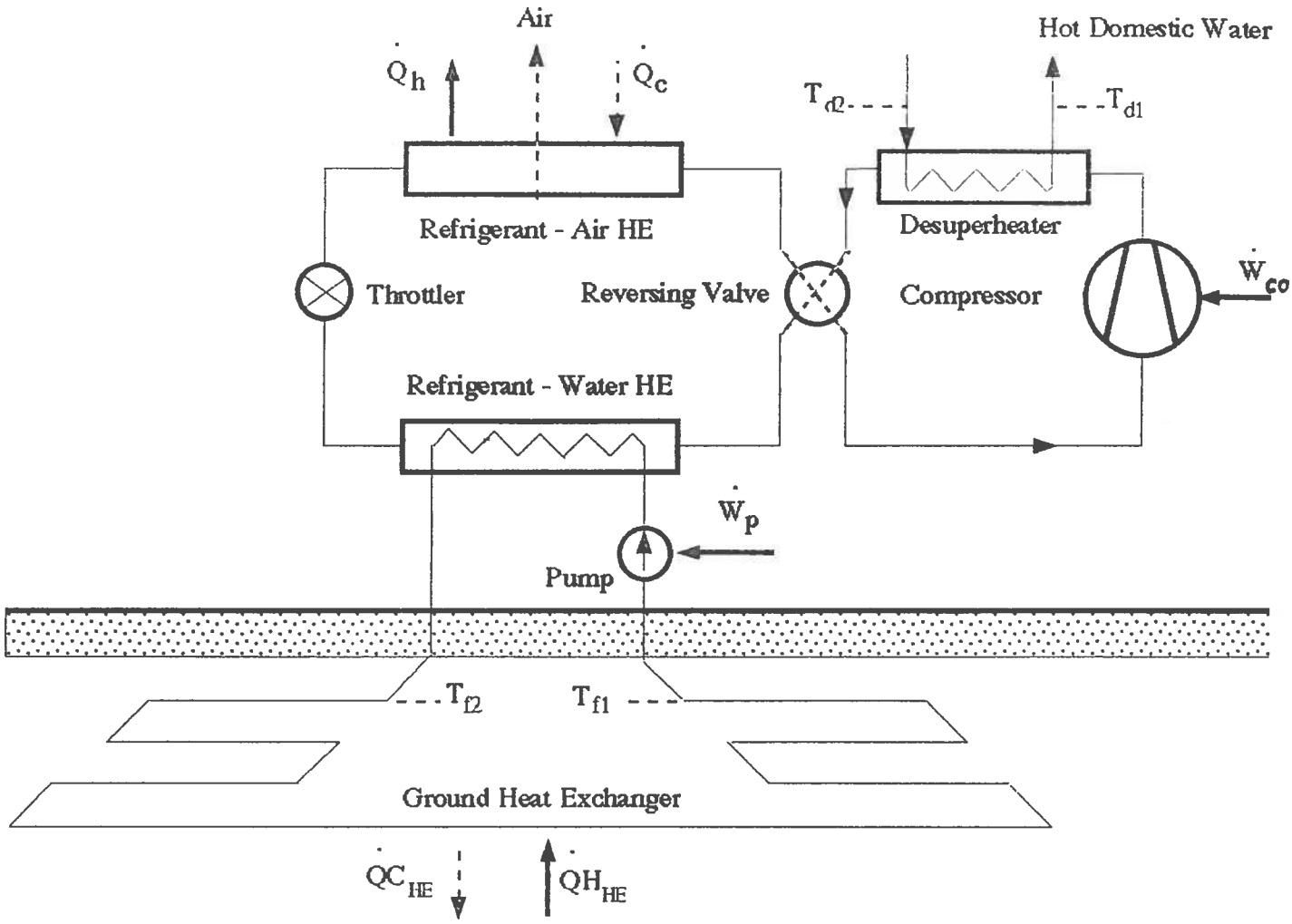


Fig.2.2 Basic Ground Heat Pump Arrangement

**Amount of heat supplied to Refrigerant - Water HE (evaporator)**

$$Q_{RWHE} = QH_{HE} = m_f c_f (T_{f1} - T_{f2}) \qquad (2 - 2h)$$

**Heating load**

$$Q_h = F2 \text{ (building thermal characteristics, weather conditions, time)} \qquad (2 - 3h)$$

**Desuperheater capacity**

$$Q_d = m_w c_w (T_{d2} - T_{d1}) \qquad (2 - 4h)$$

**Power input to the compressor**

$$W_{co} = QH_{HE} - Q_h - Q_d \qquad (2 - 5h)$$

The coefficient of performance

$$COP_h = \frac{Q_h}{W_{co}+W_p} \qquad (2 - 6h)$$

Amount of heat extracted from the ground

$$QH_{HE} = Q_h \frac{COP_h - 1}{COP_h} \qquad (2 - 7h)$$

Cooling Mode

Amount of heat rejected to the ground

$$QC_{HE} = F_1 (T_{f1}, T_{f2}, T_{s1}, T_{s2}, L_{GHE}, D_{pi}, U) \qquad (2 - 1c)$$

More information about the method used to calculate $QC_{HE}$ can be found in Chapter 2.7

Amount of heat to be removed from Refrigerant - Water HE (condenser)

$$Q_{RWHE} = QC_{HE} = m_f c_f (T_{f1} - T_{f2}) \qquad (2 - 2c)$$

Cooling load

$$Q_c = F2 \text{ (building thermal characteristics, weather conditions, time)} \qquad (2 - 3c)$$

Desuperheater capacity

$$Q_d = m_w c_w (T_{d2} - T_{d1}) \qquad (2 - 4c)$$

Power input to the compressor

$$W_{co} = - QC_{HE} + Q_c - Q_d \qquad (2 - 5c)$$

The coefficient of performance

$$COP_c = \frac{Q_c}{W_{co}+W_p} \qquad (2 - 6c)$$

Amount of heat rejected to the ground

$$QC_{HE} = Q_c \frac{COP_c - 1}{COP_c} \qquad (2 - 7c)$$

## 2.3 Heat Pump Capacity Data

For modelling purposes of the entire GHPS, liquid source heat pumps manufactured by WaterFurnace International (1989), were selected for this report. They are designed for heating and cooling mode of operation and have a relatively wide range for the entering fluid temperature $T_{f1}$, from -1 to 45 °C. The technical data provided by the manufacturer and used to generate the necessary information for modelling of the GHPS is listed below:

- coefficient of performance (COP)
- total heat rejected to the ground(HR) - $QC_{HE}$
- total heat extracted from the ground (HE) - $QH_{HE}$
- total cooling capacity (TC) - $Q_c$
- total heating capacity (TH) - $Q_h$
- temperature of ground-coil fluid (water) entering a heat pump unit (EWT) - $T_{f1}$.

The temperature $T_{f1}$ is the main factor that determines other capacity data listed above. Other factors that effect heat pump capacity data are: the type of the ground coil fluid, its mass flow rate, and entering air temperature (EA = $T_{air}$).

A balanced operation of the heat pump unit is considered i.e., the condensing temperature, $T_{con}$, in winter, and evaporating temperature, $T_{evp}$, in summer, are constant. Therefore all capacity data of the selected heat pump unit, are functions of the $T_{f1}$ , and valid only for fixed values of the air flow rate $V_a$ , ground coil fluid flow rate $V_f$, entering air wet bulb temperature $T_{WB}$, and dry bulb temperature $T_{DB}$ for summer and winter. The following approximations were obtained:

heating operation

$$COP_h = COPh(1) + COPh(2) * T_{f1} + COPh(3) * T_{f1}^2 \quad (2\text{-}8a)$$

$$QH_{HE} = HE(1) + HE(2) * T_{f1} + HE(3) * T_{f1}^2 \quad (2\text{-}8b)$$

cooling operation

$$COP_c = COPc(1) + COPc(2) * T_{fl} + COPc(3) * T_{fl}^2 \quad (2\text{-}8c)$$

$$QC_{HE} = HR(1) + HR(2) * T_{fl} + HR(3) * T_{fl}^2 \quad (2\text{-}8d)$$

Figure 2.3 and 2.4 show a graphical interpretation of the above performance data for the two following heat pumps:

| | | |
|---|---|---|
| - model type | WX041 | WX012 |
| - air flow rate | 2336 $m^3/h$ (1375 cfm) | 637.5 $m^3/h$ (375 cfm) |
| - water flow rate | 1.136 $m^3/h$ (5.0 gpm) | 0.568 $m^3/h$ (2.5 gpm) |
| - air temperature (cooling) | 26.6/19.4 °C (75/63 °F) | 26.6/19.4°C (75/63°F) |
| - air temperature (heating) | 21.1 °C (60 °F) | 21.1 °C (60 °F) |

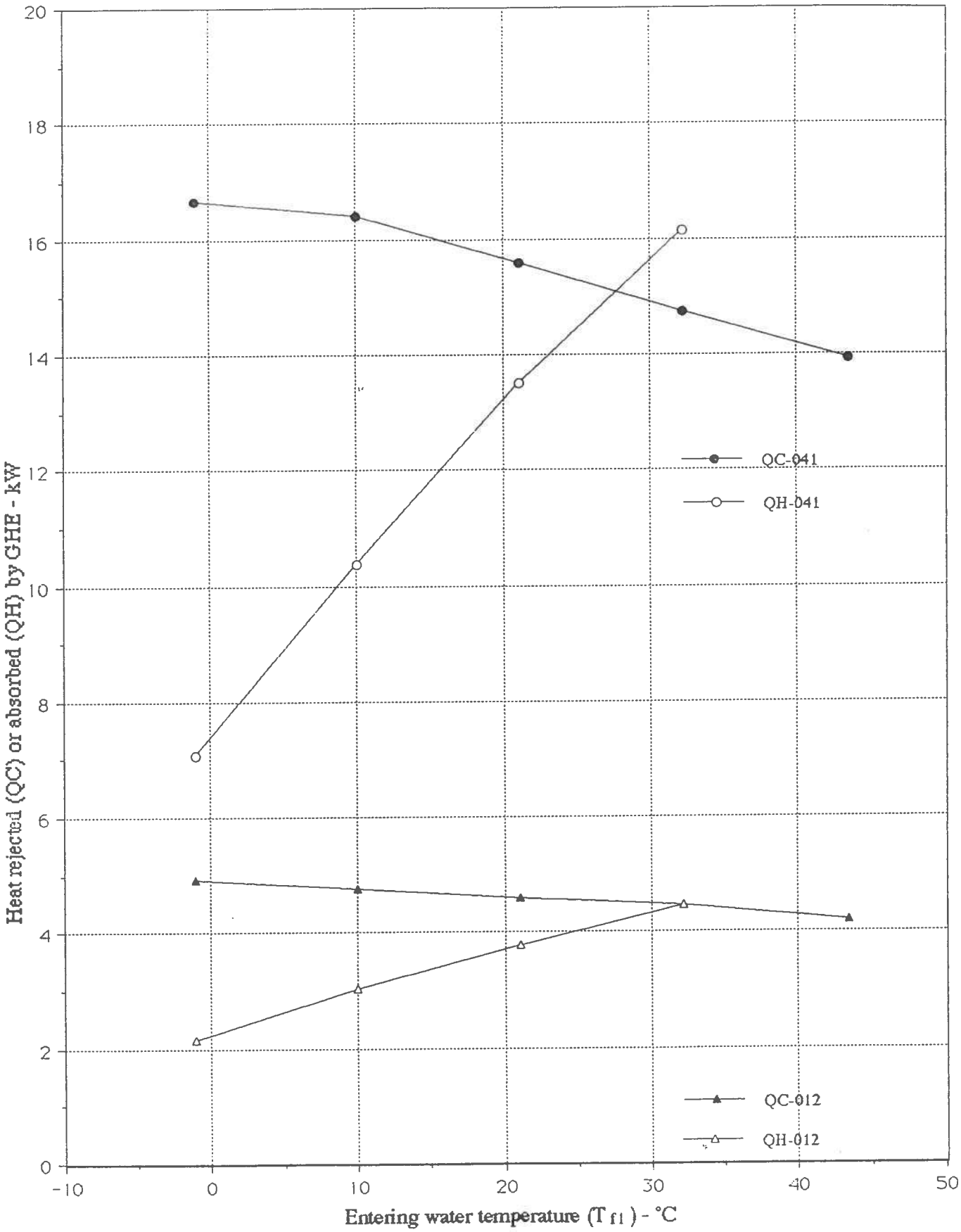


Fig. 2.3 Heat Pump Capacity Data vs. Entering Water Temperature $T_{fl}$

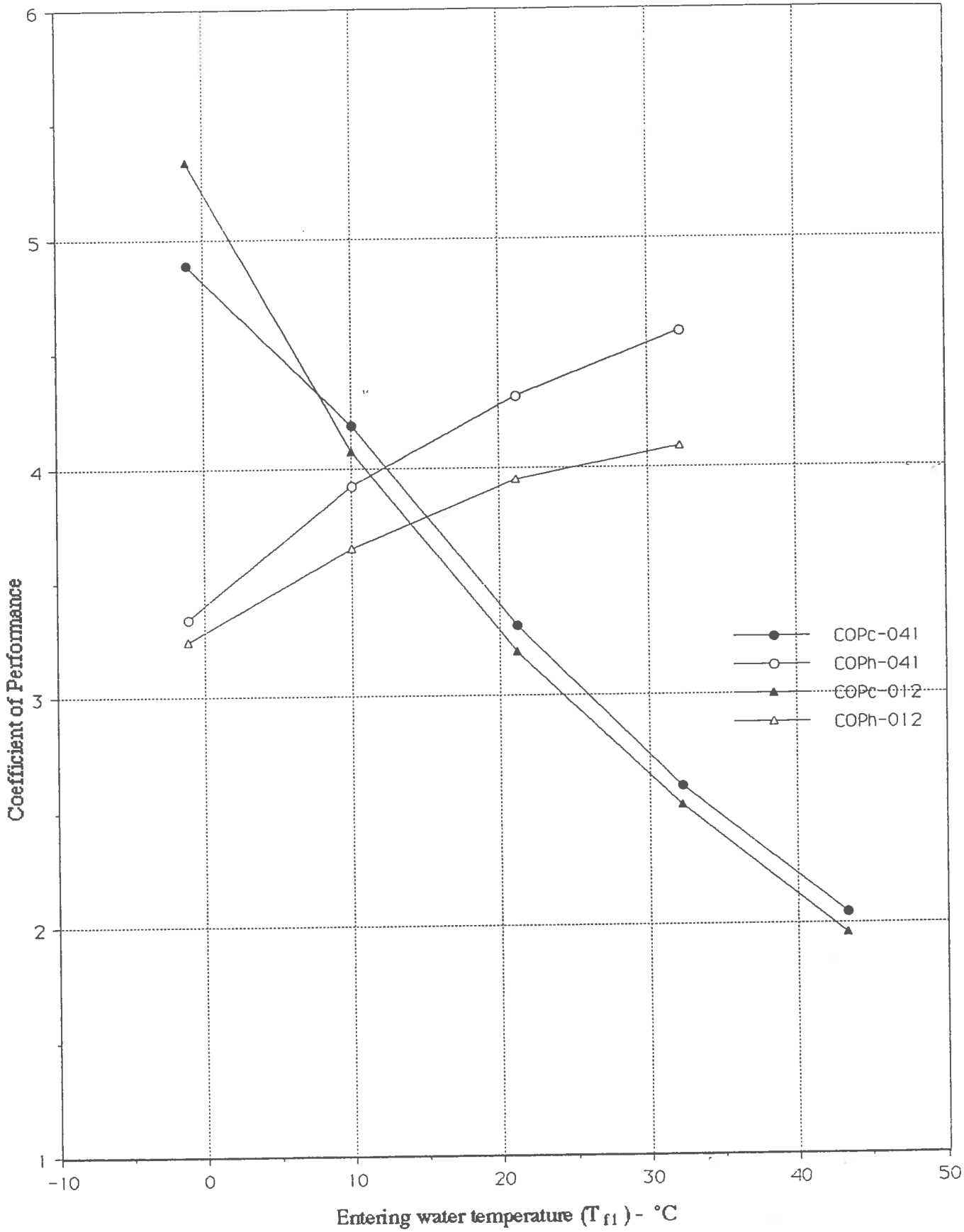


Fig. 2.4 Coefficient of Performance (COP) vs. Water Entering Temperature ($T_{f1}$)

## 2.4 Ground Heat Exchanger Configurations

In this report only the horizontal system of the GHE is considered. This system can be designed in series or parallel flow of the ground coil fluid over the GHE, (Fig. 2.5). It is worth noting that the series flow system requires a larger pipe diameter and more expensive pipe than the parallel one.

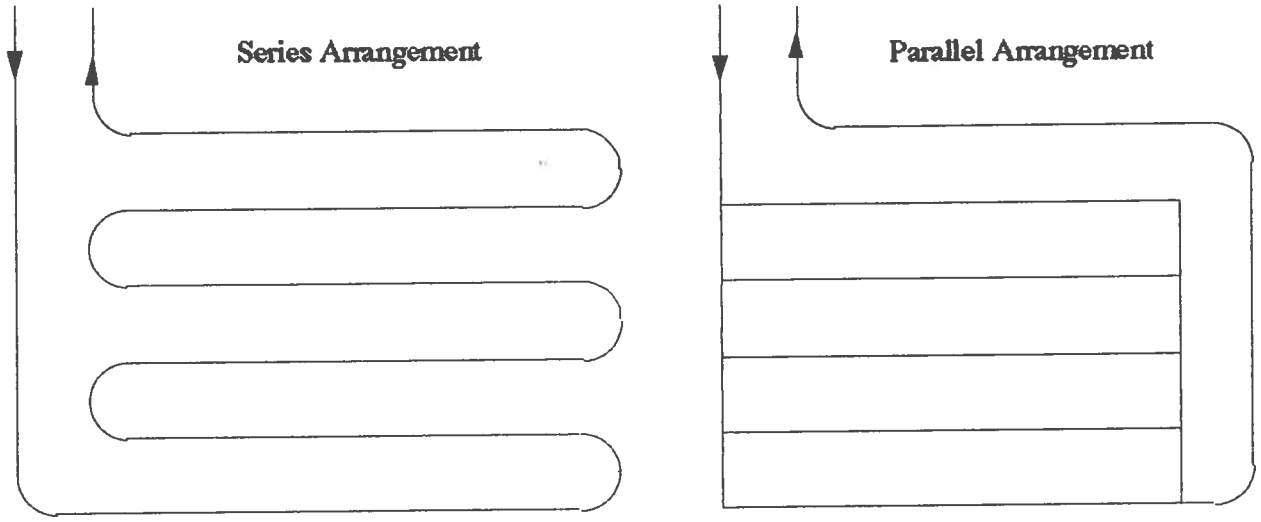


Fig. 2.5 Series and parallel arrangement of the horizontal GHE

Parallel systems in turn require smaller pipe diameter and therefore are less costly. There is however a problem with even distribution of the ground coil fluid and removing trapped air in the system.

The requirement of a large free ground area is, in general, a limitation of the horizontal system. This requirement can be considerably reduced by using the multiple-layer pipe system (Fig. 2.6).

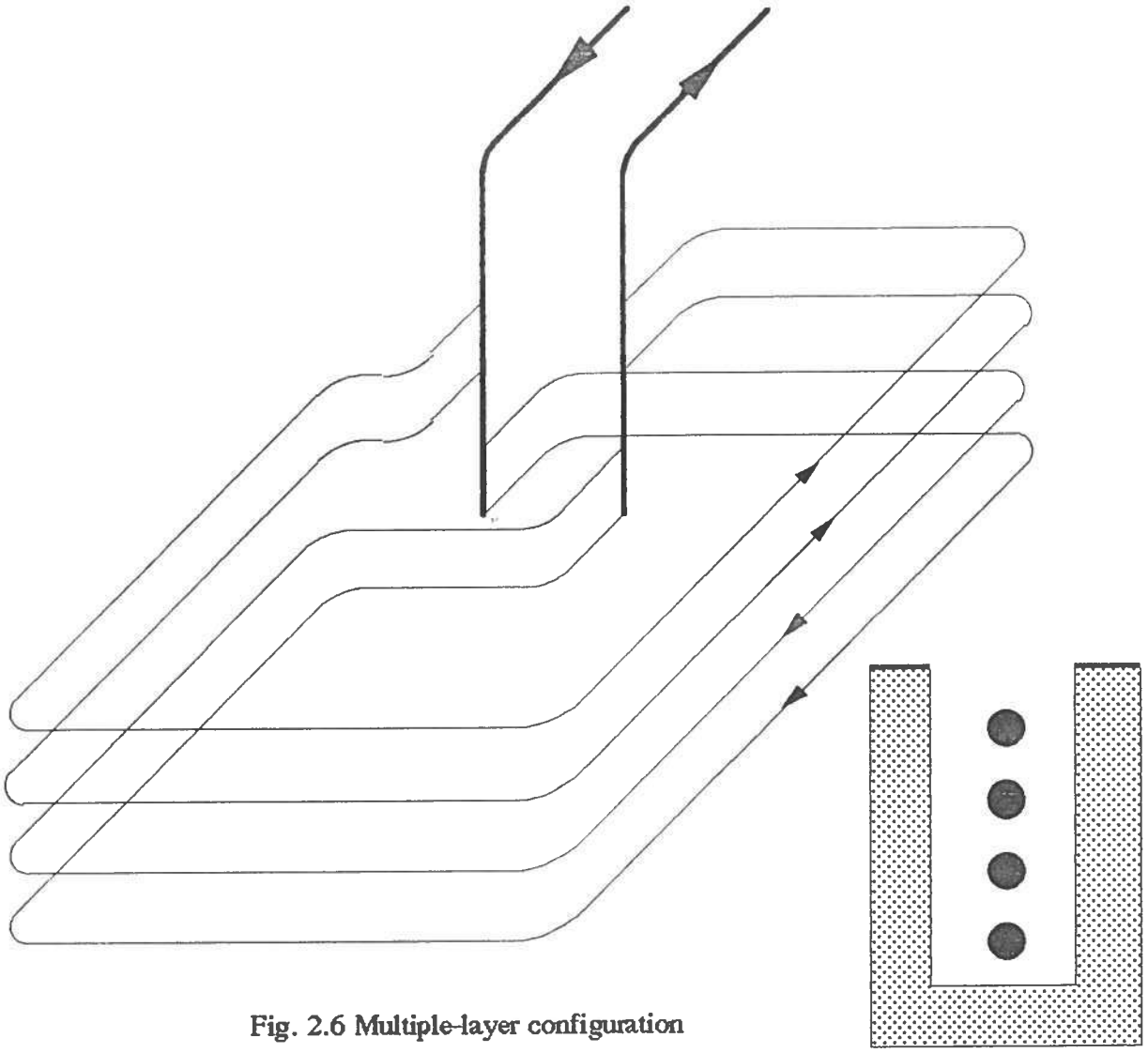

Fig. 2.6 Multiple-layer configuration

More information about horizontal ground heat exchangers can be found in the User Manual of the computer package G-HEADS which is attached to this report.

## 2.5 Building Design Loads

Detailed information on the heating and/or cooling loads of the house is required for a proper selection of heat pump units and the design of the ground coil and air distribution system. These rates of energy and the COP of the heat pump determine the rate of thermal energy to be extracted or rejected from/to the ground by the use of the GHE, called the ground heat exchanger load. It

should be noted that the COP of the heat pump can be obtained from the manufacturers specifications and it is fixed by the entering water temperature $T_{fl}$. For the cooling mode of operation the amount of heat rejected to the ground equals to the sum of the building cooling load and the power input to the heat pump compressor and water circulating pump. For the heating mode of operation, the amount of heat extracted from the ground is the difference between heating load and power input to the compressor and to the circulating pump.

Ground heat exchanger operation (on/off) is very sensitive to weather conditions and building thermal characteristics and therefore varies from hour to hour. Therefore many researchers support a model reflecting the hourly performance of the entire ground heat pump system and long time simulation in terms of years at the expense of simplifying coupled heat and moisture transport equations. Hourly simulation however, would require a lot of computer time and would not be practical for use by industry, even if a mainframe computer were available. One way to reduce computer time is to simplify the model while keeping up acceptable accuracy [Mei, 1986]. According to Forsmand (1981) the deviation of the COP caused by using daily average data is within 3% with respect to hourly simulation and thus it is pointless to use a very complex computer program. Bose et al.(1985) even suggest the use of monthly values for ground heat exchanger design. Moreover for a steady-state model of a heat pump an hourly simulation appears to be too short to obtain a steady state condition. Bearing this in mind, the authors of this report decided to put more emphasis on a detailed modeling of the coupled heat and moisture flow in ground heat storage, and a long term simulation on a daily basis (12 hrs). The heating and cooling loads for a given building shall be obtained on the basis of the meteorological data.

The current state-of-the-art practice is to use personal computers for heating and/or cooling load calculations. The computer can provide the data loads at twelve or more different hours from one set of input data. This is very helpful in determining maximum overall loads and selecting the appropriate size of a heat pump unit. A computerized approach speeds up lengthy and strenuous calculations providing more reliable and consistent results. Sophisticated computer software for

heating and/or cooling load calculations and estimating energy consumption is available on today's market. Some of the software is briefly reviewed below:

- LDCAL5 (Cooling and Heating Load Calculations ) developed by Oklahoma State University. It includes methodologies of load calculations for all types of buildings.
- BESA Design, version 1.2 developed by Candaplan Resources Inc., Hamilton, Ontario, Canada. Building models may contain up to 25 zones and can be run alone or in a batch ofup to 10 models. Each run can consist of loads and sizes, analysis, a typical day analysis or full hourly analysis. This package is designed for personal computers such as the IBM XT, AT, PS/2 and compatibles.
- BLAST (Building Loads Analysis and System Thermodynamics) developed by the U.S. Army Corps of Engineers Construction Engineering Research Laboratory, Champaign, Illinois. It performs hourly simulations of building loads using a detailed room heat balance method combined with conduction transfer functions.
- Right-J Residential Load Calculation Software from Air Conditioning Contractors of America, Washington, D.C. It performs accurate, detailed load and cfm calculations. The package calculates whole-house or room by room loads .

In this report a simplified formula for estimating heating and cooling loads is used (Appendix H).

## 2.6 Thermal Behavior of Ground-Coupled Systems

The performance of ground-coupled heat pump systems depends strongly on the soil thermo -and transport properties which in turn are influenced by weather conditions. For example, soil thermal conductivity and soil moisture diffusivity depend strongly on soil moisture content. When a ground coil is discharging or extracting heat, the soil in the immediate vicinity of the heat source or heat sink, is exposed to large temperature gradients, thus generating a driving force for moisture migration from the high to the low temperature region. As the moisture content of the soil adjacent

to the heat source decreases the local thermal conductivity may drop sharply and thus dry soil surrounding the coil acts as an insulating annulus. This results in an increase of the temperature of the working fluid (water, brine) leaving the ground heat exchanger. Its magnitude depends upon the soil conditions, the coil length and the amount of heat rejected by the ground coil, i.e., condenser load of the heat pump. The return temperature controls the performance of the heat pump and its capacity. The latter determines the run time (on) of the heat pump for a given cooling load of the building.

The soil temperature gradient has the opposite direction whilst the ground coil acts as the heat sink, so that soil moisture has a tendency to migrate toward the heat sink surface. If the rate of heat extraction is high, soil moisture in the vicinity of the ground coil may undergo phase change. During the freezing process, the thermal -and transport properties of soil are changing significantly and a unique and complex set of soil conditions is created, such as, for example, the liberation of latent heat from the fusion of water and the occurrence of water migration to the freezing front which may result in frost heave. The latent heat liberated on freezing has a very positive effect on ground coil performance. If the ground coil is not long enough, the exit temperature of the working fluid from the coil may be very low resulting in low performance in the ground heat pump unit.

The knowledge of long term effects of ground coupling is very important at the design stage to prevent the future failure of the system. Such failure could wreck a potentially prosperous market for ground coupled heat pumps. For example, the question of full thermal recovery of the ground, coupled with the heat pump operating mainly in heating mode, must be answered. If the ground did not regain heat during summer, i.e., presence of frozen soil or a very low soil temperature around the ground heat exchanger, a lower performance of the heat pump may result. This may be a permanent problem unless an additional source of heat will be used in order to reduce heat pump heating load. A similar situation may appear in systems operating mainly in cooling load where the ground did not regain moisture content and/or deposited heat was not completely dissipated during winter time.

## 2.7 Computerized Design of a Ground Heat Pump System

The most troublesome element of the entire GHPS to be designed is without any doubts the GHE. Heat deposition and/or heat extraction to/from the ground induces a simultaneous heat and mass transfer in soils and may lead to additional complex problems related to the phase change phenomena of soil moisture such as drying/rewetting and freezing/thawing. This makes the design of the GHEs extremely complex and difficult since there is no analytical solution to the coupled heat and mass flow problem in the ground.

Off all the design methods, only a computerized approach is able to handle this complex task successfully. This approach, described below, assumes a fixed length of ground coil and then the daily performance of the entire heat pump system is tested using a detailed mathematical model of ground heat storage, a steady state model of heat pump units, the heating and cooling loads of the house, and comprehensive climatological data. In order to select the best alternative for a given house, site and weather conditions, the designer will be able to test various dimensions, configurations, and arrangements of the GHE, different kind of ground coil fluids, coil materials, soils and heat pump units over a very long period of time.

Longitudinal variation of the fluid temperature along the buried GHE is dependent upon the heat flux from the fluid into the ground or vice versa which causes either an increase or decrease of temperature. The amount of heat exchanged between the circulating fluid in the ground coil and surrounding soil over the pipe wall can be expressed as:

$$Q = U * \pi D_{pi} L_{GHE} * \Delta T_m \qquad (2-9)$$

where: $U$ = overall heat transfer coefficient, per unit length of pipe

$D_{pi}$ = inside pipe diameter

$L_{GHE}$ = length of the ground heat exchanger

$\Delta T_m$ = mean logarithmic temperature difference.

The overall heat transfer coefficient for the GHE - soil system is defined as.

$$\frac{1}{U} = \frac{1}{h_f} + \frac{D_{pi}}{2}\left[\frac{\ln \frac{D_{po}}{D_{pi}}}{K_p} + \frac{\ln \frac{D_s}{D_{po}}}{K_s}\right] \qquad (2 - 10)$$

where: $h_f$ = film heat transfer coefficient (fluid-pipe wall)

$K_p$ = thermal conductivity of the pipe wall

$K_s$ = thermal conductivity of the soil in the vicinity of the pipe

$D_{po}$ = outside diameter of the pipe

$D_s$ = soil effective diameter.

The value of $D_s$ is determined by a calibration of the mathematical model to fit the experimental data. In general excessive values for $D_s$ lead to the so called insulation effect of the pipe and thus to a heat flux decrease. For example, for the steady - state operation of a pipeline, Haynes (1974) recommends that:

$$D_s \approx 3 * D_{po} \qquad (2 - 11)$$

Thermal conductivity of the soil, $K_s$, depends on the type of soil, mineral composition, dry density , and moisture content which in turn is influenced by the temperature gradient. Again the accurate values of soil moisture content are needed and can be obtained from the mathematical model.

The film heat transfer coefficient, $h_f$, between the circulating fluid and the pipe wall is calculated from empirical equations. For a laminar flow in smooth circular tubes, the Nusselt number is constant and according to Incropera and de Witt (1985) is equal to:

$$Nu_D = \frac{h\ D}{K_f} = 4.3636 \qquad (2 - 12)$$

If the fluid flow is in transitional and turbulent zones, i.e. Re ≥ 2300, the following relation proposed by Gnielinski (1976) can be used.

$$Nu_D = \frac{(Re - 1000) * Pr * 0.5\ f}{1.0 + 12.7 * (Pr^{2/3} - 1)\ \sqrt{f/2}} \qquad (2 - 13)$$

where: f = the friction factor

Pr = Prandtl number

Re = Reynolds number

The friction factor value, for turbulent fully developed flow in a smooth pipe, is given by Petukhov (1970).

$$f = (1.58 \ln Re - 3.28)^{-2} \qquad (2 - 14)$$

For variable properties of ground coil fluids the following corrections are recommended:

$$Nu_{Db} = Nu_D \left\{ \frac{Pr_b}{Pr_w} \right\}^n \qquad (2 - 15)$$

where: n = 0.11 - heating mode

n = 0.25 - cooling mode

b = evaluated at local bulk temperature

w = evaluated at local wall temperature

The mean logarithmic temperature difference is defined as:

$$\Delta T_m = \frac{\Delta T_1 - \Delta T_2}{\ln \frac{\Delta T_1}{\Delta T_2}} \qquad (2 - 16)$$

where: $\Delta T_1 = T_{f1} - T_{s1}$

$\Delta T_2 = T_{f2} - T_{s2}$

$T_{s1}$ = mean soil temperature at exit from the GHE and for the effective soil diameter $D_s$

$T_{s2}$ = mean soil temperature at inlet to the GHE and for the effective soil diameter $D_s$

$T_{f1}$ = mean temperature of the circulating fluid at exit from the GHE

$T_{f2}$ = mean temperature of the circulating fluid at inlet to the GHE

Applying the principle of energy conservation to the heat exchange apparatus of the heat pump linked with the GHE we have:

$$\dot{Q}_{HE} = \dot{m}_f * c_f ( T_{f2} - T_{f1}) \qquad (2 - 17)$$

where: $Q_{HE}$ = total heat of extraction (QH) or rejection (QC) to the ground by the GHE

The above equation is used to calculate the value of $T_{f2}$, whilst in the first iteration $T_{f1}=T_{s1}$ .

Combining (2-9), (2-16) and (2-17) the following relation is obtained.

$$\pi D_{pi} * U * L_{GHE} * \frac{(T_{f1}-T_{s1}) - (T_{f2}-T_{s2})}{\ln \frac{T_{f1}-T_{s1}}{T_{f2}-T_{s2}}} = \dot{m}_f * c_f ( T_{f2} - T_{f1}) \qquad (2 - 18)$$

Assuming that $T_{s1}=T_{s2}=T_s$ the first approximate value of fluid temperature, $T_{f1}$, entering the heat pump unit, for the given temperature, $T_{f2}$, can be obtained from:

$$T_{f1} = T_s + (T_{f2} - T_s)\, e^{-\pi D_{pi} * U * L_{GHE} / ( m_f * c_f)} \qquad (2 - 19)$$

The case where $T_{s1}=T_{s2}=T_s$ takes place when the GHE is out of operation for a long time. In practice, the soil temperature, $T_s$, varies along the ground coil length, L, and depends on the outer boundary conditions at the ground surface, time varying heating and/or cooling loads handled by the heat pump unit . Therefore much more accurate values of $T_{f1}$ are obtained from the Eq.(2 - 18) by using numerical methods such as for example, Newton-Raphson or False Position. It is clear, from the Eq.(2 - 18), that $T_{f1}$ depends on the amount of heat to be extracted or rejected from/to the ground, and the heat transfer capability of the GHE.

The amount of heat $Q_{HE}$ depends strongly on the time of compressor operation. The relative time of compressor operation at steady state condition is defined as:

$$r = \frac{t_{on}}{t_{on}+t_{off}} = \frac{Q_B}{Q_{HP}} \qquad (2 - 20)$$

where: $r$ = relative time of compressor operation at steady state condition

$t_{on}$ = *on-cycle* theoretical compressor time

$t_{off}$ = *off-cycle* theoretical compressor time

$Q_B$ = heating or cooling load of the building

$Q_{HP}$ = heating/cooling capacity of the heat pump.

Heating/cooling capacity, $Q_{HP}$, and the COP of the heat pump unit are, in turn, straight functions of $T_{w1}$ and are described in Section 2.1. The heating or cooling load of the building, $Q_B$, depends in turn on weather conditions and building thermal characteristics. Manufacturer's capacity data for heat pump equipment assume however full-loaded steady-state operation whilst in fact it operates at partial load most of the time [McQuiston and Parker, 1988]. For small unit type equipment such as water-to-water heat pumps the detailed part-load performance is not always available. In this case a method developed by National Bureau of Standards is normally used. A partial-load factor is defined as follows:

$$PLF = 1 - \delta_c (1 - r) \qquad (2 - 21)$$

where: $\delta_c$ = degradation coefficient, given by manufacturer or taken as 0.25

For unitary heat pumps the PLF can also be expressed as follows:

$$PLF = \frac{t_{on}}{t_{ona}} \qquad (2 - 22)$$

where: $t_{ona}$ = *on-cycle* actual compressor time

Therefore the actual run time of the heat pump unit operating at partial load is expressed as:

$$t_{ona} = \frac{t_{on}}{1 - \delta_c (1 - r)} \qquad (2 - 23)$$

Continuous computerized testing of the performance of the ground heat pump unit linked with the GHE having a selected length, $L_{GHE}$, requires the knowledge of soil moisture content and

temperatures at any time of on/of operation. In traditional design approaches these values are usually not available and therefore a transient mathematical model of ground heat storage is necessary to provide continuous information about these data.

## 2.8 Sizing the Heat Pump Unit

It is a common problem encountered at the design stage whether the size of a ground heat pump should be selected on the basis of the heating or the cooling load. Usually there is a problem to accommodate both loads, i.e the selected unit is too small or too large. The over- or undersized heat pump unit creates number of undesired operational and economical problems, such as: frequent on-off operation, lower operating efficiency, reduction of equipment life time, higher initial and operating costs, or comfort reduction and necessity for supplementary heating or cooling. There are, however , no nation wide guidelines regarding ground heat pump selection. According to the rule of thumb the heat pump sizing can be based either on the design heating load, or the cooling load with substantial oversizing. In the northern climate the heating load is more dominant than cooling load and this factor shall be taken into account as well. In this report, the following procedure is suggested:

$$\frac{Q_c * t_c}{Q_h * t_h} \geq 1.25 \qquad \text{selection is based on the cooling load } Q_c$$

$$0.75 \leq \frac{Q_c * t_c}{Q_h * t_h} < 1.25 \qquad \text{selection is based on } Q_c * 1.25$$

$$0.50 \leq \frac{Q_c * t_c}{Q_h * t_h} < 0.75 \qquad \text{selection is based on } \frac{Q_c + Q_h}{2}$$

$$0 < \frac{Q_c * t_c}{Q_h * t_h} < 0.5 \qquad \text{selection is based on } Q_h$$

where: $Q_c$ = cooling load

$Q_h$ = heating load

$t_h$ = total time of the cooling season

$t_c$ = total time of the heating season

# 3. GROUND HEAT STORAGE CHARACTERISTICS

## 3.1 Introduction

The knowledge of ground heat storage characteristics is very important in the design process since it has a direct influence on the performance of the ground heat exchanger and as a consequence the entire ground coupled heat pump system (GCHPS).

During the cooling mode, when heat is transferred to the ground by the ground heat exchanger, warming of the soil takes place. Heat is transferred mainly by conduction, and by moisture migration in the form of vapor and/or liquid. Vapor diffusion, away from the ground coil, occurs due to the highest vapor pressure at the pipe-soil interface. On reaching a cool zone the vapor condenses releasing latent heat. Migration of liquid moisture is due to pressure gradients influenced by increased soil temperature which in turn is responsible for lowering liquid surface tension forces. Therefore liquid moisture has a tendency to migrate from warmer to colder regions. These two combined moisture fluxes generate a moisture content gradient in the soil, which is a driving force for liquid moisture migration back to the heat source. Depending on the type of soil the system may remain in dynamic equilibrium or a net loss of moisture will occur with a resulting decrease of thermal conductivity of the soil.

During the heating mode, heat is extracted from the ground and soil moisture freezing, in a vicinity adjacent to the ground coil, may take place. This in turn induces migration of moisture from warm to cold zones. The frozen soil behaves as a sink, therefore the migration of water lasts so long as the temperature gradient exists and soil moisture is available. This eventually may lead to soil expansion (frost heave), if the soil pores are overfilled with ice, and cause damage to the ground coils. Therefore in this case, a soil less sensitive to frost heave should be selected as a backfill. In turn, freezing of the soil next to the ground coil may generate additional pressure improving heat transfer due to thermal contact resistance. Moreover the thermal conductivity of frozen soil, higher than that of unfrozen soil, increases the rate of heat transfer to the ground coil.

From the above discussion it is clear that in order to establish a solid design basis for ground heat storage the following information about the site shall be collected and analyzed:

- types of soils and stratification data
- geotechnical data (grain size distribution, bulk density of dry soil, water content, void and saturation ratio, and permeability)
- thermo -and mass transfer characteristics of unfrozen and frozen soils (heat capacity, thermal conductivity, hydraulic conductivity, and soil-moisture diffusivity)
- climatological data over the full heating and cooling season (ambient temperature, rainfall, solar radiation, wind velocity, snow precipitation, temperature of undisturbed soil etc.)
- geohydrological data (depth of ground water table, ground water flow, etc.).

For example, values for the heat capacity and thermal conductivity of soils are expected to be high to minimize the storage volume and enhance a heat exchange. Thermal conductivity varies with the type of soil and is very sensitive to its moisture content. If the ground coil performance is to be good it is desirable to have, in the immediate vicinity of the ground coil, a densely packed soil with high moisture content. Sound knowledge of soil moisture transport characteristics is also necessary in order to predict dynamic changes of soil moisture content. The diffusion of moisture in ground heat storage under the influence of the temperature gradient is of considerable importance, since it may drastically reduce soil thermal properties in the direct vicinity of the ground heat exchanger.

Experimental data on moisture transport characteristics in various soils is very scarce. The available data is only for sand , silty loam, and to a certain extent for clay loam. This data however is extended over the full soil texture, containing 12 different soil types, by reckoning a weighted contribution of the basic soil components such as sand, silt, and clay.

## 3.2 General Characteristics of Soils

According to the US Department of Agriculture (USDA) there are twelve soil texture classes. Table 3.1 gives the common textural class names and their per cent ranges of soil separates as well as dry bulk densities.

Table 3.1 General Characteristics of Common Textural Classes of Soils

| Soil Texture | Clay, $m_{cl}$ Mass Fraction - | Silt, $m_{si}$ Mass Fraction - | Sand, $m_{sa}$ Mass Fraction - | Soil* Density, $\rho_b$ $kg/m^3$ |
|---|---|---|---|---|
| Sand | 0.00 - 0.10 | 0.00 - 0.15 | 0.85 - 1.00 | 1480-1785 |
| Loamy sand | 0.00 - 0.15 | 0.00 - 0.30 | 0.70 - 0.90 | 1410-1775 |
| Sandy loam | 0.00 - 0.20 | 0.00 - 0.50 | 0.40 - 0.80 | 1290-1760 |
| Loam | 0.07 - 0.27 | 0.28 - 0.50 | 0.23 - 0.52 | 1270-1695 |
| Silt loam | 0.00 - 0.27 | 0.50 - 0.88 | 0.00 - 0.50 | 1230-1550 |
| Silt | 0.00 - 0.12 | 0.80 - 1.00 | 0.00 - 0.20 | 1120-1600 |
| Sandy clay loam | 0.20 - 0.35 | 0.00 - 0.28 | 0.45 - 0.80 | 1405-1725 |
| Clay loam | 0.27 - 0.40 | 0.15 - 0.53 | 0.20 - 0.45 | 1270-1560 |
| Silty clay loam | 0.27 - 0.40 | 0.40 - 0.73 | 0.00 - 0.20 | 1260-1565 |
| Sandy clay | 0.35 - 0.45 | 0.00 - 0.20 | 0.45 - 0.65 | 1395-1710 |
| Silty clay | 0.40 - 0.60 | 0.40 - 0.60 | 0.00 - 0.20 | 1200-1545 |
| Clay | 0.40 - 1.00 | 0.00 - 0.40 | 0.00 - 0.45 | 1265-1535 |

* Calculated from porosity data reported by Clapp and Hornberger (1978)

Each soil from this list has a completely different distribution of grain sizes and shapes which in turn determines its density, porosity and pore size distribution. These parameters directly influence

the soil thermal -and mass transfer coefficients. These 12 soils can be divided into three textural groups:

(i) sandy: sands

(ii) loamy: loamy sands, sandy loams, loams

(iii) clayey: clay loams, silty clay loams, clays.

Natural soils form a mixture of sand, silt, and clay and therefore have an intermediate structure and properties.

## 3.3 Thermal Properties of Soils

The thermal properties of ground depend on various factors such as the type and structure of the soil, its water/ice content, and its dry bulk density, $\rho_b$. Ground structure is very complex and depends on the type of soil and alternate cycles of freezing/thawing or drying/rewetting which are encountered during heat extraction or deposition to the ground. The above cycles may result in changes in the soil structure what then leads to variation in its thermal properties.

Drying of soil leads to shrinkage and soil cracks leading to thermal resistance. Subsequent wetting causes so called swelling. Alternate cycles of drying and rewetting lead to a loosening of soil on the interface with the GHE. This is very common in clayey soils of high plasticity.

Cycles of freezing and thawing can disturb the natural structural bonds in soil and generate additional thermal contact resistance. Again a loosening of soil around the GHE takes place. Therefore backfilling is used to replace a clayey soil with better packed soil such as sand with higher dry density and thermal conductivity.

In general ground heat storage may contain a large variety of soils having different thermal -and mass transfer characteristics, a good knowledge of which is essential for computer simulation of the entire system. Therefore the available thermal -and mass transfer properties of all twelve

textural classes of soils will be briefly reviewed. Thermal properties of soil are described by heat capacity and thermal conductivity.

### 3.3.1 Heat Capacity

The volumetric heat capacity of soil can be estimated simply as a mixture of solid matter, water or ice and air [de Vries, 1963].

$$C = \sum_{i=1}^{n} C_i \ \theta_i \qquad (3 - 1)$$

where: $C$ = volumetric heat capacity of soil

$C_i$ = volumetric heat capacity for each constituent

$\theta_i$ = respective volume fraction

$n$ = number of components

For a soil-water-ice mixture, if the dry density of the soil $\rho_b$ is known, the volumetric heat capacity can be obtained by the equation

$$C = \rho_b \, ( c + 4.184 \, w_u + 2.1 \, w_I) \qquad (3 - 2)$$

where: $C$ = volumetric heat capacity of soil, $kJ/m^3K$

$c$ = specific heat of dry soil, kJ/kgK

$w_u$ = unfrozen water content based on the dry mass of the soil

$w_I$ = ice content based on the dry mass of the soil

$\rho_b$ = bulk density of soil

Most of the minerals composing soils have nearly the same values of density $\rho_m$= 2650 $kg/m^3$ and specific heat capacity $c_m$= 0.836 kJ/kgK. Since it is difficult to separate the different kinds of

organic matters present in soils, all of them are lumped into a single constituent with an average density $\rho_b$= 1300 kg/m$^3$, and an average specific heat capacity c = 0.711 kJ/kg.K. Ice and water have specific heat capacities 2.1 kJ/kg.K and 4.184 kJ/kg.K respectively.

### 3.3.2 Thermal Conductivity

Heat flow through the soil occurs by conduction, convection, and radiation. If the size of the solid particles is small, the contribution of convection to the heat transfer is negligible. When the soil temperature is low, the radiation effect will also be very small. The thermal conductivity of soils is a function of several factors. The most important are density, moisture content, temperature, texture, mineral composition, and saturation.

The most comprehensive study of the thermal conductivity of soils was made by Kersten [1949]. He concluded his study by providing a set of empirical equations based on the dry density and water content of the soils and the grain size. Kersten's equations follow his experimental data, and for most conditions, they enable the calculation of soil thermal conductivities to within 25%.

For unfrozen soils:

Fine-grained (50% or more of silt and clay sizes)

$$K_u = 0.13 \left\{ \log w - 0.22 \right\} 10^{0.000624\rho_b} \qquad (3-3)$$

Coarse-grained (less than 50% of silt and clay sizes)

$$K_u = 0.1 \left\{ \log w + 0.57 \right\} 10^{0.000624\rho_b} \qquad (3-4)$$

where $K_u$ = thermal conductivity of unfrozen soil, W/m K

$w$ = mass water content ($w_I + w_u$), % dry weight

$\rho_b$ = dry bulk density of soil, kg/m$^3$

Eq. (3 - 3) is applicable, for the water content, w, equal or greater than 7% and for Eq. (3 - 4) water content w shall be equal or greater to 1%.

The relation of the thermal conductivity of silt loam and sand versus volumetric moisture content, published by Nakshabandi and Kohnke (1965) and Jury and Miller (1974) respectively, can be approximated by the following equations:-

Silt loam

$$K_u = 0.48468 - 3.8677\theta + 127.16\,\theta^2 - 346.35\,\theta^3 + 274.13\,\theta^4 \qquad (3 - 5)$$

Sand

For $0 \le \theta \le 0.025$

$$K_u = 1.15 + 306\,\theta \qquad (3 - 6a)$$

For $0.025 \le \theta \le 0.35$

$$K_u = 4.1677 + 14.823\,\theta - 14.016\,\theta^2 \qquad (3 - 6b)$$

Graphical presentation of thermal conductivity for a medium sand and silt-loam against volumetric moisture content is shown in Fig. 3.1.

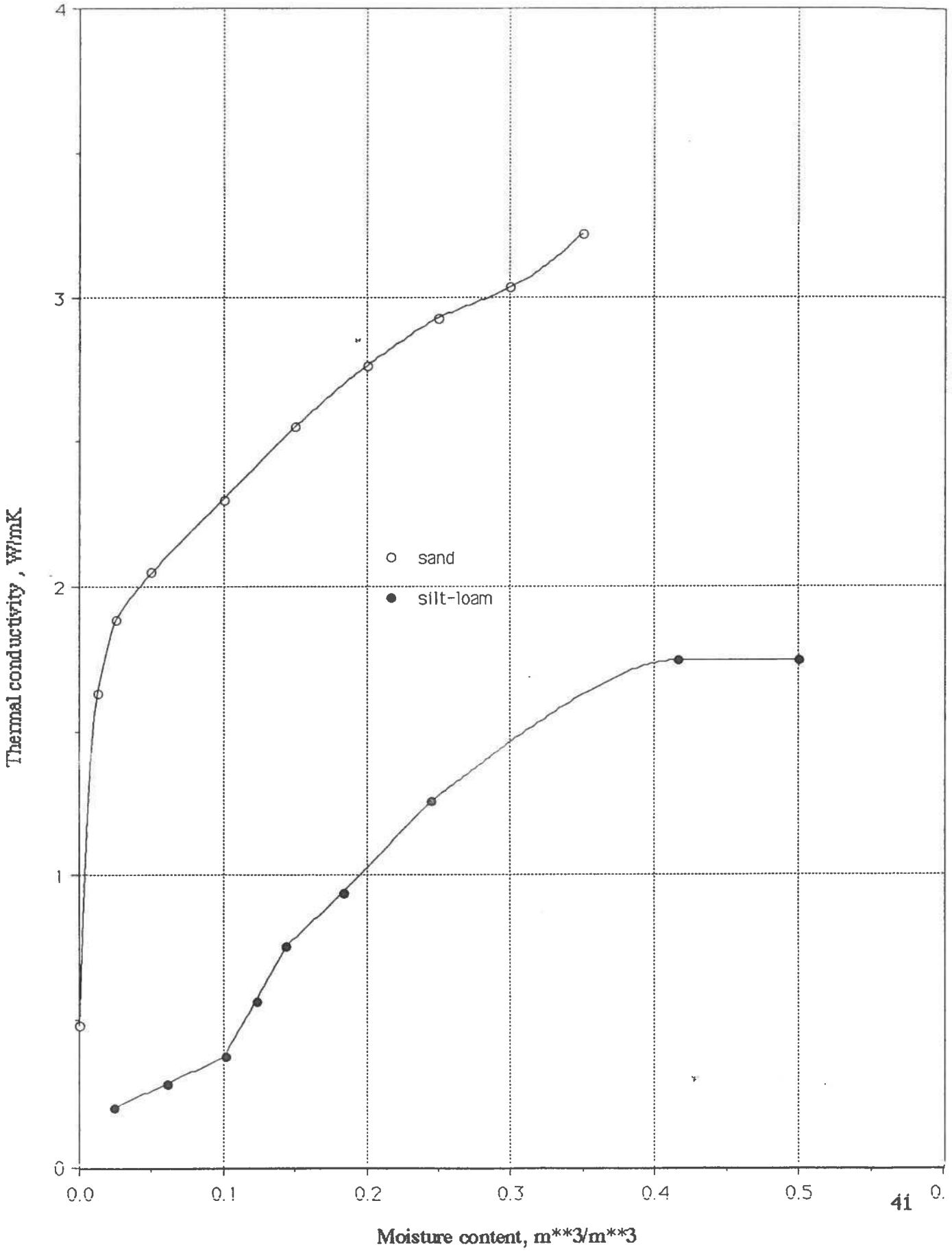
4
3
2
1
0
0.0
0.1
0.2
0.3
0.4
0.5
0.
sand
silt-loam
Thermal conductivity , W/mK
Moisture content, m**3/m**3

For frozen soils:

Kersten (1949) also reported empirical equations for calculating the thermal conductivity of frozen soils.

Fine-grained (50% or more of silt and clay sizes)

$$K_f = 0.012\left\{ w\, 10^{0.0005\rho_b} + 0.117 * 10^{0.00137\rho_b} \right\} \qquad (3-7)$$

Coarse-grained (less than 50% of silt and clay sizes)

$$K_f = 0.0046\left\{ w\, 10^{0.0009\rho_b} + 2.375 * 10^{0.0008\rho_b} \right\} \qquad (3-8)$$

where: $w$ = mass water content ($w_I + w_u$), % dry weight

These equations are applicable for the typical soil textural groups discussed in Section 3.1. Therefore in this report only Kersten's equations will be used to calculate soil thermal conductivity for unfrozen and frozen soils.

For partially frozen soils

The following equation is used in this report to calculate the thermal conductivity of partially frozen soils.

$$K_{pf} = K_u \xi + K_f (1 - \xi) \qquad (3-9)$$

where: $K_{pf}$ = thermal conductivity of partially frozen soil,

$K_u$ = thermal conductivity of unfrozen soil,

$K_f$ = thermal conductivity of frozen soil,

$\xi$ = volume fraction of unfrozen soil.

## 3.4 Transport Characteristics of Soils

In order to evaluate accurately the performance of the ground heat exchanger, it is necessary to carry out an analysis of coupled heat and moisture transport in ground heat storage caused by the ground coil operation and/or environmental effects. This analysis, however, requires knowledge of soil moisture transport characteristics such as:

- hydraulic conductivity, $K_h$
- isothermal vapor diffusivity, $D_{\theta v}$
- isothermal liquid diffusivity, $D_{\theta l}$
- thermal vapor diffusivity, $D_{Tv}$
- thermal liquid diffusivity, $D_{Tl}$

### 3.4.1 Hydraulic Conductivity

Unfrozen soils

For saturated soils the hydraulic conductivity is dependent on soil texture and dry bulk density. The following relations are given by Campbell (1974) and can be used to obtain the hydraulic characteristics of soils.

$$K_{hs} = 0.14112\left(\frac{1300}{\rho_b}\right)^{1.3\,b} \exp\left(-6.5\, m_{cl} - 3.7\, m_{si}\right) \qquad (3 - 10)$$

where: $K_{hs}$ = hydraulic conductivity of saturated soil, m/h

$\rho_b$ = bulk density of soil, $kg/m^3$

b = empirical power of soil moisture characteristic function

$m_{cl}$ = mass fraction of clay

$m_{si}$ = mass fraction of silt

The power of soil moisture characteristic function can be obtain from the following relation:

$$b = d_g^{-0.5} + 0.2\,\sigma_g \qquad (3 - 10a)$$

where: $d_g$ = geometric mean diameter of soil particle, mm

$$d_g = \exp\left[\, m_{cl} \ln 0.001 + m_{si} \ln 0.026 + (1 - m_{cl} - m_{si}) \ln 1.025\right]$$

for the three classes of soils normally used in determining texture

$d_{clay} = 0.001$ mm , $d_{silt} = 0.026$ mm , $d_{sand} = 1.025$ mm

$\sigma_g$ = geometric standard deviation of particle diameter, mm

$$\sigma_g = \exp\left[\left(m_{cl}(\ln 0.001)^2 + m_{si}(\ln 0.026)^2 + (1-m_{cl} - m_{si})(\ln 1.025)^2\right) - \left(m_{cl}\ln 0.001 + m_{si}\ln 0.026 + (1-m_{cl} - m_{si})\ln 1.025\right)^{0.5}\right]$$

For all soil textures the expected range of $d_g$ is 0.003 to 0.7 mm, while the range of $\sigma_g$ is 1 to 30. The above relations are generally valid for soils at bulk density of 1300 kg/m$^3$. The calculations made by the authors of this report show an acceptable agreement with experimental data published by Clapp and Hornberger (1979) and de Jong (1982) for the bulk density range of 1100 to 1600 kg/m$^3$.

Comprehensive experimental data regarding hydraulic conductivity of saturated soils is also available and was provided by Clapp and Homberger (1979). For unsaturated soils the hydraulic conductivity is not constant and depends on soil composition, gradation, void ratio and moisture content. This is a reason that this property is very difficult to determine experimentally in field or laboratory tests. The values of hydraulic conductivity for unsaturated soils can vary by many orders of magnitude between their full saturation and desiccation. According to Shapiro et al.(1978) the gravity induced flow in silty loam is very small in comparison to that generated by moisture and temperature gradients and therefore can be disregarded . Campbell (1974) proposed the following empirical equation for unsaturated hydraulic conductivity.

$$K_h = K_{hs} \left( \frac{\theta}{\theta_s} \right)^{2b+3} \qquad (3-11)$$

Clapp and Hornberger (1978) published the values of empirical power, b, for the hydraulic conductivity of of 11 textural groups of soils. They obtained these values from desorption data reported by Holtan et al.(1976) which consisted of 176 sampled soil types from 34 locations in the United States. This approach was assessed by De Jong (1982) for the data from soils found in Canada. In total 271 soil samples, from 81 different Canadian locations, were analyzed. The average coefficients, b, were found to be similar to those reported by Clapp and Hornberger. The representative values of the hydraulic parameters are shown in Table 3.2. As one can see, not all soils were included in the final analysis, mainly due to insufficient data regarding soil water characteristics. Variations of b for the same type of soil texture are caused by differences in mineralogy, types of organic matter, and climatic effects. Therefore saturated water contents, $\theta_s$, for Canadian conditions ranged from 0.391 in the loamy sand to 0.573 in the silty clay loam, whereas for the U.S. the figures ranged from 0.395 in the sand to 0.492 in the silty clay.

Table 3.2 Values of hydraulic parameters

| Soil Texture | Soil* Density, $\rho_b$ | American b | American Data $\theta_s$ | Canadian b | Canadian Data $\theta_s$ |
|---|---|---|---|---|---|
| | kg/m$^3$ | - | m$^3$/m$^3$ | - | m$^3$/m$^3$ |
| Sand | 1480-1785 | 4.05 | 0.395 | 3.21 | 0.401 |
| Loamy sand | 1410-1775 | 4.38 | 0.410 | 4.09 | 0.391 |
| Sandy loam | 1290-1760 | 4.90 | 0.435 | 4.78 | 0.393 |
| Silt | 1120-1600 | - | - | - | - |
| Silt loam | 1230-1550 | 5.30 | 0.485 | 7.34 | 0.482 |

| | | | | | |
|---|---|---|---|---|---|
| Loam | 1270-1695 | 5.39 | 0.451 | 6.60 | 0.493 |
| Sandy clay loam | 1405-1725 | 7.12 | 0.420 | - | - |
| Silty clay loam | 1260-1565 | 7.75 | 0.477 | 7.95 | 0.573 |
| Clay loam | 1270-1560 | 8.52 | 0.476 | 9.84 | 0.504 |
| Sandy clay | 1395-1710 | 10.4 | 0.426 | - | - |
| Silty clay | 1200-1545 | 10.4 | 0.492 | 10.26 | 0.532 |
| Clay | 1265-1535 | 11.4 | 0.482 | 12.71 | 0.522 |

* Calculated from porosity data reported by Clapp and Hornberger (1978)

Haverkamp et al. (1979) published the relation for hydraulic conductivity of Yolo light clay (clay loam) which closely follows experimental data :

$$K_h = K_{hs} \frac{124.6}{124.6 + (-\psi)^4} \qquad (3-12)$$

where: $K_{hs} = 1.23 * 10^{-5}$ (cm/s)

$\psi$ = matric potential (cm)

For the Yolo light clay, sand mass fraction can be assumed to be close to 24%, whereas the critical volumetric moisture content at which liquid continuity fails, $\theta_{lk} = 0.2$ .

### 3.4.2 Soil Moisture Diffusivity

In general, when unsaturated soil is under the influence of a thermal gradient, soil moisture flow in the form of liquid and/or vapor may take place.The equation describing this process was derived by Philip and de Vries (1957).

$$\frac{q_m}{\rho_l} = \frac{q_l}{\rho_l} + \frac{q_v}{\rho_l} = -D_\theta \nabla\theta - D_T \nabla T - K_h \nabla y \qquad (3-13)$$

The isothermal and thermal soil moisture diffusivities are split into liquid and vapor components:

$$D_\theta = D_{\theta l} + D_\theta \qquad (3 - 14)$$

$$D_T = D_{Tl} + D_{Tv} \qquad (3 - 15)$$

The liquid diffusivities have a principal meaning at high soil moisture contents, whilst the remaining two vapor coefficients are more dominant at low moisture contents. Reliable data on diffusion coefficients for the liquid and vapor fluxes is required in order to accurately simulate soil moisture profiles in ground heat storage.

Experimental data on soil moisture diffusivity coefficients is scarce and very difficult to obtain. There are only a few publications about soil moisture diffusivity for isothermal conditions. Staple et al. (1954) obtained isothermal soil moisture diffusivity for clay loam within a wide range of soil moisture contents from just below saturation to the air-dry condition. Philip (1955) reported the relation between isothermal soil moisture diffusivity and volumetric moisture content for Yolo light clay (clay loam). Dirksen and Miller (1966) gave the isothermal diffusivity relationship for silt loam. Bruce and Klute (1956) and Whisler et al.(1968) published some data regarding fine sand and sandy loam. Baladi (1975) suggested an exponential form of isothermal diffusivity for loam.

Very little data is available with respect to the thermal diffusivity of soil moisture. Philip and de Vries (1957) provided values of thermal and isothermal liquid and vapor diffusivities for Yolo light clay and for a medium sand. These values were obtained from general equations of soil-water diffusivity based on measurements of matric suction head, $\psi$, and unsaturated soil hydraulic conductivity, $K_h$. Jackson et al. (1965) published data on soil-water diffusivity regarding isothermal and temperature dependent conditions for relatively dry loam and silty clay. Gee (1966) provided some experimental data for both isothermal and thermal soil water diffusivity of silt loam. Jury et al.(1974) obtained thermal and isothermal soil-moisture diffusivities for moist sand whose moisture content varied from 20 to 90% of saturation values. Shapiro et al.(1978) evaluated soil-

moisture diffusivities for silt loam using a phenomenological method based upon measured one-dimensional temperature and moisture content profiles. More recently Evgin and Svec (1988) obtained thermal and moisture transfer characteristics for compacted silt using a dual gamma-ray scanner.

### 3.4.2.1 Isothermal Moisture Diffusivity

Unfrozen Soils

There are only four sets of available experimental data regarding isothermal moisture diffusivity in liquid and vapor form, for the following soils: medium sand, silt loam, compact silt , and clay loam.

Jury and Miller (1974) published some experimental data regarding isothermal moisture diffusivity for a medium sand. This data is extremely difficult to approximate therefore a polynomial fit is used:

$$0 \le \theta \le 0.03$$

$$D_\theta = 4.844*10^{-17} + 12.38\,\theta + 2.5228*10^{4}\,\theta^2 + 1.1396*10^{6}\,\theta^3 - 6.4425*10^{7}\,\theta^4 \qquad (3 - 16a)$$

$$0.03 < \theta \le 0.056$$

$$D_\theta = -126.82 + 1.2251*10^{4}\,\theta - 4.1497*10^{5}\,\theta^2 + 5.7417*10^{6}\,\theta^3 - 2.5445*10^{7}\,\theta^4 \qquad (3 - 16b)$$

$$0.056 < \theta \le 0.180$$

$$D_\theta = -1710.8 + 7.1682*10^{4}\,\theta - 1.0487*10^{6}\,\theta^2 + 6.4552*10^{6}\,\theta^3 - 1.3462*10^{7}\,\theta^4 \qquad (3 - 16c)$$

$$0.180 < \theta \le 0.219$$

$$D_\theta = -1.497\,!0^{5} + 2.3082*10^{6}\,\theta - 1.1748*10^{7}\,\theta^2 + 1.9822*10^{7}\,\theta^3 \qquad (3 - 16d)$$

$$0.219 < \theta \leq 0.35$$

$$D_\theta = 2.0051 * 10^6 - 3.8129 * 10^7 \theta + 2.8823 * 10^8 \theta^2 - 1.0816 * 10^9 \theta^3 + 2.0126 * 10^9 \theta^4 - 1.4832 * 10^9 \theta^5 \qquad (3 - 16e)$$

Gee (1966) measured the total isothermal moisture diffusivity ($cm^2$/day) for silt-loam and his data can be approximated by the following polynomial.

$$D_\theta = |-426.55 + 2.9589 * 10^4 \theta - 5.2695 * 10^5 \theta^2 + 3.6079 * 10^6 \theta^3 - 1.0428 * 10^7 \theta^4 + 1.0903 * 10^7 \theta^5| \qquad (3 - 17)$$

The experimental values of soil isothermal diffusivity obtained by Jury and Miller (1974) for sand, Gee (1966) for silt loam, and Evgin and Svec (1988) for compact silt are summarized in Fig. 3.2.

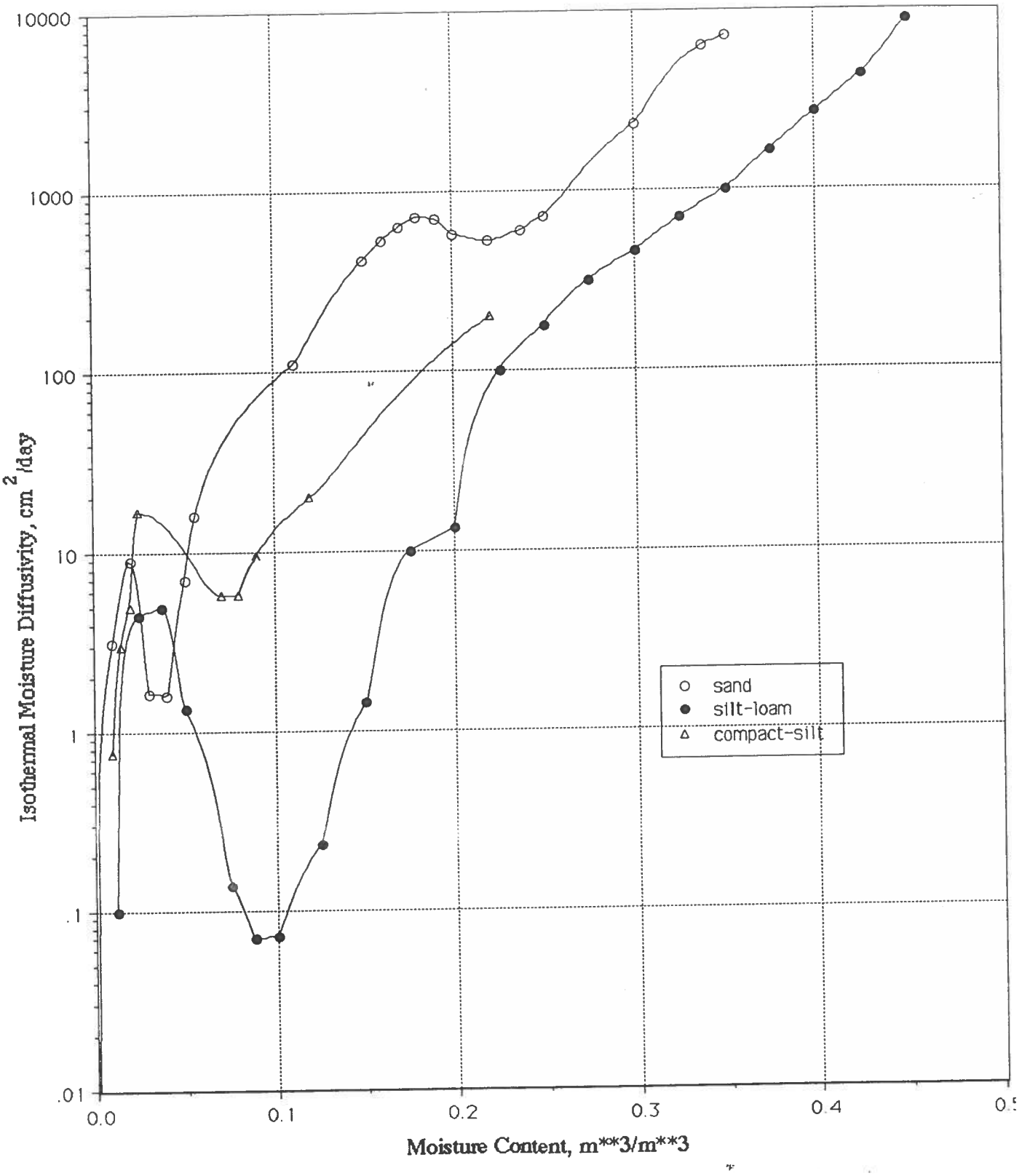


Fig. 3.2 Isothermal moisture diffusivity vs. volumetric water content

As one can see, the available data regarding liquid and vapor isothermal diffusivity is basically for four types of soils and this imposes a serious limitation on computer simulation of ground heat storage containing various soil layers. Therefore, in this report, the isothermal moisture diffusivity is calculated according to the Philip - de Vries model assuming that $\psi$ and $K_h$ are known as functions of volumetric water content $\theta$.

The isothermal soil moisture diffusivity function for a liquid flux is defined by the equation.

$$D_{\theta l} = - K_h \frac{\partial \psi}{\partial \theta} \qquad (3 - 18)$$

Experimental values of soil water suction head, $\psi$, and hydraulic conductivity, $K_h$, for 11 different soil textures, can be obtained from the data published by Clapp and Hornberger (1978). They suggest the standardized relations for $K_h(\theta)$ and $\psi(\theta)$ so that a change in soil type would only require substitution of the empirical parameters. Standardized relations used by Clapp and Hornberger (1978) have the following form:

$$\psi(\theta) = \psi_s \left(\frac{\theta}{\theta_s}\right)^{-b} \qquad 0<\theta \le \theta_x = 0.92\ \theta_s \qquad (3 - 19)$$

$$K_h(\theta) = K_s \left(\frac{\theta}{\theta_s}\right)^{2b+3} \qquad 0<\theta \le \theta_s \qquad (3 - 20)$$

where b, $\theta_s$, $\psi_s$ and $K_s$ are the empirical parameters to be specified [Clapp and Hornberger (1978); Campbell (1985)].

The use of Eq.(3 - 19 ) however, leads to a sharp discontinuity in soil water suction head close to the saturation state. Therefore this equation is modified to account for air entry potential. Following de Jong (1982) a moisture content $\theta_x = 0.92\ \theta_s$ is selected, and a quadratic relation for $\psi$ is assumed between $\theta_x$ and $\theta_s$.

$$\psi(\theta) = - a_0 \left(\frac{\theta}{\theta_s} - a_1\right) + \left(\frac{\theta}{\theta_s} - 1\right) \qquad \theta_x < \theta \leq \theta_s \qquad (3-21)$$

where

$$a_0 = \frac{\psi_x}{\left(1 - \frac{\theta_x}{\theta_s}\right)^2} - \frac{\psi_x}{\frac{\theta_x}{\theta_s}\left(1 - \frac{\theta_x}{\theta_s}\right)} b$$

$$a_1 = 2\frac{\theta_x}{\theta_s} - \frac{\psi_x}{\frac{\theta_x}{\theta_s} a_0} b - 1$$

The relation for the matric potential of the Yolo light clay was provided by Haverkamp et al. (1979) and had the following form:

$$\theta = 0.124 + \frac{274.2}{739 + \ln(-\psi)^4} \qquad (3-22)$$

where: $\psi$ = matric potential (cm)

After simple rearrangements the following relations for isothermal liquid moisture diffusivity are obtained.

$$D_{\theta l} = b\, K_{hs}\, \psi_s\, \theta_s^{-b-3}\, \theta^{b+2} \qquad 0 < \theta \leq \theta_x = 0.92\, \theta_s \qquad (3-23)$$

$$D_{\theta l} = a_0\, K_{hs} \frac{\theta^{2b+4}}{\theta_s^{2b+5}} \left[2 - \frac{\theta_s}{\theta}(a_1 + 1)\right] \qquad \theta_x < \theta \leq \theta_s \qquad (3-24)$$

The average values of b, $\theta_s$, $\psi_s$ and $K_s$ for 11 textural groups are presented by Clapp and Hornberger (1978) and are shown in Table 3.3. A large standard deviation of the $\psi_s$ for each soil textural group, was however obtained. Therefore they suggested the use of the geometric mean i.e. $\psi_s$ (log).

Table 3.3 Representative Values of Soil Hydraulic Parameters *

| Soil Texture | Mean Clay Fraction | b | $\psi_s$ (log) | $\theta_s$ | $K_s$ |
|---|---|---|---|---|---|
| Sand | 0.03 | 4.05 | 3.50 | 0.385 | 1.056 |
| Loamy sand | 0.06 | 4.38 | 1.78 | 0.410 | 0.938 |
| Sandy loam | 0.09 | 4.90 | 7.18 | 0.435 | 0.208 |
| Silt loam | 0.14 | 5.30 | 56.6 | 0.485 | 0.0432 |
| Loam | 0.19 | 5.39 | 14.6 | 0.451 | 0.0417 |
| Sandy clay loam | 0.28 | 7.12 | 8.63 | 0.420 | 0.0378 |
| Silty clay loam | 0.34 | 7.75 | 14.6 | 0.477 | 0.0102 |
| Clay loam | 0.34 | 8.52 | 36.1 | 0.476 | 0.0147 |
| Sandy clay | 0.43 | 10.4 | 6.16 | 0.426 | 0.0130 |
| Silty clay | 0.49 | 10.4 | 17.4 | 0.492 | 0.0062 |
| Clay | 0.63 | 11.4 | 18.6 | 0.482 | 0.0077 |

* Data reported by Clapp and Hornberger (1978)

The isothermal soil moisture diffusivity function for a vapor flux is defined by the following equation developed by Philip and de Vries (1957).

$$D_{\theta v} = f(\theta_a)\, D\, \frac{p}{p - p_v}\, \frac{g}{R_v\, T_v}\, \frac{\rho_v}{\rho_l}\, \frac{\partial \psi}{\partial \theta_l} \qquad (3-25)$$

where:

$f(\theta_a) = \theta_a + \theta_l = PO$ for $\theta_l \le \theta_{lk}$

$f(\theta_a) = \theta_a + \theta_a \dfrac{PO - \theta_a}{PO - \theta_{lk}}$ for $\theta_l > \theta_{lk}$

$D = 21.7 * 10^{-6} \dfrac{p}{p_o} \left[ \dfrac{T}{T_o} \right]^{1.88}$ $(m^2/s)$

$R_v$ = 0.4615 (kJ/kg K)

$g$ = 9.81 ($m/s^2$)

$\rho_v = 6.0957 * 10^{-3} * 10^{2.1747 * 10^{-2}Tvc}$

$\rho_l \approx 1000$ $kg/m^3$

$\frac{\partial \psi}{\partial \theta_l}$ = ... Eqs. (3 - 18) and (3 - 20)

Walker et al. (1981) found that $\theta_{lk}$ was best equated to: 0.25*PO for soils with high clay contents, and 0.125*PO for very sandy soils. To evaluate this value for any soil texture the following weighted relation is used in this report .

$$\theta_{lk} = m_{cl} * 0.25 + m_{si} * 0.1875 + m_{sa} * 0.125 \qquad (3 - 26)$$

where: $m_{cl}$, $m_{si}$ ,$m_{sa}$ = mass fractions of clay, silt,and sand respectively

Thus numerical values of isothermal soil moisture diffusivity for various soils are calculated from the Eqs: (3 - 23), (3 - 24), (3 - 25), using soil parameters $K_h(\theta)$ and $\psi(\theta)$ given by Clapp and Hornberger (1978). The relation of total isothermal soil moisture diffusivity $D_\theta$ vs. volumetric moisture content, for selected soils, are shown in Figures 3.3, 3.4, and 3.5.

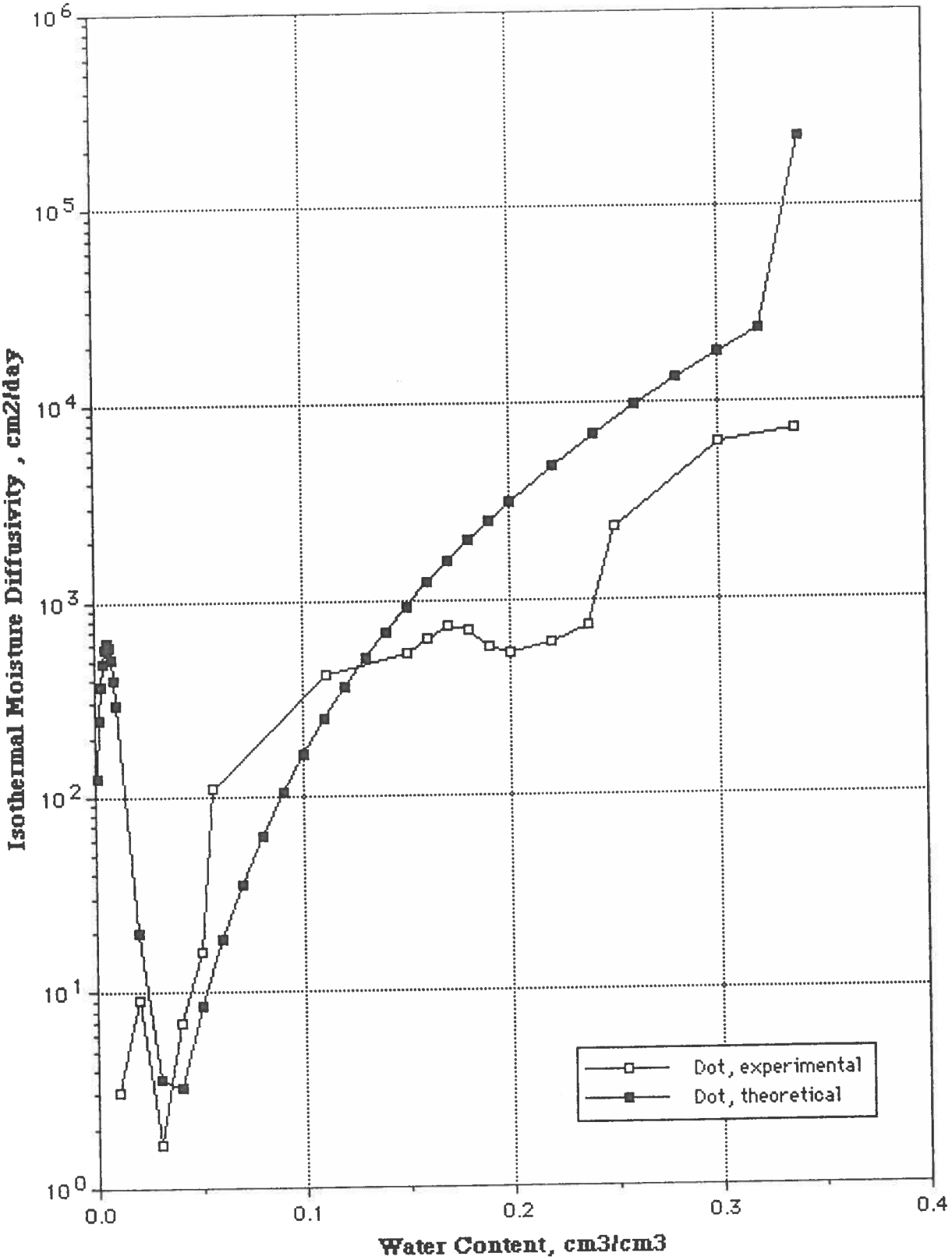


Fig. 3.3 Isothermal soil moisture diffusivity of sand vs. volumetric water content.

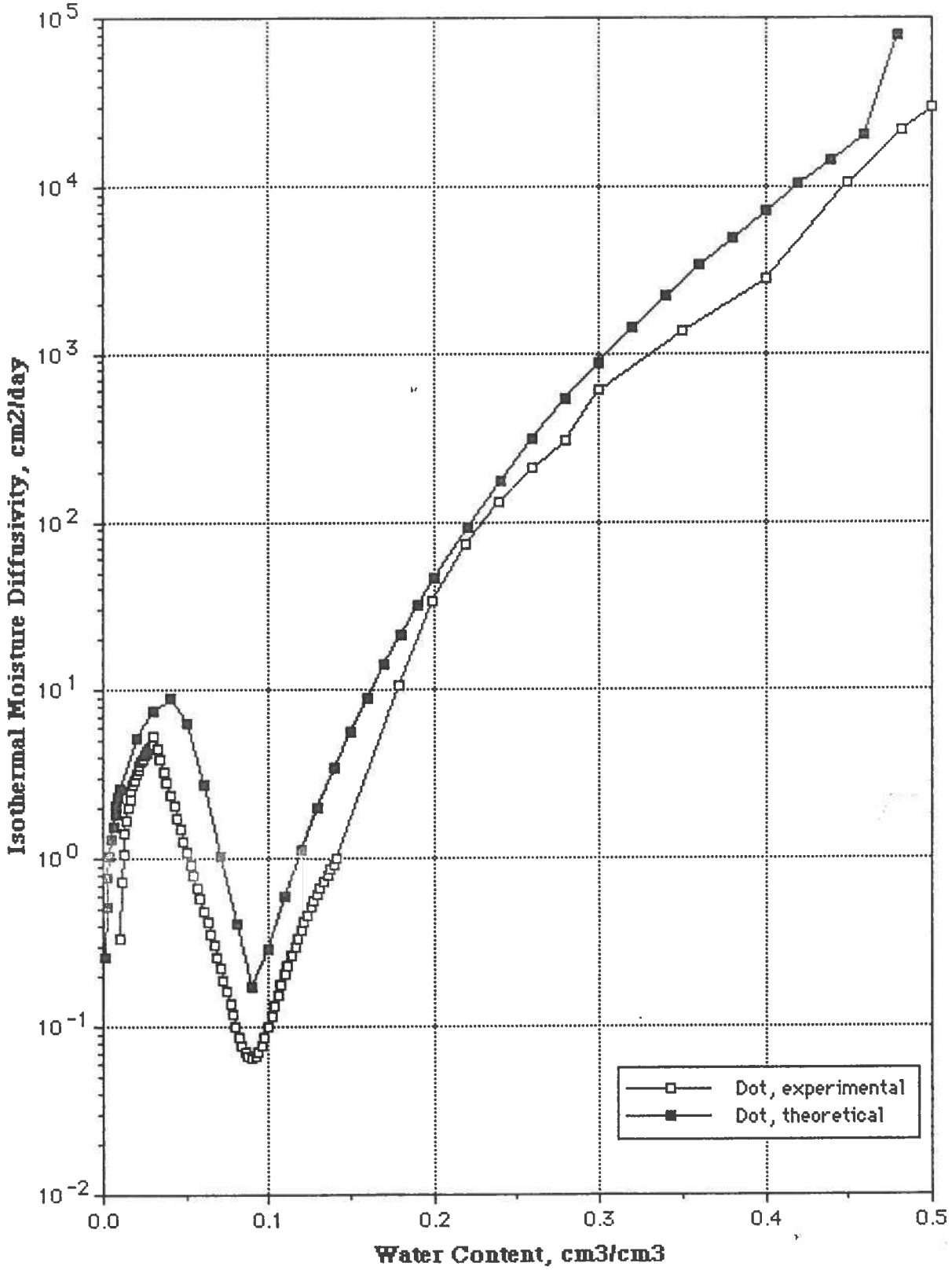


Fig. 3.4 Isothermal soil moisture diffusivity of silt vs. volumetric water content.

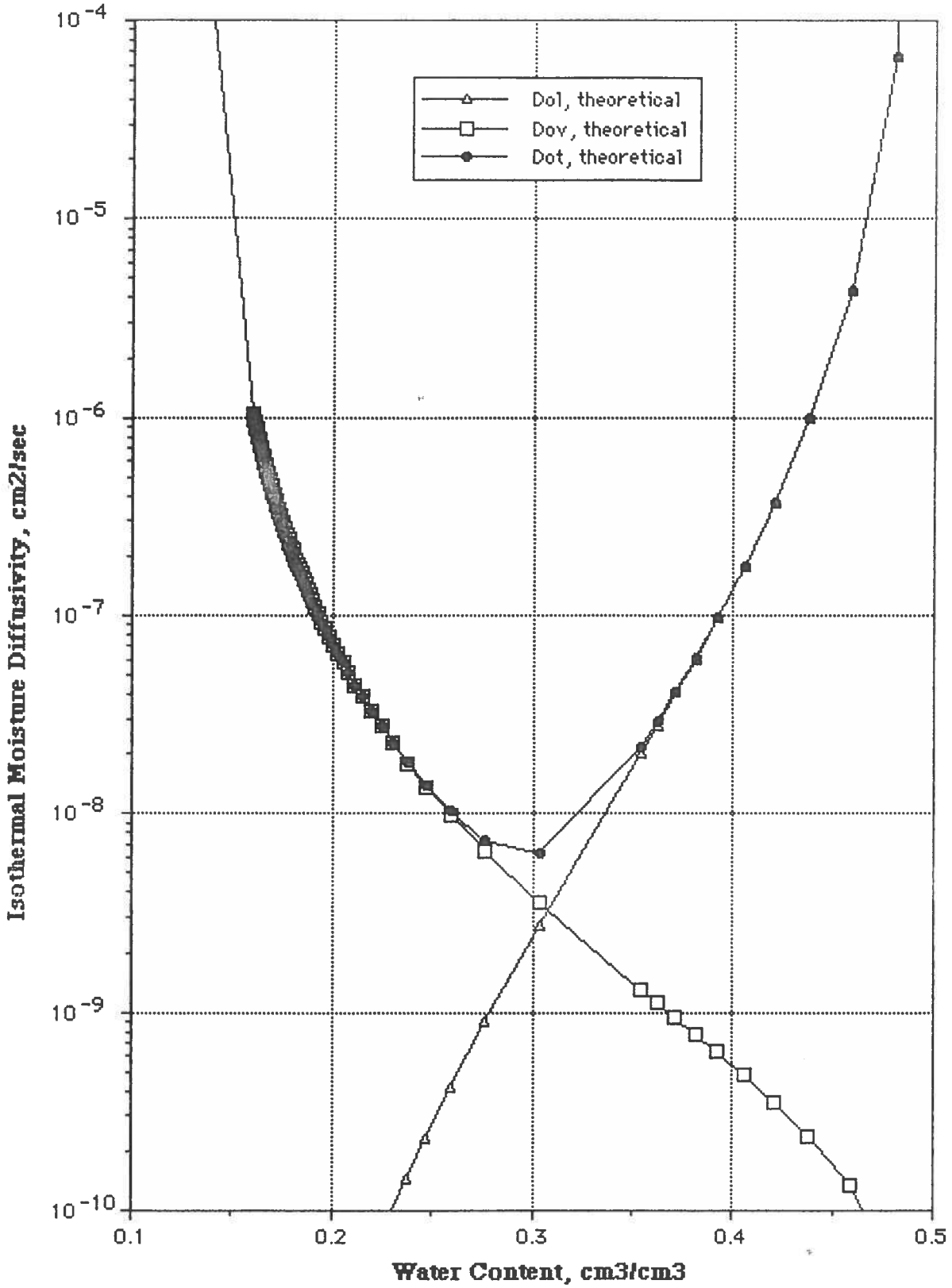


Fig. 3.5 Isothermal soil moisture diffusivity of Yolo light clay vs. volumetric water content.

3.4.2.2 Thermal Moisture Diffusivity

Unfrozen Soils

As in the case of isothermal moisture diffusivity, the experimental data on thermal moisture diffusivity, in liquid and vapor form, is very scarce and that available is only for: medium sand, silt loam, compact silt , and clay loam.

Jury and Miller (1974) provided some experimental data regarding thermal moisture diffusivity ($cm^2/day°C$) for a medium sand. Equations describing this moisture transport coefficient have the following form:

$0 \le \theta \le 0.1$

$$D_T = 1.2072 * 10^{-2} * 10^{10.642\theta} \qquad (3 - 27a)$$

$0.1 \le \theta < 0.35$

$$D_T = 8.5486 * 10^{-2} * 10^{7.5689\theta} \qquad (3 - 27b)$$

The approximation of Gee's (1966) experimental data for silt-loam ($cm^2/day°C$) has the following form:

$0.025 \le \theta \le 0.30$

$$D_T = -4.0591 * 10^{-2} + 2.9668\,\theta - 46.877\,\theta^2 + 349.4\,\theta^3 - 1232.2\,\theta^4 + 1646.3\,\theta^5 \qquad (3 - 28a)$$

$0.3 < \theta \le 0.45$

$$D_T = 1.865 * 10^{-5} * 10^{12.394\theta} \qquad (3 - 28b)$$

Experimental values of soil thermal diffusivity obtained by Jury and Miller (1974) for sand, Gee (1966) for silt loam, Evgin and Svec (1988) for compact silt, and Philip and de Vries (1957) for clay loam are summarized in Fig. 3.6.

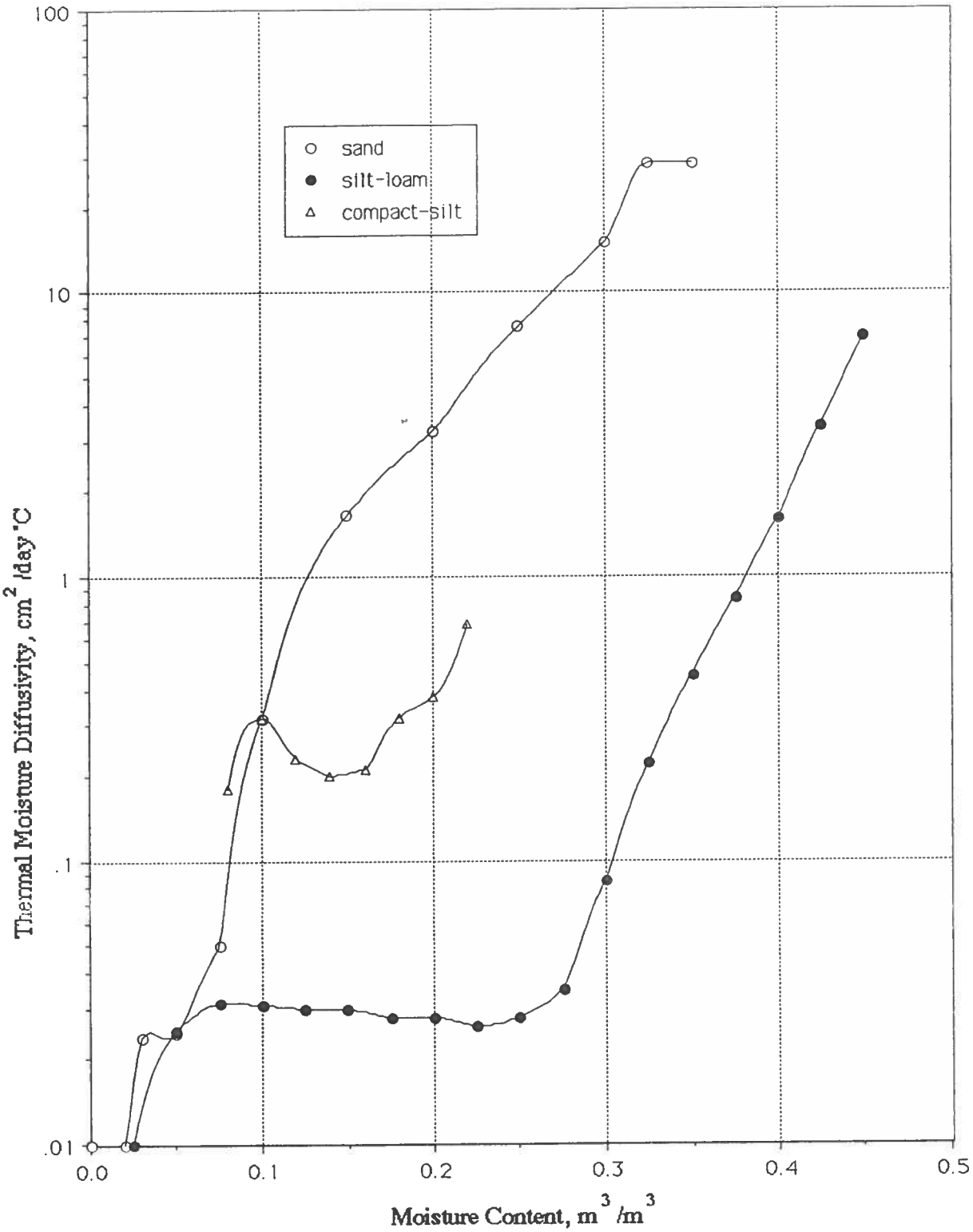


Fig. 3.6 Thermal moisture diffusivity as a function of volumetric water content

The available data regarding liquid and vapor thermal diffusivity is only for four types of soils and therefore in this report this relation is calculated according to the Philip - de Vries model assuming that $\psi$ and $K_h$ are known as functions of volumetric water content $\theta$.

In general the thermal soil moisture diffusivity for a liquid flux is defined by the following equation [de Vries (1958)] .

$$D_{Tl} = - K_h \frac{1}{\sigma} \frac{d\sigma}{dT} \psi \qquad (3 - 29)$$

where: $K_h$ = hydraulic conductivity of unsaturated soil - Eq. (3 - 19)

$\sigma$ = surface tension of water against air ($\sigma = 0.076217 - 0.00016985\ T$) [N/m]

$T$ = temperature of water (° C)

$\psi$ = matric suction head

Taking into account a gradual air entry in the soil region near saturation, the following expressions for thermal moisture diffusivity in liquid form are obtained.

$$D_{Tl} = - K_{hs} \psi_s \sigma^{-1} \frac{d\sigma}{dT} \left[\frac{\theta}{\theta_s}\right]^{b+3} \qquad 0<\theta \le \theta_x = 0.92\ \theta_s \quad (3 - 30)$$

$$D_{Tl} = - K_{hs} a_0 \sigma^{-1} \frac{d\sigma}{dT} \left(\frac{\theta}{\theta_s} - a_1\right)\left(\frac{\theta}{\theta_s} - 1\right)\left(\frac{\theta}{\theta_s}\right)^{2b+3} \qquad \theta_x<\theta \le \theta_s \quad (3 - 31)$$

where: $a_0, a_1$ = coefficients of Eq.(3 - 20)

$\psi_s$ = saturation suction

$\frac{d\sigma}{dT}$ = $- 1.6985 * 10^{-4}$

$\theta_s$ = saturated water content

$b$ = empirical constant

Thus values of $D_{Tl}$ for 11 different soil textures can be calculated on the basis of experimental data provided by Clapp and Hornberger (1978) or empirical equations published by Campbell (1985).

The thermal soil moisture diffusivity for a vapor flux is defined by the following equation [de Vries (1958)].

$$D_{\theta v} = f(\theta_a)\, D \frac{p}{p - p^v} \frac{\rho v}{\rho l} \frac{\zeta}{p_{vs}} \frac{\partial p_{vs}}{\partial T} \qquad (3 - 32)$$

where: $\zeta = \frac{(\nabla T)_a}{\nabla T}$ $\frac{\text{the average temperature gradient in the air-filled pores}}{\text{overall temperature gradient}}$

For soils such as: sandy soils $\zeta \approx 2.37$; silty soils $\zeta \approx 1.78$; clayey soils $\zeta \approx 1.46$

For any soil texture the following weighted relation is used:

$$\zeta = 1.46\, m_{cl} + 1.78\, m_{si} + 2.37\, m_{sa}$$

$p_{vs}$ = partial pressure of saturated water vapor ($= 0.73848 * 10^{2.3867 * 10^{-2} T}$)

$$\frac{\partial p_{vs}}{\partial T} = 0.040583758 * 10^{0.023867\, T}$$

The total values of isothermal soil moisture diffusivity $D_T$ vs. volumetric moisture content, for selected soils, are shown in Figures 3.7, 3.8, and 3.9.

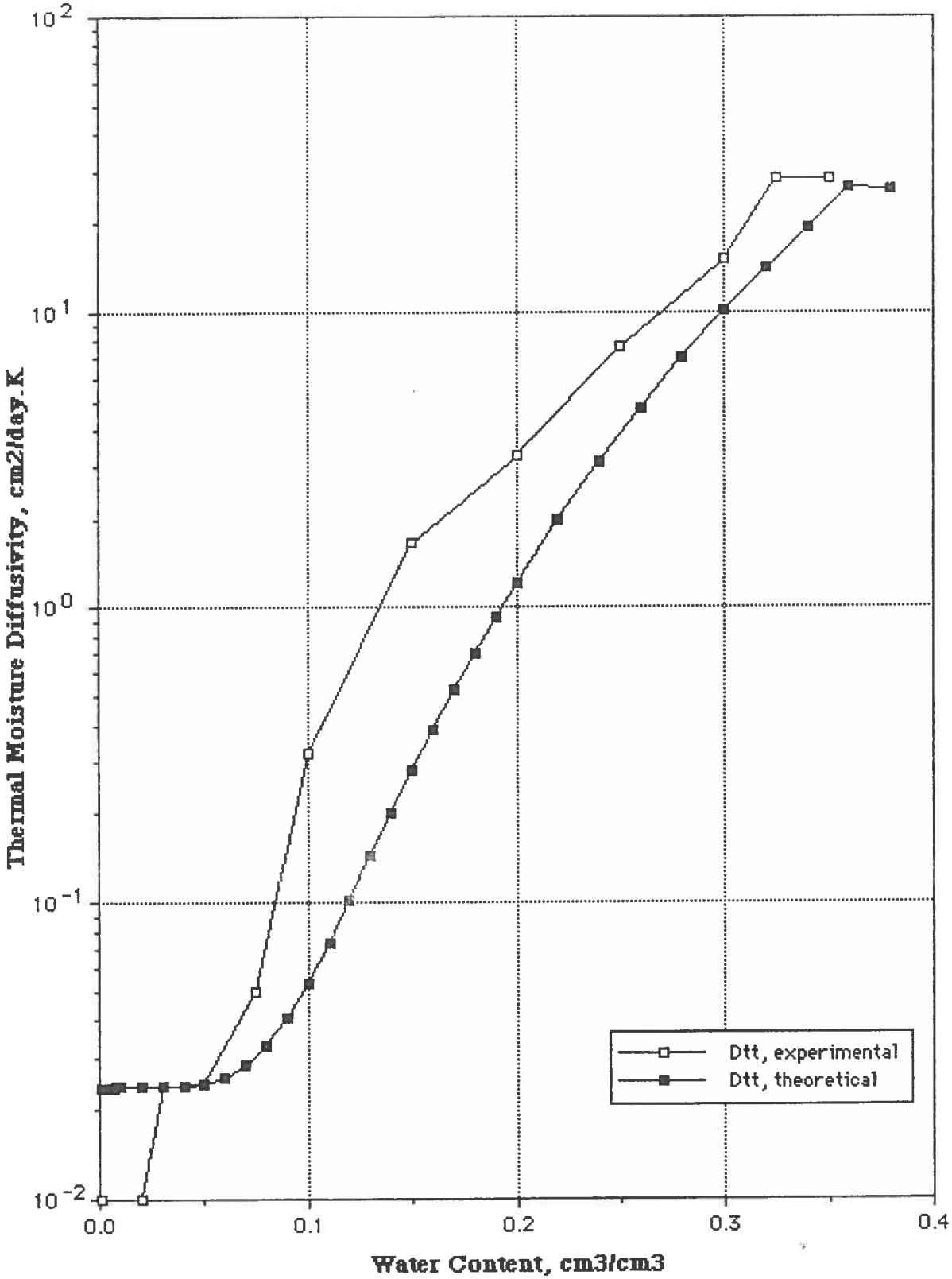


Fig. 3.7 Thermal soil moisture diffusivity of sand vs. volumetric water content.

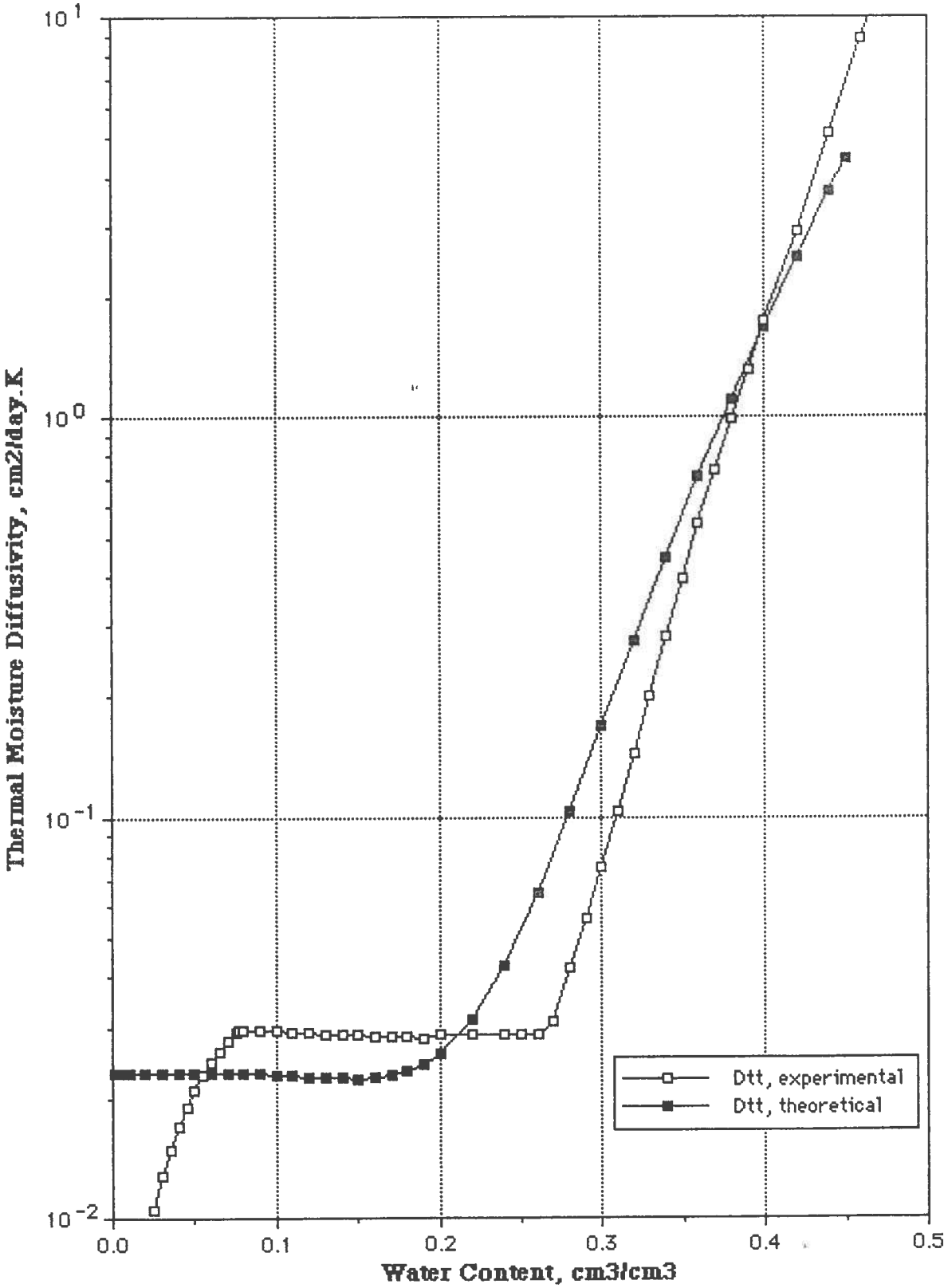


Fig. 3.8 Thermal soil moisture diffusivity of silt vs. volumetric water content.

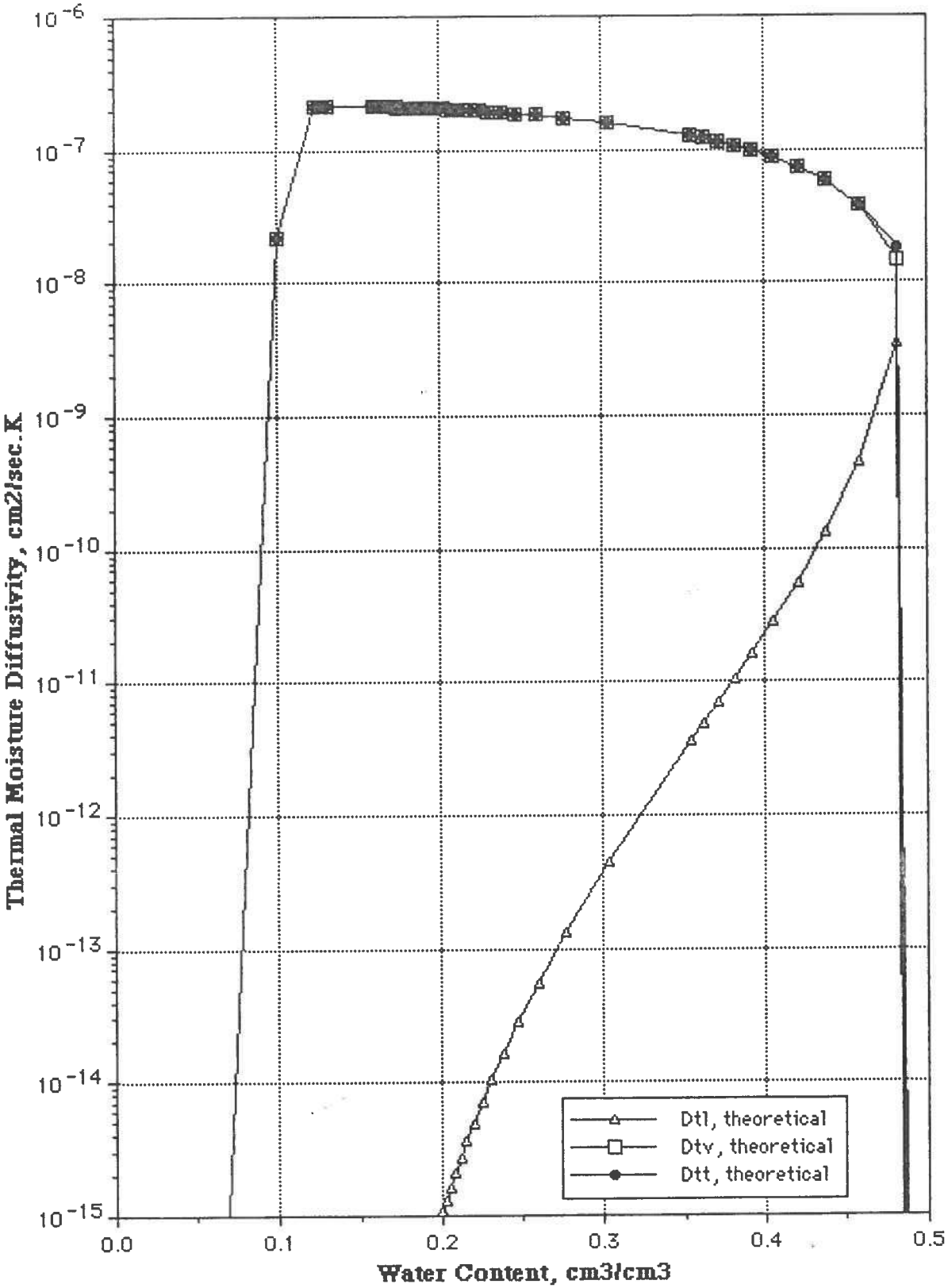


Fig. 3.9 Thermal soil moisture diffusivity of Yolo light clay vs. volumetric water content.

### 3.4.2.3 Soil Water Diffusivity Model - Summary

In previous sections it was shown that modelling soil water diffusivity, for soil conditions with and without the presence of a thermal gradient, could be achieved using equations derived by Philip and de Vries (1957) and experimental data provided for various soils by Clapp and Hornberger (1979), and Campbell (1985).

Calculated results of the isothermal diffusivity of soil moisture in a liquid form conform rather well to results published by other researchers. As far as soil moisture flow in vapor form is concerned calculated results show the same increasing trend but only within the range of $0.5\theta_{lk} < \theta < \theta_{lk}$. Below that there is a further increase in calculated values whereas the experimental ones decline to zero. The calculated results could be greatly improved if different values of power coefficient b were used above and below critical volumetric moisture content, $\theta_{lk}$. Unfortunately, the available experimental data on isothermal soil moisture diffusivity, which allows the right selection of b for the soil moisture content range where liquid continuity does not exist, is very limited.

Regarding thermal soil moisture diffusivity, the agreement between calculated results and experimental data was found to be satisfactory in almost the whole range of volumetric moisture content, with one exception at $\theta < \theta_{lk}$ where experimental results tend to be zero whereas calculated ones tend to be constant.

Bearing this in mind the following model of soil moisture diffusivity is used in this report:

Isothermal Diffusivity

For $\theta_{lk} \leq \theta < \theta_s$

$D_\theta = D_{\theta l} + D_{\theta v}$ ( Philip-deVries model + Campbell empirical equations)

For $0.5\ \theta_{lk} \leq \theta < \theta_{lk}$

$D_\theta = (D_\theta)_{\theta_{lk}}$ ( Philip-deVries model + Campbell empirical equations)

For $0 \le \theta < 0.5\ \theta_{lk}$

$D_\theta = 0$

Thermal Diffusivity

For $0.5\ \theta_{lk} \le \theta < \theta_s$

$D_T = D_{Tl} + D_{Tv}$ ( Philip-deVries model + Campbell empirical equations)

For $0 \le \theta < 0.5\ \theta_{lk}$

$D_T = 0$

### 3.4.2.4 Thermal and Isothermal Moisture Diffusivity of Freezing Soils

According to Harlan (1973), water migration in frozen and unfrozen soil under isothermal conditions is about the same when the liquid water contents are the same. He regards moisture migration in a vapor form as negligible and mass transport involves only liquid flow. A numerical simulation based on this analogy did not correspond with experimental data (Taylor and Luthin, 1978; Jame, 1978). In order to obtain a consensus between their experimental data (Jame, 1978; Burt and Williams 1976), and Harlan's model, an impedance factor was introduced to decrease the diffusivity of moisture by a magnitude order of two to three.

$$D_{pf} = \frac{D_\theta}{I} \qquad (3 - 33)$$

where: $D_\theta$ = isothermal moisture diffusivity in unfrozen soil, $m^2/s$

$I$ = impedance factor, $10^{10\theta_I}$

$\theta_I$ = volumetric ice content, $m^3/m^3$

The diffusivity relationship, $D_\theta$, for silt - loam was given by Dirksen and Miller (1966).

$$D_\theta = 9.4 * 10^{-5} * 10^{5.88\theta - 10\theta_I} \qquad (3 - 34)$$

## 3.5 Thermo - Physical Properties of Snow

The presence of snow cover on the surface of the ground heat storage strongly effects the temperature conditions in the soil. Snow protects the ground from freezing in winter but it also increases the soil moisture content in summer, thus contributing to lower summer ground temperatures. The cover of snow protects the soil to a great extent from excessive heat losses during the winter mainly due to the low thermal conductivity of snow (averages less than 0.1 of that of compact soil), and the very high value of snow albedo. This is one of the reasons that the soil temperature in winter is considerably higher than that of the ambient air and is dependent upon the thickness and thermal properties of snow.

The thermo-physical properties of snow are very difficult to measure since snow undergoes constant metamorphism as soon it falls to the ground. The morphological changes in snow are, (according to Snow Hydrology, 1956) caused by: heat exchange, compaction due to its own weight, mass flux in snow cover, wind, and temperature and water vapor variations within the snowpack.

The density of new snow increases approximately from 50 $kg/m^3$ when falling at an ambient temperature of -8 °C to 125 $kg/m^3$ when falling at 0 °C (Raudkivi, 1979).The density variation caused by wind can exceed the initial value by as much as five times. The snowpack density generally increases with depth. In packs several meters deep the lower half may have densities of 350 - 400 $kg/m^3$, while in the younger surface layers the densities may be only 70 - 100 $kg/m^3$ . With time, the snowpack tends to become more homogeneous and it finally reaches the "ripe" state i.e., it can not hold more liquid water against gravity.

The insulating effect of snow mainly depends on its thermal conductivity. Many researchers have expressed this parameter as a function of the bulk density of snow. Yen (1981) gave a excellent

survey of most of the available empirical formulae and in his opinion the effective thermal conductivity of snow can be obtained from the following expression.

$$K_{sn} = 2.213 * 10^{-6} \rho_{bs}^{1.885} \qquad (3 - 35)$$

where: $K_{sn}$ = effective thermal conductivity of snow, W/m K

$\rho_{bs}$ = bulk density of snow, kg/m$^3$

It is worth mentioning that this expression does not specify snow temperature ranges. Snow temperature may have a noticeable effect on effective thermal conductivity. According to Pitman and Zuckermann (1967) the thermal conductivity of snow decreases with decreasing snow temperature and and can be approximated as follows.

$$K_{sn} = 0.0688 \exp(0.0088\, T_{sn} + 0.0046682\, \rho_{bs}) \qquad (3 - 26)$$

where: $T_{sn}$ = temperature of snow, °C

This equation is valid in the snow density range of 100 to 600 kg/m$^3$ . The specific heat of snow has the same value as the specific heat of ice, i.e. 2.12 kJ/kg/K. The latent heat of snow is also identical to that of ice. Precise values for the latent heat of fusion, $L_f$, and sublimation, $L_{sub}$ ,of pure ice at 0 °C used in this report are 333.5 kJ/kg and 2838 kJ/kg respectively.

## 3.6 Geological and Hydrogeological Aspects

Geological and hydrogeological information about the site is of a great importance in the design of ground heat storage. It is recommended that proper geotechnical site investigation be carried out i.e. soil sampling, and laboratory testing [Porsvig (1983)] before any final design is made. The following characteristics of the ground should be examined before any decision regarding selection

of the ground coupled heating/cooling system is made: soil strata, ground water table, soil infiltration.

A good knowledge on the ground strata is required in order to use right soil thermal and mass transport characteristics describing simultaneous heat and moisture movement in the vicinity of the GHE caused by heat extraction or deposition to the ground. The soil characteristics listed above have a strong influence on the performance of the GHE, therefore refilling of a coil trench with a better soil may be necessary.

The presence of ground water at the site can be a key factor for selecting the heat source i.e., ground water or soil. If the ground water flow is rather small and not causing any soil temperature drop, a closed-loop system is recommended. If the ground water flow is excessive there is a good possibility for applying an open loop system where the ground water itself is a source of heat. Regardless of what kind of system is selected the following information should be known and considered in the design process if a firm dimensioning of ground heat storage is to be made: variations of a ground water table over a one year period, temperature of the ground water over a one year period, and the direction of the ground water flow. The presence of ground water in soil surrounding the horizontal GHE is very beneficial during the heating and cooling modes of operation. As far as heat extraction from the ground is concerned freezing of soil water leads to utilization of a huge amount of latent heat from the fusion of water and considerable improvement of soil thermal characteristics. When heat is rejected to the ground the presence of soil water around the GHE keeps up its performance since soil thermal characteristics do not change.

Soil infiltration is the term applied to the process of water entry into soil by downward flow from the soil surface or upward flow from a high water table. Good hydraulic properties of soil between the coil and a ground surface will speed up soil moisture content increase due to external precipitation such as rain or snow.

This in turn will improve soil thermal characteristics and the performance of the GHE. The knowledge of site topography is also important in order to select a runoff case (sloping terrain) or ponding case (valley or flat terrain)

The mathematical model being developed takes into account all the geological factors discussed above.

# 4. HEAT AND MOISTURE FLOW IN GROUND HEAT STORAGE

This chapter deals with the various aspects of energy and mass exchange in ground heat storage and at the soil-air interface.

## 4.1 Heat and Moisture Transfer in Unfrozen Soils

Three different approaches were developed in the past for the analysis of the relationship between soil moisture migration and heat flow in soils.

The first approach postulated by Philip and de Vries (1958) is a mechanistic one which employs the concept of fluid mechanics and heat conduction. The effects of liquid migration by capillarity and vapor diffusion, due to temperature gradients, are combined into a dynamic mass balance equation. The heat flux is described in terms of conduction, latent heat transport, and sensible heat flow. A thermal energy balance equation together with a mass balance of one describes the coupled heat and moisture flow in a soil system. The final model contains a set of transient simultaneous partial differential equations containing many soil parameters which are not easily available.

The second approach to this problem is based on the use of the thermodynamics of irreversible processes. This model was formulated first by Taylor and Cary (1964). This approach is more general than the first one as it incorporates several driving forces other than pressure or temperature gradients. However, there are serious difficulties in obtaining the transport coefficients of the partial differential equations describing heat and moisture migration in soils.

Finally Luikov (1966), applying the theory of the thermodynamics of irreversible processes, derived a coupled system of partial differential equations representing simultaneous heat and mass transfer in porous bodies. The thermal -and transport characteristics of various porous materials were determined experimentally to verify the model.

In this report the modified de Vries model is used to formulate the problem of simultaneous heat and moisture flow in unfrozen soils.

General assumptions

The following, more important, limitations and assumptions are applied to the Philip-de Vries model (de Vries , 1987):

1. The soil is unsaturated, homogeneous and isotropic in a macroscopic sense,
2. Soil mass transport and thermal characteristics are non-hysteretic,
3. The phenomena of boiling, freezing, and thawing are not included,
4. The model does not apply when the matrix is not rigid,
5. The liquid in soils has the proprties of pure bulk water,
6. Liquid movement is driven by capillary and adsorptive forces,
7. Vapor movement is by diffusion in the gas-filled pores,
8. Free convection in the gas phase can be neglected,
9. Heat transfer by radiation is negligible,
10. The temperature dependence of $\rho_l$, c, K and L is neglected.

In general capillary forces (matrix potential) can be expressed in two ways i.e., as a gradient of volumetric moisture content, $\theta$, or as a capillary head, $\psi$.

The volumetric moisture content approach leads to a nonlinear diffusion equation and is valid only for homogeneous and unsaturated soils. If the pressure head is used as the driving force, the model can be extended from unsaturated to saturated soil conditions, and to multi-layer systems [Sophocleous, 1979; Milly, 1982]. This approach has been succesfully applied only to one-dimensional soil systems. However, the numerical solution of that model extended for more complex systems (two -or three dimensional) can be more difficult to obtain since it often leads to a

stiff system of highly nonlinear equations. Therefore the modified Philip-de Vries model, based on the volumetric moisture content approach, is used in this report.

Moisture Transfer

Nonisothermal mass transfer in an unsaturated soil takes place in both the liquid and vapor phases, in response to both a volumetric moisture content and a temperature gradient, de Vries (1958). This behavior can be described mathematically by Eq. (4.1) and (4.2), which are for liquid and vapor transfer in an unsaturated soil.

$$\frac{q_l}{\rho_l} = -D_{\theta l}\nabla\theta_l - D_{Tl}\nabla T - K_h\nabla y \qquad (4-1)$$

$$\frac{q_v}{\rho_l} = -D_{\theta v}\nabla\theta_v - D_{Tv}\nabla T \qquad (4-2)$$

The total moisture flux density, $q_m$, in unsaturated soils is the sum of the liquid flux, $q_l$, and vapor flux, $q_v$, and can be written as follows:

$$\frac{q_m}{\rho_l} = \frac{q_l}{\rho_l} + \frac{q_v}{\rho_l} = -D_\theta\nabla\theta - D_T\nabla T - K_h\nabla y \qquad (4-3)$$

where $q_m$ = total moisture flux density

$q_l$ = liquid flux density

$q_v$ = vapor flux density

$D_{\theta l}$ = isothermal liquid diffusivity

$D_{Tl}$ = thermal liquid diffusivity

$D_{\theta v}$ = isothermal vapor diffusivity

$D_{Tv}$ = thermal vapor diffusivity

$D_\theta$ = isothermal moisture diffusivity, $D_\theta = D_{\theta l} + D_{\theta v}$

$D_T$ = thermal moisture diffusivity, $D_T = D_{Tl} + D_{Tv}$

$\theta_l$ = volumetric liquid content

$\theta_v$ = volumetric vapor content

$\theta$ = total volumetric moisture content, $\theta = \theta_l + \theta_v$

T = temperature

$K_h$ = unsaturated hydraulic conductivity

$\rho_l$ = density of liquid water

y = elevation

The principle of mass conservation applied to the liquid and vapor phases respectively leads to:

$$\frac{\partial \theta_l}{\partial t} = - \nabla \cdot \left( \frac{q_l}{\rho_l} \right) - E \qquad (4 - 4)$$

$$\frac{\partial \theta_v}{\partial t} = - \nabla \cdot \left( \frac{q_v}{\rho_l} \right) + E \qquad (4 - 5)$$

where: E = an evaporation term introduced to represent the source or sink of water as liquid is transferred into vapor

t = time

Liquid and vapor fluxes are additive (de Vries, 1962), therefore the following equation for moisture flow in nonisothermal unsaturated soil is valid:

$$\frac{\partial \theta}{\partial t} = \frac{\partial \theta_l}{\partial t} + \frac{\partial \theta_v}{\partial t} = - \nabla \cdot \left( \frac{q_l}{\rho_l} + \frac{q_v}{\rho_l} \right) = - \nabla \cdot \left( \frac{q_m}{\rho_l} \right) \qquad (4 - 6)$$

and hence

$$\frac{\partial \theta}{\partial t} = \nabla \cdot (D_\theta \nabla \theta_l) + \nabla \cdot (D_T \nabla T) + \frac{\partial K_h}{\partial y} \qquad (4 - 7)$$

where: $\theta$ = total volumetric moisture content

The above equation holds terms containing the soil temperature gradient. The numerical solution of this equation is possible on the condition that an equation describing heat flux in unsaturated soils is known.

Heat Flow

Heat transfer in a soil system can be represented by the following modes: conduction, latent heat due to pressure vapor driven flux, and sensible heat carried by the liquid flux. According to the Philip-de Vries model, the heat flux density in the soil can be written as follows.

$$q = - K \nabla T + C_l ( T - T_O) q_m - L \rho_l D_{\theta v} \theta_v$$

By applying the principle of energy conservation, while ignoring sensible heat transfer and convection effects, the following relation is developed.

$$C \frac{\partial T}{\partial t} + L \rho_l \frac{\partial \theta_v}{\partial t} = \nabla \cdot (K \nabla T) - L \nabla \cdot (q_v) \qquad (4 - 8)$$

where: C = volumetric heat capacity of soil

L = latent heat of vaporization of water

K = thermal conductivity of soil

Substitution of Eq. (4 - 5) into Eq. (4 - 8) yields

$$C \frac{\partial T}{\partial t} = \nabla \cdot (K \nabla T) - L \rho_l E \qquad (4 - 9)$$

According to Luikov (1958) the soil liquid moisture content is dependent on the phase change (pc) of liquid moisture i.e., condensation of vapor or evaporation of liquid and moisture flow due to its migration (m).

$$(\rho_l\theta_l) = (\rho_l\theta_l)_m + (\rho_l\theta_l)_{pc}$$

The total differential change of the soil liquid moisture content has the following form.

$$d(\rho_l\theta_l) = d(\rho_l\theta_l)_m + d(\rho_l\theta_l)_{pc}$$

Denoting that

$$\beta = \frac{d(\rho_l\theta_l)_{pc}}{d(\rho_l\theta_l)_m}$$

the phase conversion factor $\varepsilon$ is introduced

$$\varepsilon = \frac{\beta}{\beta+1} = \frac{d(\rho_l\theta_l)_{pc}}{d(\rho_l\theta_l)} = \frac{D_{\theta v}}{D_{\theta v} + D_{\theta l}} \qquad (4\text{-}10)$$

If $\varepsilon = 1$, then moisture transfer occurs only in vapor form while the transport of liquid is absent. Since the soil moisture content is equal to the liquid content then with $\varepsilon = 1$ a change of soil moisture content occurs due to the evaporation of the liquid or condensation of vapor. If $\varepsilon = 0$, then the moisture content changes only as the result of liquid transfer. In the majority of cases this factor is less than unity . The use of the phase conversion factor therefore enables the evaporation term to be expressed within clearly defined limits as $\varepsilon$ varies from 0 to 1. Following modifications of the de Vries -Philip model made by Thomas (1985) we have:

The rate change in liquid moisture content

$$\frac{\partial}{\partial t}(\rho_l\theta_l) = \frac{\partial}{\partial t}(\rho_l\theta_l)_m + \frac{\partial}{\partial t}(\rho_l\theta_l)_{pc} \qquad (4-11)$$

Substituting the term $\frac{\partial}{\partial t}(\rho_l\theta_l)_{pc}$ from Eq. (4 - 10) into Eq.(4 - 11), after rearranging we have

$$\frac{\partial}{\partial t}(\rho_l\theta_l) = -\nabla \cdot q_l + \varepsilon \frac{\partial}{\partial t}(\rho_l\theta_l) \qquad (4-12)$$

From Eq. (4 - 4), $\frac{\partial}{\partial t}(\rho_l\theta_l)$ may also be expressed as

$$\frac{\partial}{\partial t}(\rho_l\theta_l) = -\nabla \cdot q_l - \rho_l E \qquad (4-13)$$

Comparing the last two equations we have

$$-\rho_l E = \varepsilon \frac{\partial}{\partial t}(\rho_l\theta_l) \qquad (4-14)$$

Substituting this term into Eq. (4 - 9) gives the following

$$C\frac{\partial T}{\partial t} = \nabla \cdot (K\nabla T) + L\varepsilon \frac{\partial}{\partial t}(\rho_l\theta_l) \qquad (4-15)$$

The mass of vapor is usually negligible in comparison with the mass of the liquid and therefore

$$\frac{\partial}{\partial t}(\rho_l\theta_l) \approx \frac{\partial}{\partial t}(\rho_l\theta) \qquad (4-16)$$

The combination of Eqs. (4 - 16) , (4 - 7) and (4 - 15) gives the general form of the governing differential equation for heat transfer in unsaturated soils.

$$C\frac{\partial T}{\partial t} = \nabla \cdot (K + L\varepsilon\rho_l D_T)\nabla T + \nabla \cdot (L\varepsilon\rho_l D_\theta)\nabla\theta_l + L\rho_l \frac{\partial(\varepsilon K_h)}{\partial y} \qquad (4-17)$$

In a similar way by merging Eqs. (4 - 10) and (4 - 7) the governing differential equation for soil moisture transfer is obtained, viz.:

$$\frac{\partial \theta_l}{\partial t} = \nabla \cdot (D_\theta \nabla \theta_l) + \nabla \cdot (D_T \nabla T) + \frac{\partial K_h}{\partial y} \qquad (4\text{-}18)$$

Relations (4 - 17) and (4 - 18) form a coupled set of differential highly nonlinear equations. In order to obtain variations of both T and $\theta_l$ in time and space the numerical solution must be applied. The equations can be written more conveniently as

$$\nabla \cdot (K^* \nabla T) + \nabla \cdot (D_\varepsilon \nabla \theta_l) - C \frac{\partial T}{\partial t} + L\rho_l \frac{\partial (\varepsilon K_h)}{\partial y} = 0 \qquad (4\text{-}19)$$

$$\nabla \cdot (D_T \nabla T) + \nabla \cdot (D_\theta \nabla \theta_l) - \frac{\partial \theta_l}{\partial t} + \frac{\partial K_h}{\partial y} = 0 \qquad (4\text{-}20)$$

where: $K^*$ = apparent thermal conductivity of soil , $K + L\varepsilon\rho_l D_T$

$D_\varepsilon = L\varepsilon\rho_l D_\theta$ (4 - 21)

## 4.2 Soil-Water Phase Change Effects

Heat extraction from the ground by means of the GHE may lead to soil-moisture freezing in the vicinity of the ground coil. This operation usually takes place in the winter and therefore additional soil freezing may also appear close to the ground surface. The soil freezing is characterized by a release of a large amount of latent heat from the fusion of water and soil moisture migration towards a freezing zone which may produce an undesirable phenomenon called frost heaving. The movement of soil due to heave can be so huge that it can easily damage the GHE , lawns, drive-ways, parking lots and other (engineering) structures.

The soil temperature gradient in the winter has an opposite sign to that in the summer, i.e. soil heat flows into the GHE or by flowing upwards to the ground surface is lost to the surrounding air. When the ground is freezing, soil-water migrates, under the influence of the temperature gradient and a moisture sink in the freezing front, from the unfrozen soil region to the freezing interface. Thus, during heat extraction soil moisture content around the GHE is increasing. The moisture migration may be accomplished by the diffusion of water in the form of liquid or vapor phases. The main motive force, a suction gradient, driving soil moisture towards the phase change interface is related by most of the theories to the unfrozen water films in the interface and their coaction with the soil surfaces. According to Koopmans and Miller (1966) the freezing of soil-moisture is analogous to soil drying and thawing and is similar to rewetting, i.e. the ice cristals play a role similar to air pockets in soils. This is a reason that many researchers have developed a theory of heat and moisture transfer in freezing/thawing soils on a basis similar to that proposed by Philip and de Vries (1957).

### 4.2.1 Coupled Heat and Moisture Transport in Freezing/Thawing Soils

Many mathematical models describing the coupled heat and moisture flow in freezing soils have been proposed by numerous researchers over the last two decades. The analogy between moisture transport processes in unsaturated unfrozen soil and freezing soil is in common use. In general two different modeling approaches can be distinguished.

The apparent heat capacity approach assumes that the soil water content in a freezing zone is a function of soil temperature.

$$\theta = \theta\,(T) \qquad T < 0^{\circ}\,C \tag{4 - 22}$$

Soil-water migration in freezing soils is modeled in a manner similar to that used for unsaturated porous systems, i.e. in all of the available models, Darcy's law is assumed to be valid.

$$\frac{\partial \theta_l}{\partial t} + \frac{\rho_I}{\rho_w} \frac{\partial \theta_I}{\partial t} = \nabla \cdot (D_\theta \nabla \theta_l) \qquad (4 - 23)$$

where: $D_\theta$ = isothermal soil moisture diffusivity

$\rho_I$ = density of ice

$\theta_I$ = volumetric ice content

The isothermal soil moisture diffusivity in frozen soil is assumed to be equal to that of the unfrozen soil with the water content equal to the unfrozen water content of the frozen soil. Moisture migration by vapor diffusion is usually assumed to be negligible [Jumikis 1957; Dirksen and Miller 1966; Fuch et al.,1978].

The heat transfer in freezing soils is modeled as follows:

$$C_{pf} \frac{\partial T}{\partial t} - L_f \frac{\rho_I}{\rho_w} \frac{\partial \theta_I}{\partial t} = \nabla \cdot (K_{pf} \nabla T) \qquad (4 - 24)$$

where: $C_{pf}$ = volumetric heat capacity of soil-water-ice mixture

$L_f$ = volumetric latent heat of fusion of water

$K_{pf}$ = thermal conductivity of partially freezing soil.

By combining Eqs. (4 - 22), (4 - 23) and (4 - 24) we have

$$(C_{pf} + L_f \frac{\partial \theta_l}{\partial T}) \frac{\partial T}{\partial t} = \nabla \cdot (K_{pf} \nabla T) - L_f \nabla \cdot (D_\theta \nabla \theta_l) \qquad (4 - 25)$$

where: $C_a = (C_{pf} + L_f \frac{\partial \theta_l}{\partial T})$ - apparent heat capacity

This approach was used in the mathematical models proposed by Harlan (1973), Jame and Norum (1977), Outcalt (1976), Kay et al. (1978), and Taylor and Luthin (1978) to simulate soil-water

freezing on a small laboratory scale only . Taylor and Luthin (1978) and Jame and Norum (1977) obtained a close correlation with the experimental data only after adjusting the isothermal soil moisture diffusivity in the freezing zone. It was proven by Hromadka et. al (1981) that for coupled heat and moisture transport in freezing soils, the effects of latent heat overshadow the parabolic nature of differential equations (4 - 23, 4 - 25) and this in turn may lead to inconsistent models with undesirable restraints on parameters and solution discretization. This approach usually requires small time-steps in the order of seconds, small spatial discretization in the order of centimeters and may create instability problems for long simulations of a year or more.

An alternative approach, based on the concept of the isothermal phase change of soil moisture, was developed first by Bafus and Guymon (1976) and was further expanded by Guymon et. al (1984) for the two-dimensional case. This approach assumes that the effects of the latent heat of fusion of soil-moisture can be modelled as an isothermal process. The calculation procedure is very simple, the temperature of a soil volume undergoing phase change is not permitted to change (T=0 °C) until the latent heat $L_f$ of all the soil-moisture available for a phase change is extracted or added to the control volume. The amount of heat extracted from the soil volume in a time interval of $\Delta t$ causing a drop of soil temperature of $\Delta T$ can be expressed as follows:

$$\Delta Q = L_f [\, \theta^* - \theta(T_o)] - L_f \frac{\partial \theta_l}{\partial T} \Delta T - C_{pf} \Delta T \qquad (4 - 26)$$

where: $\theta^*$ = volumetric soil-moisture content at the beginning of the process

$\theta(T_o)$ = volumetric unfrozen moisture content as a function of temperature $T_o$

$T_o$ = initial temperature of the system

$\Delta T$ = Temperature drop (assumed to be negative)

$\Delta Q$ = amount of heat extracted from the system during time step $\Delta t$

Three cases can be considered for a strictly freezing process modelled as an isothermal phase change.

$$L_f [\, \theta^* - \theta(T_o)] = \Delta Q \quad \text{isothermal freezing (static regime of T and } \theta\,) \tag{4 - 27}$$

$$L_f [\, \theta^* - \theta(T_o)] > \Delta Q \quad \text{isothermal freezing with moisture accumulation} \tag{4 - 28}$$

$$L_f [\, \theta^* - \theta(T_o)] < \Delta Q \quad \text{temperature change } \Delta T \text{ takes place} \tag{4 - 29}$$

A moisture sink due to ice formation is modeled as follows:

$$\frac{\rho_I}{\rho_w} \frac{\partial \theta_I}{\partial t}\, dt = \frac{\Delta Q}{L_f} \qquad \text{if} \quad L_f [\, \theta^* - \theta(T_o)] \geq \Delta Q$$

$$\frac{\rho_I}{\rho_w} \frac{\partial \theta_I}{\partial t}\, dt = [\, \theta^* - \theta(T_o)] - \frac{\partial \theta_I}{\partial T} \Delta T \qquad \text{if} \quad L_f [\, \theta^* - \theta(T_o)] < \Delta Q \tag{4 - 30}$$

According to Hromadka (1981) this approach allows relatively large time steps $\Delta t$, expressed in hours, and the spatial discretization can alo be relatively large, in the order of 0.5 meters. This approach is able to accurately simulate the temperature and moisture content of freezing soils over long periods of time , in the order of years.

Taking into account the above comments, the soil-moisture phase change modeling in this report will be based on the isothermal approach. More important assumptions made for two-dimensional model development are listed below:

(i) Soil moisture migrates in liquid and vapor form and is driven by the thermal and moisture gradient.

(ii) Heat and moisture is transferred according to Eq. (4 - 31) (4 -32).

(iii) Soil moisture phase change is approximated as an isothermal process.

(iv) Thermal - and transport properties of soil are obtained from experimental data.

(v) Soil moisture transport properties are adjusted by a phenomenological parameter obtained from field data, laboratory experiments, or theory.

(vi) Soil moisture migration in a completely frozen soil is assumed to be negligible.

(vii) Hysteresis effects due to freezing/thawing cycles are negligible.

The final mathematical model simulating heat and moisture flow in the freezing zone has the following form:

$$C_{pf}\frac{\partial T}{\partial t} - L_f S = \nabla \cdot (K^* \nabla T) + \nabla \cdot (D_\varepsilon^* \nabla \theta_l) + L_v \rho_l \frac{\partial (\varepsilon K_h^*)}{\partial y} \qquad (4-31)$$

$$\frac{\partial \theta_l}{\partial t} + S = \nabla \cdot (D_T^* \nabla T) + \nabla \cdot (D_\theta^* \nabla \theta_l) + \frac{\partial K_h^*}{\partial y} \qquad (4-32)$$

where: $K^* = K_{pf} + L_v \varepsilon \rho_l D_T^*$

$D_\varepsilon^* = L_v \varepsilon \rho_l D_\theta^*$

$K_h^* = K_h \, 10^{-I\theta_I}$

$D_T^* = D_T \, 10^{-I\theta_I}$

$D_\theta^* = D_\theta \, 10^{-I\theta_I}$

$S = \frac{\rho_I}{\rho_w}\frac{\partial \theta_I}{\partial t}$

$I$ = calibration factor

## 4.3 Heat Transfer in Frozen Soils

For frozen soil the following mathematical model is applied

$$C_f \frac{\partial T}{\partial t} = \nabla \cdot (K_f \nabla T) \qquad (4-33)$$

$$\frac{\partial \theta_l}{\partial t} = 0 \qquad (4-34)$$

## 4.4 Boundary Conditions at the Ground Storage Surface

This section deals with the various aspects of energy and water exchange at the soil-air interface.

In general there are many very complex processes involved at the boundary conditions. These processes almost defy mathematical description. This is because the numerous variables involved are difficult to quantify or define. Taking into account the climate and the topographic conditions, the following parameters and phenomena are involved in the boundary conditions model at the surface of ground heat storage:

(i) Soil characteristics of heat and mass transfer

(ii) Composition of the surface cover and soil

(iii) Solar radiation, cloud cover, the surface albedo, air temperature, relative humidity

(iv) Rainfall

(v) Snow cover

(vi) Wind speed

(vii) Evaporation, evapotranspiration, sublimation and condensation.

A physical description of the soil surface-atmosphere system is based on the energy and water budgets which are inextricably coupled when water changes phase. More details about that can be found in Tarnawski (1982).

### 4.4.1 Heat Balance

The heat balance at the ground/snow surface, for year round conditions has the following form:

$$q_{si} - q_{sr} + q_{li} - q_{lr} + q_{gs} + q_h - q_e + q_{adv} + q_n = 0 \qquad (4 - 35)$$

where: $q_{si}$ = incident shortwave radiation

$q_{sr}$ = reflected shortwave radiation

$q_{li}$ = longwave radiation incoming from cloudy sky

$q_{lr}$ = longwave radiation from the ground

$q_{gs}$ = penetration of solar radiation through the snowpack

$q_h$ = convective heat transfer of sensible heat from air

$q_e$ = latent heat flux by evaporation, evapotranspiration, melting snow or sublimation

$q_{adv}$ = advection of heat by precipitation

$q_n$ = conduction of heat from underground

Flux components carrying heat toward the surface are positive, those carrying heat away from the surface are negative. Of all these fluxes, the radiation exchange is the most important. The convective heat transfer is of secondary importance. Heat flow by evaporation is also of secondary importance. Rainfall has an important influence on the water movement in the boundary layer of soil and on soil properties, but is of minor importance as an energy flux. Replacing radiant energy terms by $q_{sn}$ and $q_{ln}$ Eq. (4 - 35) is reduced to

$$q_{sn} + q_{lo} + q_h - q_e + q_{adv} + q_n = 0 \qquad (4 - 36)$$

where $q_{sn} = q_{si} - q_{sr}$

$q_{lo} = q_{li} - q_{lr}$

Radiation

The radiation that arrives at the surface of the earth is considered as two separate streams: shortwave radiation originating from the sun, which is generally considered to fall within the wavelength range of 0.3 to 3 μm and longwave radiation from the sky and surroundings, between 5 to 80 μm. Shortwave radiation reaches the ground in two main forms. Direct shortwave radiation includes the shadow-casting rays of the unclouded sun. Diffusive shortwave radiation consists in part of mainly blue radiation scattered by air molecules, and in part of nearly white radiation diffusely reflected by clouds and suspended particles. The net shortwave radiation (solar radiation) at the surface of the earth can be expressed as:

$$q_{sn} = q_{si} - q_{sr} = q_{si}\,(1-a) \qquad (4 - 37)$$

where a = albedo of the soil surface (surface reflectivity)

$q_{si}$ = incident shortwave radiation (total radiation)

The total radiation $q_{si}$ is recorded at meteorological stations. On reaching the ground surface, the total shortwave radiation is reflected from it. The reflectivity or albedo is understood to be the ratio of reflected radiation to insolation. In nature, there are three different kinds of surface on the earth, soil, water, and snow. From the point of view of ground heat pumps, only the first and the last surface is important. Soil shows the greatest variability, even without considering the varied vegetation which may cover it. Typical rough albedo values for various soils without vegetation are presented in Table 4.1[Eagleson, 1970]. The results show a great variability of albedo, dependent upon soil quality. It is seen that albedo is essentially dependent on soil moisture content. The decrease of soil albedo by water is significantly less at soil surfaces. The albedo shows a significant decrease with the increase of surface roughness. Also the color of the soil has an influence on albedo variation. By changing the soil surface color, it is possible to change the thermal level of the soil.

Table 4.1. Soil Albedo

| Soil | Albedo | Soil | Albedo |
|---|---|---|---|
| Black, dry soil | 0.14 | Ploughed field, moisted | 0.14 |
| Black, moist soil | 0.08 | Surface of clayly desert | 0.29-0.31 |
| Gray, dry soil | 0.25-0.30 | Yellow sand | 0.35 |
| Gray, moist soil | 0.10-0.12 | White sand | 0.34-0.40 |
| Blue, dry loam | 0.23 | Gray sand | 0.18-0.23 |
| Blue, moist loam | 0.16 | River sand | 0.43 |
| Fallow field, dry surface | 0.08-0.12 | Bright, fine sand | 0.37 |
| Fallow field, wet surface | 0.05-0.07 | Rock | 0.12-0.15 |

The albedo of vegetation is also very variable. Approximate albedo values of different vegetative covers are given in Table 4.2 [Eagleson, 1970].

Table 4.2. Vegetation Albedo

| Vegetation | Albedo | Vegetation | Albedo |
|---|---|---|---|
| Summer wheat | 0.10 - 0.25 | Tops of oak | 0.18 |
| Winter wheat | 0.16 - 0.23 | Tops of pine | 0.14 |
| Winter rye | 0.18 - 0.23 | Tops of fir | 0.10 |
| High, dense grass | 0.18 - 0.23 | Lettuce | 0.22 |
| Green Grass | 0.26 | Beets | 0.18 |
| Grass dried in sun | 0.19 | Potatoes | 0.15 - 0.25 |
| Meadow | 0.15 - 0.25 | Heather | 0.10 |

For snow, the albedo is highly variable and is a function of its age, water content, depth, grain size, solar angle, and degree of contamination. For fresh snow the albedo value is about 0.8 but as the snow ages its value decreases to 0.4. Typical values of snow albedo are given in Table 4.3 [Geiger, 1965].

Table 4.3. Snow Albedo

| Type of Snow | Albedo | Ice / Water | Albedo |
|---|---|---|---|
| Fresh cover | 0.75 - 0.95 | Sea ice | 0.36 - 0.50 |
| Dense cover | 0.60 - 0.90 | Water | 0.03 - 0.10 |
| Old cover | 0.40 - 0.70 | | |
| Clean firn | 0.50 - 0.65 | | |
| Dirty firn | 0.20 - 0.50 | | |

Most natural surfaces can be treated as "full" radiators which emit longwave radiation in contrast to the solar radiation emitted by the sun. Longwave radiation from the atmosphere $q_{li}$ is nearly all absorbed at the surface of the earth, because the latter acts as a nearly perfect absorber for long wavelengths. The surface in turn emits a stream of upward radiation $q_{lr}$ of similar wavelengths. Hence, net longwave radiation is expressed by the formula.

$$q_{lo} = q_{li} - q_{lr} \qquad (4 - 38)$$

The available observational data do not allow any adequate characterization of the regularities of the spatial and temporal variability of effective radiation and downward atmospheric emission. In practice, empirical formulae are commonly applied, of which those best known are the Ångstrom

(Eq. 4 - 39) and Brunt (Eq. (4 - 40)) formulae. Both formulae have the following form, for cloudless sky:

$$q_{lo} = \sigma T_{ka}^4 (A_1 + B_1 10^{-G_1 e_a}) \qquad (4 - 39)$$

$$q_{lo} = \sigma T_{ka}^4 (A_2 + B_2 \sqrt{e_a}) \qquad (4 - 40)$$

where $q_{lo}$ = effective outgoing radiation under a cloudless sky, $W/m^2$

$\sigma$ = Stefan-Boltzmann constant, $W/m^2K^4$

$T_{ka}$ = ambient absolute temperature at a height of 1.5 - 2.0 m from the earth's surface

$e_a$ = water-vapor pressure in the air at height of 1.5 - 2.0 m, mbar

$A_1$, $B_1$, $G_1$, $A_2$, and $B_2$ = constants

The coefficient in formulae (4 - 39) and (4 - 40) were determined, from observational data, by many investigators. For the Ångstrom formula the following constants are the most reliable.

$$A_1 = 0.180;\ B_1 = 0.250;\ G_1 = 0.0945$$

These values were obtained by Boltz and Falkenberg [1949]. For the Brunt's formula, the following constants are the most frequently used in climatological calculations [Budyko, 1958].

$$A_2 = 0.39;\ B_2 = 0.05$$

In reality the sky is almost always cloudy. The problem of the influence of cloudiness on the effective outgoing radiation is very important. To estimate this effect, Budyko [1958] suggested the following formula

$$q_{ln} = q_{lo} (1 - s_1 N^2) + 4\sigma s_2 T_{ka}^3 (T_{ksur} - T_{ka}) \qquad (4 - 41)$$

where: $q_{ln}$ = net longwave radiation for cloudy sky

$q_{lo}$ = net longwave radiation for cloudless sky

$s_1$ = empirical constant, $s_1 = 0.78$

N = relative amount of cloudiness (0 - 1)

$s_2$ = empirical constant, $s_2 = 0.90$

$T_{ksur}$ = absolute temperature of the earth's surface

Values $T_{ka}$, $e_a$, N can be obtained from any climatological station. The second term of Eq. (4 - 41) permits the estimation of the effect of temperature differences between the underlying surface and the air on the outgoing radiation. When there is a difference in temperatures, the effective outgoing radiation change is approximately equal to

$$\sigma s_2(T_{ksur}^4 - T_{ka}^4) \approx 4\sigma s_2 T_{ka}^3(T_{ksur} - T_{ka})$$

Convective heat transfer

Convective heat transfer at the ground surface is a process of energy transport by the combined action of heat conduction, energy storage, and the mixing motion between the ground surface and the air. The convection at the surface is calculated using a convective heat transfer coefficient and the difference between the ambient air temperature and the surface temperature.

$$q_h = h\,(T_{sur} - T_a) \qquad (4 - 42)$$

where h = convection heat transfer coefficient

$T_{sur}$ = ground surface temperature

$T_a$ = ambient air temperature

Assuming the convection mechanism to be similar to that on a flat plate of turbulent flow, the coefficient of heat transfer by convection h, is obtained from a correlation which uses the 0.8 power of the wind velocity and appropriate properties of the air, as follows:

$$h = \kappa_c K_a \left( \frac{v \rho_a}{\eta_a} \right)^{0.8} \qquad (4 - 43)$$

where $\kappa_c$ = constant coefficient

$K_a$ = thermal conductivity of air

$v$ = apparent wind velocity at 2 m above the surface

$\rho_a$ = density of air

$\eta_a$ = dynamic viscosity of air

The constant coefficient $\kappa_c$ was obtained from a series of year-long calculations which matched the cumulative heat flux over the geothermal flux for a given year [Hwang, 1976]. Experience shows that normally, $\kappa_c = 0.01867$ .

Usually, the measured wind velocity from meteorological stations is at 10 m above the ground surface. Appendix B shows the derivation of the apparent wind velocity.

Release of latent heat of evapotranspiration

Evaporation occurs in the equations of both heat and water balance. This arises because the evaporation of liquid water needs a great deal of heat. In fact, evaporation is usually an important mode of heat transfer. The latent heat contribution can be calculated as,

$$q_e = \upsilon_{et} L \qquad (4 - 44)$$

where $L$ = latent heat of vaporization of water

$\upsilon_{et}$ = flux density of evapotranspiration (Eq. (4 - 48))

The processes of vaporization or evapotranspiration from the soil will be described in the subsection on water balance at the ground surface.

The moisture flux at the ground surface can be expressed in term of ground surface temperature (Appendix C).

Advective energy contributions

The temperature of raindrops falling upon a ground surface is usually different from the surface temperature. This means that there will be a transfer between the drops and the surface. The amount of heat transferred to the surface is directly proportional to the mass of the rainwater and to its temperature. Thus, approximately,

$$q_{adv} = m_r c_w (T_{rain} - T_{sur}) \qquad (4 - 45)$$

where $m_r$ = mass of rainfall

$c_w$ = specific heat of water

$T_{rain}$ = temperature of rain

$T_{sur}$ = temperature of the surface

Eq. (4 - 45) can be written in terms of the amount of rainfall, and with the assumption that $T_{rain} \approx T_a$:

$$q_{adv} = \frac{R_f c_w}{86400} (T_a - T_{sur}) \qquad (4 - 46)$$

where $q_v$ = advection of heat by rainfall, $W/m^2$

$R_f$ = amount of rainfall, mm/day

$\rho_l$ = density of water, $kg/m^3$

$c_w$ = specific heat of water, kJ/kg.K

## 4.4.2 Moisture Balance

The water balance at the ground/snow surface for year round conditions has the following form:

$$\upsilon_r + \upsilon_m - \upsilon_{et} + \upsilon_{ex} = 0 \qquad (4 - 47)$$

where: $\upsilon_r$ = flux of rainfall

$\upsilon_m$ = flux of snowmelt

$\upsilon_{et}$ = flux of evapotranspiration

$\upsilon_{ex}$ = flux of moisture exfiltration from the underground

As in the energy balance equation, the fluxes toward the surface are positive. In Eq. (4 - 47), the interception of water by plant canopies and surface storage in puddles were disregarded. These phenomena are very temporary and the water thus detained ends up as delayed infiltration or as evaporation. Also the sublimation flux and flux of water by vapor diffusion are very small and they are usually neglected.

Flux of rainfall

Rainfall is measured daily or more frequently at meteorological stations expressed in millimeters on horizontal surface ( 1mm corresponds to 1 $kg/m^2$).

Flux of snowmelt

The model assumes that water from melting snow may either infiltrate into the soil or accumulate and flow from the ground heat storage area as a surface runoff.

Flux of evapotranspiration

Evapotranspiration is a term used to describe the combined process of evaporation from soil and plant surfaces and the transpiration of plants. Evaporation is the process by which a liquid is changed into vapor. Transpiration is defined as the process by which water evaporate from apertures on the surfaces of the leaves and green stems. Evapotranspiration can be a significant percentage of water and energy budget at the surface. Numerous formulae have been proposed for estimating the rate of evapotranspiration [Tornthwaite, 1948; Penman, 1948; Van Bavel,1966]. The most detailed is the energy budget method introduced by Van Bavel [1966]. The basic equation takes the following form.

$$\upsilon_{et} = \frac{(\Delta/\gamma)\ q_r\ A_e\ +\ B_v\ P_d}{(\Delta/\gamma)\ +\ 1} \qquad (4-48)$$

where $\upsilon_{et}$ = flux of evapotranspiration, $kg/m^2h$

$\Delta/\gamma$ = weighting factor in assessing the relative effects of energy supply and ventilation on evapotranspiration,-

$\Delta/\gamma = 0.702636 + 0.030111T_a + 0.002135T_a^2 \quad 0< T_a<30\ °C$

$\gamma$ = psychrometric constant, c/mbar

$T_a$ = ambient temperature, °C

$q_r$ = net radiation, long and short-wave, $q_r = q_{sn} - q_{ln}$, $W/m^2$

$A_e$ = conversion factor $\left(A_e = \frac{1}{678}\right), \frac{m^2\ mm}{Wh}$

$B_v$ = 7.27 + 3.9v, van Bavel transport function, mm/hmbar

v = wind velocity at a height of 2 m, m/s

$P_d$ = vapor pressure deficit ( $P_d = e_s - e_a$ ), mbar

$e_s$ = saturated vapor pressure in air, mbar

$e_a$ = actual vapor pressure in air, mbar

The moisture flux at the ground surface can be expressed in terms of ground surface temperature.

Flux of exfiltration

The process of migration of water from the underground to the soil surface is called exfiltration. The opposite movement of water is called infiltration and is due to rainfall or snowmelt.

## 4.5 Heat Transfer at Ground Coil - Soil Interface

The flux of heat loss/gain per unit length of the GHE is represented by the following relation

$$q' = \frac{T_f - T_{sp}}{R_T'} \qquad (4 - 55)$$

where: $T_f$ = temperature of the working fluid circulating in the GHE

$T_{sp}$ = temperature of the pipe-soil interface

$R_T'$ = total thermal resistance between the working fluid and the surrounding soil.

The total thermal resistance, $R_T'$, consists of three components

$$R_T' = R_c' + R_p' + R_{th}' \qquad (4 - 56)$$

where: $R_c'$ = internal convective resistance

$R_p'$ = thermal resistance of a pipe wall

$R_{th}'$ = thermal contact resistance

### Internal Convective Resistance

For a smooth circular tube, the internal convective resistance is expressed by

$$R_c' = \frac{1}{\pi D_{pi}\, h} \qquad (4 - 57)$$

where: $D_{pi}$ = inside diameter of the pipe

$h$ = internal convective heat transfer coefficient

Equations describing internal heat transfer coefficient are discussed in section 2.7.

Thermal Resistance of the Pipe Wall

For the circular pipe, the thermal resistance is expressed as follows.

$$R_p' = \frac{\ln(D_{po}/D_{pi})}{2\pi\ K_p} \qquad (4-58)$$

where: $D_{po}$ = outside diameter of the pipe

$D_{pi}$ = inside diameter of the pipe

$K_p$ = thermal conductivity of the pipe wall

Thermal Contact Resistance

In the real cases there is no perfect surface contact between the ground coil and adjacent layers of soil and contacting points are only at discrete locations. This is mainly due to soil surface roughness, interspersed with void spaces filled with air or soil-water/ice and by the cycling operation of the GHE (heating/cooling). Thus heat can be transferred by conduction through the contact spots and/or across the voids by convection. The outcome of this phenomenon is a drop of temperature at the interface of the pipe surface and soil. The development of the thermal contact resistance model is beyond the scope of this report, and therefore, it is assumed that $R_{th}' = 0$.

The flux of heat gain/loss per unit length of the GHE are defined as

$$q' = \frac{Q}{L_{GHE}} = U * \pi\ D_{pi} * \Delta T_m \qquad (4-59)$$

where: Q = rate of heat exchanged between ground coil fluid and surrounding soil

$U$ = overall heat transfer coefficient defined in terms of inside pipe area

$D_{pi}$ = inside pipe diameter

$L_{GHE}$ = length of the ground heat exchanger

$\Delta T_m$ = mean logarithmic temperature difference.

A detailed description all components of this equation is provided in Chapter 2.

Thus, the temperature at the pipe-soil interface can be obtained from the following relation.

$$T_{sp} = T_f - U * \pi D_{pi} L * \Delta T_m * R_T' \qquad (4 - 60)$$

## 4.6 Initial Temperature and Moisture Profiles in the Ground

Initial ground temperature and moisture profiles are essential in order to commence any computer simulation. Therefore a general relation for temperature distribution in the ground, proposed by Lettau (1962) and van Wijk (1963) , is used in this report.

$$T(y,t) = Ts_{ave} - (Ts_{ave} - Ts_{min}) \exp\left[- y \sqrt{\frac{\pi}{365\ \alpha}}\right] * \cos\left\{\frac{2\pi}{365}\left(t - t_{min} - \frac{y}{2}\sqrt{\frac{\pi}{365\ \alpha}}\right)\right\} \qquad (4 - 61)$$

where: $T(y,t)$ = soil temperature as a function of the ground depth, y, and time, t, expressed in days counted since January 1st

$Ts_{max}$ = maximum surface temperature in a year

$Ts_{min}$ = minimum surface temperature in a year

$Ts_{ave} = \frac{Ts_{min}+Ts_{max}}{2}$

$y$ = depth of the ground

$\alpha = \frac{K_s}{\rho_b\ c}$ thermal diffusivity of soil

$K_s$ = thermal conductivity of soil

$c$ = soil specific heat

$\rho_b$ = bulk density of soil

t = current time expressed in days counted since January 1st

$t_{min}$ = time when $Ts_{min}$ was recorded (expressed in days counted since January 1st )

Initial volumetric moisture content profile in the ground can be obtained from the similar relationship, i.e.:

$$\theta(y,t) = \theta_{save} - (\theta_{save} - \theta_{smax}) \exp\left[ (y - y_w) \left( \frac{\pi}{365\ D_\theta} \right)^{0.5} \right] * \cos\left\{ \frac{2\pi}{365} \left( t - t_{minI} + \right. \right.$$

$$\left. \left. + \frac{(y - y_T)}{2} \left[ \frac{\pi}{365\ D_\theta} \right]^{0.5} \right\} \right. \quad (4 - 62)$$

where: $\theta(y,t)$ = soil volumetric moisture content as a function of the ground depth, y, and time, t, expressed in days counted since January 1st.

$\theta_{smax}$ = maximum volumetric moisture content at the ground surface in a year

$\theta_{smax}$ = minimum volumetric moisture content at the ground surface in a year

$\theta_{save} = \frac{\theta_{smax} + \theta_{smin}}{2}$

$y_T$ = total depth of the finite element domain

$y_w$ = depth of water table

$D_\theta$ = isothermal moisture diffusivity

y = depth of the ground

t = current time expressed in days counted since January 1st

$t_{minI}$ = time when $\theta_{smin}$ was recorded (expressed in days counted since January 1st )

Maximum and minimum values of Ts and $\theta_s$ can be obtained from the records of agrometeorological stations in Canada available in Land Resource Research Centre of Agriculture Canada. Some useful data in this regard can be found in the report published by Edey and Joynt (1975).

# 5. MATHEMATICAL MODEL OF A GROUND HEAT PUMP SYSTEM

## GROUND HEAT STORAGE

### Unfrozen Soil

$$\nabla \cdot (K^* \nabla T) + \nabla \cdot (D_\varepsilon \nabla \theta_l) - C \frac{\partial T}{\partial t} + L\rho_l \frac{\partial (\varepsilon K_{hu})}{\partial y} = 0 \qquad (5-1)$$

$$\nabla \cdot (D_T \nabla T) + \nabla \cdot (D_\theta \nabla \theta_l) - \frac{\partial \theta_l}{\partial t} + \frac{\partial K_{hu}}{\partial y} = 0 \qquad (5-2)$$

### Freezing Soil

$$C_{pf} \frac{\partial T}{\partial t} - L_f S = \nabla \cdot (K^* \nabla T) + \nabla \cdot (D_\varepsilon{}^* \nabla \theta_l) + L_v \rho_l \frac{\partial (\varepsilon K_{hf}{}^*)}{\partial y} \qquad (5-3)$$

$$\frac{\partial \theta_l}{\partial t} + S = \nabla \cdot (D_T{}^* \nabla T) + \nabla \cdot (D_\theta{}^* \nabla \theta_l) + \frac{\partial K_{hf}{}^*}{\partial y} \qquad (5-4)$$

### Frozen Soil

$$C_f \frac{\partial T}{\partial t} = \nabla \cdot (K_f \nabla T) \qquad (5-5)$$

$$\frac{\partial \theta_l}{\partial t} = 0 \qquad (5-6)$$

### Boundary Conditions at the Ground Storage Surface

**Heat balance**

$$q_{si} - q_{sr} + q_{li} - q_{lr} + q_{gs} + q_h - q_e + q_{adv} + q_n = 0 \qquad (5-7)$$

**Water balance**

$$v_r + v_m = 0 \qquad (5-8)$$

### Boundary Conditions at the pipe-soil interface

The temperature at the pipe-soil interface can be obtained from the following relation.

$$T_{sp} = T_f - U * \pi D_{pi} * \Delta T_m * (R_c' + R_p' + R_{th}') \qquad (5 - 9)$$

GROUND HEAT PUMP UNIT

Approximations of the COP and $Q_{HE}$ for the selected heat pump unit, are functions of the $T_{f1}$, and valid only for fixed values of the air flow rate $V_a$, water flow rate $V_w$, wet and dry bulb temperature of entering air for summer and winter respectively.

heating operation

$$COP_H = COPh(1) + COPh(2) * T_{f1} + COPh(3) * T_{f1}^2 \qquad (5 - 10a)$$

$$QH_{HE} = HE(1) + HE(2) * T_{f1} + HE(3) * T_{f1}^2 \qquad (5 - 10b)$$

cooling operation

$$COP_C = COPc(1) + COPc(2) * T_{f1} + COPc(3) * T_{f1}^2 \qquad (5 - 10c)$$

$$QC_{HE} = HR(1) + HR(2) * T_{f1} + HR(3) * T_{f1}^2 \qquad (5 - 10d)$$

The entrance water temperature, $T_{f1}$, is obtained from the iteration procedure of the following equation:

$$\pi D_{pi} * U * L_{GHE} * \frac{(T_{f1}-T_{s1}) - (T_{f2}-T_{s2})}{\ln \frac{T_{f1}-T_{s1}}{T_{f2}-T_{s2}}} = \dot{m}_f * c_f (T_{f2} - T_{f1}) \qquad (5 - 11)$$

HOUSE

Heating and cooling loads data calculated on a daily basis for any house location on the condition that a climatological data file for that location is available.

$$Q_h = F_1(\text{time, location, building characteristic}) \qquad (5 - 12a)$$

$$Q_c = F_2(\text{time, location, building characteristic}) \qquad (5 - 12b)$$

# 6. NUMERICAL SOLUTION OF THE TWO DIMENSIONAL MODEL

There are generally two numerical techniques which can be used to solve the mathematical model of ground coupled heat pump systems, i.e.the finite difference method (FDM) and the finite element method (FEM). For one or two dimensional problems, FEMs are competitive with and usually superior to conventional FDMs (Pepper and Baker, 1988). The FEM provides a number of advantages over the FDMs.

The major advantage is a possibility of handling the most complex geometries of natural or constructional features of ground heat storage, e.g., layers of different soils with different material properties and variable thicknesses, ground coil-soil interface, ground surface topography, etc. Domain discretization can be chosen in a completely arbitrary fashion with node points being placed to accomodate any shape of boundary or interface and any defined variation in the thermal and physical properties of soil and a ground coil. Moreover, the smaller elements can be applied to those regions where there are noticeable changes in temperature and soil-moisture content. The computer program based on the finite element approach is very general and can be applied to solve similar problems with any desired finite element discretization.

The major disadvantage of the FEMs is the high requirement of computer memory to store coefficients of matrices. All calculations must be performed in double precision because of a higher sensitivity to numerical roundoff. The time required for program development is significantly larger with respect to the FDM. The overall computational times for both methods for results of comparable accuracy are similar (Shamsundar and Rooz, 1988).

Taking all the above into account, the FEM is selected to numerically solve a two-dimensional model described by set of equations, (5 - 1) to (5 - 11).

## 6.1 Finite Element Formulation for the Heat Storage Domain

Unfrozen and completely frozen soil

The variation of soil temperature and moisture content throughout the domain of interest

$$\Omega = \sum_{s=1}^{m} A_s \tag{6 - 1}$$

where $\Omega$ = total area of domain of interest

$A_s$ = area of an element

$m$ = total number of elements

is approximated in terms of nodal values $T_s$ and $(\theta_l)_s$ as

$$T \approx \mathbf{T} = \sum_{s=1}^{m} N_s(x,y)\, T_s(t) \tag{6 - 2}$$

$$\theta_l \approx \boldsymbol{\theta}_l = \sum_{s=1}^{m} N_s(x,y)\, \theta_{ls}(t) \tag{6 - 3}$$

where $N_s$ = the usual shape functions defined element by element.

If the approximations given by Eqs. (6 - 2) and (6 - 3) are substituted into Eqs. (5 - 1) and (5 - 2), a residual is obtained, which is then minimized using the Galerkin's method. This requires that the integral of the weighted errors over the domain must be zero, with the shape functions

$$N_r = N_s^T \tag{6 - 4}$$

being used as the weighting function, i.e.

$$\int_{\Omega} N_r \left( \nabla\bullet(D_K \nabla \mathbf{T}) + \nabla\bullet(D_\varepsilon \nabla \boldsymbol{\theta}_l) - C\frac{\partial \mathbf{T}}{\partial t} + L\rho_l \frac{\partial(\varepsilon K_h)}{\partial y} \right) d\Omega = 0 \tag{6 - 5}$$

$$\int_{\Omega} N_r \left( \nabla\bullet(D_T \nabla \mathbf{T}) + \nabla\bullet(D_\theta \nabla \boldsymbol{\theta}_l) - \frac{\partial \boldsymbol{\theta}_l}{\partial t} + \frac{\partial K_h}{\partial y} \right) d\Omega = 0 \qquad (6 - 6)$$

Expanding Eqs. (6 - 5) and (6 - 6) by the product rule of derivative lead to

$$\int_{\Omega} \left( \nabla\bullet(N_r D_K \nabla \mathbf{T}) - D_K(\nabla N_r \bullet \nabla \mathbf{T}) + \nabla\bullet(N_r D_\varepsilon \nabla \boldsymbol{\theta}_l) - D_\varepsilon(\nabla N_r \bullet \nabla \boldsymbol{\theta}_l) - N_r C \frac{\partial \mathbf{T}}{\partial t} + N_r L \rho_l \frac{\partial(\varepsilon K_h)}{\partial y} \right) d\Omega = 0 \qquad (6 - 7)$$

$$\int_{\Omega} \left( \nabla\bullet(N_r D_T \nabla \mathbf{T}) - D_T(\nabla N_r \bullet \nabla \mathbf{T}) + \nabla\bullet(N_r D_\theta \nabla \boldsymbol{\theta}_l) - D_\theta(\nabla N_r \bullet \nabla \boldsymbol{\theta}_l) - N_r C \frac{\partial \boldsymbol{\theta}_l}{\partial t} + N_r \frac{\partial K_h}{\partial y} \right) d\Omega = 0 \qquad (6 - 8)$$

The isothermal moisture diffusivity is defined as

$$D_\theta = K_h \frac{d\psi}{d\theta} \qquad (6 - 9)$$

which can also be expressed as

$$D_\theta \nabla\theta \approx D_\theta \nabla\theta_l = K_h \nabla\psi \qquad (6 - 10)$$

$$\phi = \psi + y \qquad (6 - 10a)$$

where: $\phi$ = total soil-water potential

$\psi$= matric potential

y = gravity potential

Substitution of Eq. (6 - 10a) into Eq. (6 - 10) yields

$$D_\theta \nabla\boldsymbol{\theta}_l = K_h \nabla\phi - K_h \qquad (6 - 11)$$

Substituting for this expression into the third term of Eqs. (6 - 7) and (6 - 8) yields

$$\int_{\Omega} \left( \nabla\bullet(N_r D_K \nabla \mathbf{T}) - D_K(\nabla N_r \bullet \nabla \mathbf{T}) + \nabla\bullet(N_r L \varepsilon \rho_l K_h \nabla \boldsymbol{\phi}) - \frac{\partial}{\partial y}(N_r L \varepsilon \rho_l K_h) \right.$$

$$\left. - D_\varepsilon(\nabla N_r \bullet \nabla \boldsymbol{\theta}_l) - N_r C \frac{\partial \mathbf{T}}{\partial t} + N_r L \rho_l \frac{\partial(\varepsilon K_h)}{\partial y} \right) d\Omega = 0 \qquad (6 - 12)$$

$$\int_{\Omega} \left( \nabla\bullet(N_r D_T \nabla \mathbf{T}) - D_T(\nabla N_r \bullet \nabla \mathbf{T}) + \nabla\bullet(N_r K_h \nabla \boldsymbol{\phi}) - \frac{\partial}{\partial y}(N_r K_h) - D_\theta(\nabla N_r \bullet \nabla \boldsymbol{\theta}_l) \right.$$

$$\left. - N_r C \frac{\partial \boldsymbol{\theta}_l}{\partial t} + N_r \frac{\partial K_h}{\partial y} \right) d\Omega = 0 \qquad (6 - 13)$$

Applying Green's theorem [Stasa, 1985] to the first and third terms of Eqs. (6 - 12) and (6 - 13) yields

$$\int_{\Omega} \nabla\bullet(N_r D_K \nabla \mathbf{T}) \, d\Omega = \int_{\Gamma} N_r D_K (\nabla \mathbf{T} \bullet n) d\Gamma = \int_{\Gamma} N_r D_K \frac{\partial \mathbf{T}}{\partial n} \, d\Gamma \qquad (6 - 14a)$$

$$\int_{\Omega} \nabla\bullet(N_r L \rho_l \varepsilon K_h \nabla \boldsymbol{\phi}) d\Omega = \int_{\Gamma} N_r L \rho_l \varepsilon K_h \frac{\partial \boldsymbol{\phi}}{\partial n} d\Gamma \qquad (6 - 14b)$$

$$\int_{\Omega} \nabla\bullet(N_r D_T \nabla \mathbf{T}) \, d\Omega = \int_{\Gamma} N_r D_T \frac{\partial \mathbf{T}}{\partial n} \, d\Gamma \qquad (6 - 15a)$$

$$\int_{\Omega} \nabla\bullet(N_r K_h \nabla \boldsymbol{\phi}) \, d\Omega = \int_{\Gamma} N_r K_h \frac{\partial \boldsymbol{\phi}}{\partial n} \, d\Gamma \qquad (6 - 15b)$$

Substituting of Eqs. (6 - 14a-b) and (6 - 15a-b) into Eqs. (6 - 12) and (6 - 13) and simplifying the gravitational flow terms leads to

$$\int_{\Gamma} N_r D_K \frac{\partial T}{\partial n} d\Gamma - \int_{\Omega} D_K(\nabla N_r \cdot \nabla T) d\Omega + \int_{\Gamma} N_r L \rho_l \varepsilon K_h \frac{\partial \phi}{\partial n} d\Gamma$$

$$- \int_{\Omega} D_\varepsilon(\nabla N_r \cdot \nabla \theta_l)\, d\Omega - \int_{\Omega} N_r C \frac{\partial T}{\partial t} d\Omega - \int_{\Omega} L \rho_l \varepsilon K_h \frac{\partial N_r}{\partial y} d\Omega = 0 \qquad (6-16)$$

$$\int_{\Gamma} N_r D_T \frac{\partial T}{\partial n}\, d\Gamma - \int_{\Omega} D_T(\nabla N_r \cdot \nabla T)\, d\Omega + \int_{\Gamma} N_r K_h \frac{\partial \phi}{\partial n}\, d\Gamma$$

$$- \int_{\Omega} D_\theta(\nabla N_r \cdot \nabla \theta_l)\, d\Omega - \int_{\Omega} N_r \frac{\partial \theta_l}{\partial t}\, d\Omega - \int_{\Omega} K_h \frac{\partial N_r}{\partial y}\, d\Omega = 0 \qquad (6-17)$$

Substitution of the generalized flux boundry conditions, Eqs. (6 - 27) and (6 - 29), coupled with the introduction of T and $\theta_l$ from the shape function identities, leads to

$$\int_{\Omega} D_K(\nabla N_r \cdot \nabla(N_s T)) d\Omega + \int_{\Omega} D_\varepsilon(\nabla N_r \cdot \nabla(N_s \theta_l))\, d\Omega + \int_{\Omega} N_r C \frac{\partial}{\partial t}(N_s T)\, d\Omega$$

$$+ \int_{\Omega} L \rho_l \varepsilon K_h \frac{\partial N_r}{\partial y}\, d\Omega - \int_{\Gamma} N_r F_K\, d\Gamma - \int_{\Gamma} N_r L \rho_l \varepsilon F_\theta\, d\Gamma = 0 \qquad (6-18)$$

$$\int_{\Omega} D_T(\nabla N_r \cdot \nabla(N_s T))\, d\Omega + \int_{\Omega} D_\theta(\nabla N_r \cdot \nabla(N_s \theta_l))\, d\Omega$$

$$+ \int_{\Omega} N_r \frac{\partial}{\partial t}(N_s \theta_l)\, d\Omega + \int_{\Omega} K_h \frac{\partial N_r}{\partial y}\, d\Omega - \int_{\Gamma} N_r \frac{D_T}{D_K} F_K\, d\Gamma - \int_{\Gamma} N_r F_\theta\, d\Gamma = 0 \qquad (6-19)$$

Rearrangement of the integrals yields

$$\int_{\Omega} D_K(\nabla N_r \cdot \nabla N_s)\ d\Omega\ \ T + \int_{\Omega} D_\varepsilon(\nabla N_r \cdot \nabla N_s)\ d\Omega\ \ \theta_l + \int_{\Omega} CN_rN_s\ d\Omega\ \ \frac{\partial T}{\partial t}$$

$$+ \int_{\Omega} L\rho_l\varepsilon K_h \frac{\partial N_r}{\partial y}\ d\Omega\ - \int_{\Gamma} N_rF_K\ d\Gamma\ - \int_{\Gamma} L\rho_l\varepsilon F_\theta N_r\ d\Gamma\ = 0 \qquad (6-20)$$

$$\int_{\Omega} D_T(\nabla N_r \cdot \nabla N_s)\ d\Omega\ T + \int_{\Omega} D_\theta(\nabla N_r \cdot \nabla N_s)\ d\Omega\ \ \theta_l$$

$$+ \int_{\Omega} N_rN_s\ d\Omega\ \ \frac{\partial \theta_l}{\partial t} + \int_{\Omega} K_h \frac{\partial N_r}{\partial y}\ d\Omega\ - \int_{\Gamma} N_r \frac{D_T}{D_K} F_K\ d\Gamma - \int_{\Gamma} N_rF_\theta\ d\Gamma\ = 0 \qquad (6-21)$$

These equations can be written in matrix form as

$$\mathbf{D_K\,T} + \mathbf{D_\varepsilon}\,\boldsymbol{\theta_l} + \mathbf{C_K}\,\frac{\partial \mathbf{T}}{\partial t} + \mathbf{F_K} = 0 \qquad (6-22)$$

$$\mathbf{D_T\,T} + \mathbf{D_\theta}\,\boldsymbol{\theta_l} + \mathbf{C_\theta}\,\frac{\partial \boldsymbol{\theta_l}}{\partial t} + \mathbf{F_\theta} = 0 \qquad (6-23)$$

where:

$\mathbf{D_K}$ = global conductance (stiffness) matrix in heat flow equation

$\mathbf{D_T}$ = global mass-heat diffusion matrix in moisture flow equation

$\mathbf{D_\varepsilon}$ = global mass-heat diffusion matrix in heat flow equation

$\mathbf{D_\theta}$ = global diffusion (stiffness) matrix in moisture flow equation

$\mathbf{C_K}$ = global capacitance matrix in heat flow equation

$\mathbf{C_\theta}$ = global capacitance matrix in moisture flow equation

$\mathbf{F_K}$ = global forcing vector matrix in heat flow equation

$\mathbf{F_\theta}$ = global forcing vector matrix in moisture flow equation

$\frac{\partial \mathbf{T}}{\partial t}$ = time derivative of temperature

$\frac{\partial \boldsymbol{\theta_l}}{\partial t}$ = time derivative of soil moisture content

The element matrices of $\mathbf{D}_K$ , $\mathbf{D}_\varepsilon$ , $\mathbf{C}_K$ , $\mathbf{F}_K$ , $\mathbf{D}_T$ , $\mathbf{D}_\theta$ , $\mathbf{C}_\theta$ and $\mathbf{F}_\theta$, of the above simultaneous equations for the linear triangular element is tabulated in Appendix D.

## 6.2 Generalized Mathematical Representation of Boundary Conditions

Boundary conditions at the ground surface can be expressed in a mathematical form. For the section of the boundary subjected to heat flux conditions, the conditions of the boundary are described as follows:

$$K \frac{\partial T}{\partial n} + (q_n)_\Gamma = 0 \qquad (6 - 24)$$

where: $K$ = thermal conductivity of soil at the ground surface layer

$\frac{\partial T}{\partial n}$ = temperature gradient in the normal direction of the ground surface

$(q_n)_\Gamma$ = heat flux at the ground surface $\Gamma$

The part of the boundary where moisture flux takes place is described as follows:

$$K_h \frac{\partial \phi}{\partial n} + D_T \frac{\partial T}{\partial n} + \left(\frac{v_m}{\rho_l}\right)_\Gamma = 0 \qquad (6 - 25)$$

where $K_h$ = hydraulic conductivity

$\frac{\partial \phi}{\partial n}$ = hydraulic potential gradient in the normal direction of the ground surface

$\phi$ = total potential for moisture flow

$D_T$ = thermal moisture diffusivity, $D_T = D_{Tl} + D_{Tv}$

$\rho_l$ = density of liquid water

Here $\phi$ can be expressed as

$$\phi = \psi + y \tag{6 - 26}$$

where $\psi$ = pressure head

$y$ = elevation

We rewrite Eq. (6 - 24) into the following form as

$$D_K \frac{\partial T}{\partial n} = F_K \tag{6 - 27}$$

where: $D_K = K + L\varepsilon\rho_l D_T$

$$F_K = - \frac{D_K}{K} (q_n)_\Gamma$$

From Eq. (6 - 24), the temperature gradient can be written as

$$\frac{\partial T}{\partial n} = - \frac{1}{K} (q_n)_\Gamma \tag{6 - 28}$$

Substituting Eq. (6 - 28) into Eq. (6 - 25), yields

$$K_h \frac{\partial \phi}{\partial n} = F_\theta \tag{6 - 29}$$

where: $F_\theta = \frac{D_T}{K} (q_n)_\Gamma - \frac{1}{\rho_l} (v_m)_\Gamma$

## 6.3 Lumped Capacitance Matrix Approach

The matrix form Eqs. (6 - 22) and (6 - 23) are generally valid for any known numerical method applied to solve the set of partial differential equations describing heat and moisture flow in soils (Hromadka and Guymon, 1981). There is, however, an important hidden characteristic of the global capacitance matrix obtained by the use of the FDM and the FEM, viz: the FEM approach leads to the non-diagonal matrix whilst the FDM approach produces a diagonal one.

The diagonal form of the capacitance matrix has a number of advantages over the non-diagonal one, such as:

- numerical calculations for the nodal unknowns (i.e., the nodal temperatures and/or moisture content) are more efficient and easier to perform
- produces convergent results which are smooth and do not have oscillatory behaviour
- easy and stable solution of problems involving phase-change.

There are several different techniques used for lumping the consistent capacitance matrices i.e., derived in the consistent manner with the standard Galerkin formulation, each however yielding a different lumped matrix (Zienkiewicz and Taylor, 1989).

The most common approach contains the following steps:

- scaling the entries in each given row in the consistent matrix
- dividing the result by the total capacitance
- allocating this result to the diagonal entry of each row under consideration
- assigning the off-diagonal terms to zero.

In this way the total capacitance of the consistent capacitance matrix is still preserved. It is also worth remembering that the exact maximum principle in this case is valid for the domain discretization which does not contain any obtuse triangles.

Lumping can be described as an application of a different set of shape functions just for the capacity integrals. The conditions for the matrix to be a diagonal one are as follows:

- shape functions are equal to 1 over a part of the finite element touching a given node, and zero everywhere else, (Fig 6.1)
- these parts do not overlap each other.

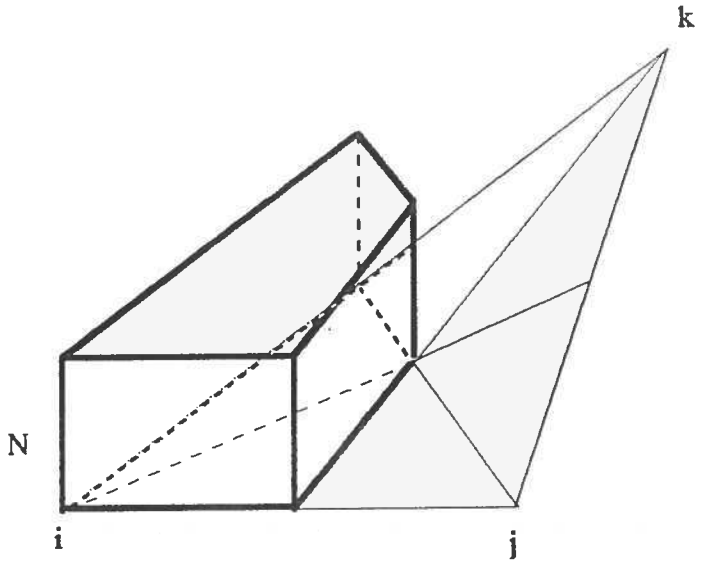


Fig. 6.1 Constant shape function for a triangular element

This idea is also utilized in the so called control -volume finite-element method (CVFEM) or sub-domain integration method (SDIM). This concept was introduced first by Wilson (1968) for the determination of temperature distribution in mass concrete structures. Later on this method has been found by numerous researchers [Narasimhan and Witherspoon, 1976; Hromadka and Guymon, 1982; Baliga and Patankar, 1980; Parkash, 1986; Hookey, 1986] to provide more accurate results than the Galerkin finite-element method.

According to the CVFEM the two-dimensional calculation domain $\Omega$ , which has a unit depth normal to the plane of interest, is discretized into a number of triangular finite elements (Fig. 6.2a). The triangular elements are next further subdivided into subareas by the centroids joined to the midpoints of the corresponding sides (Fig. 6.2b). This procedure generates so called control volumes around each node in the domain $\Omega$ (Fig. 6.2c).

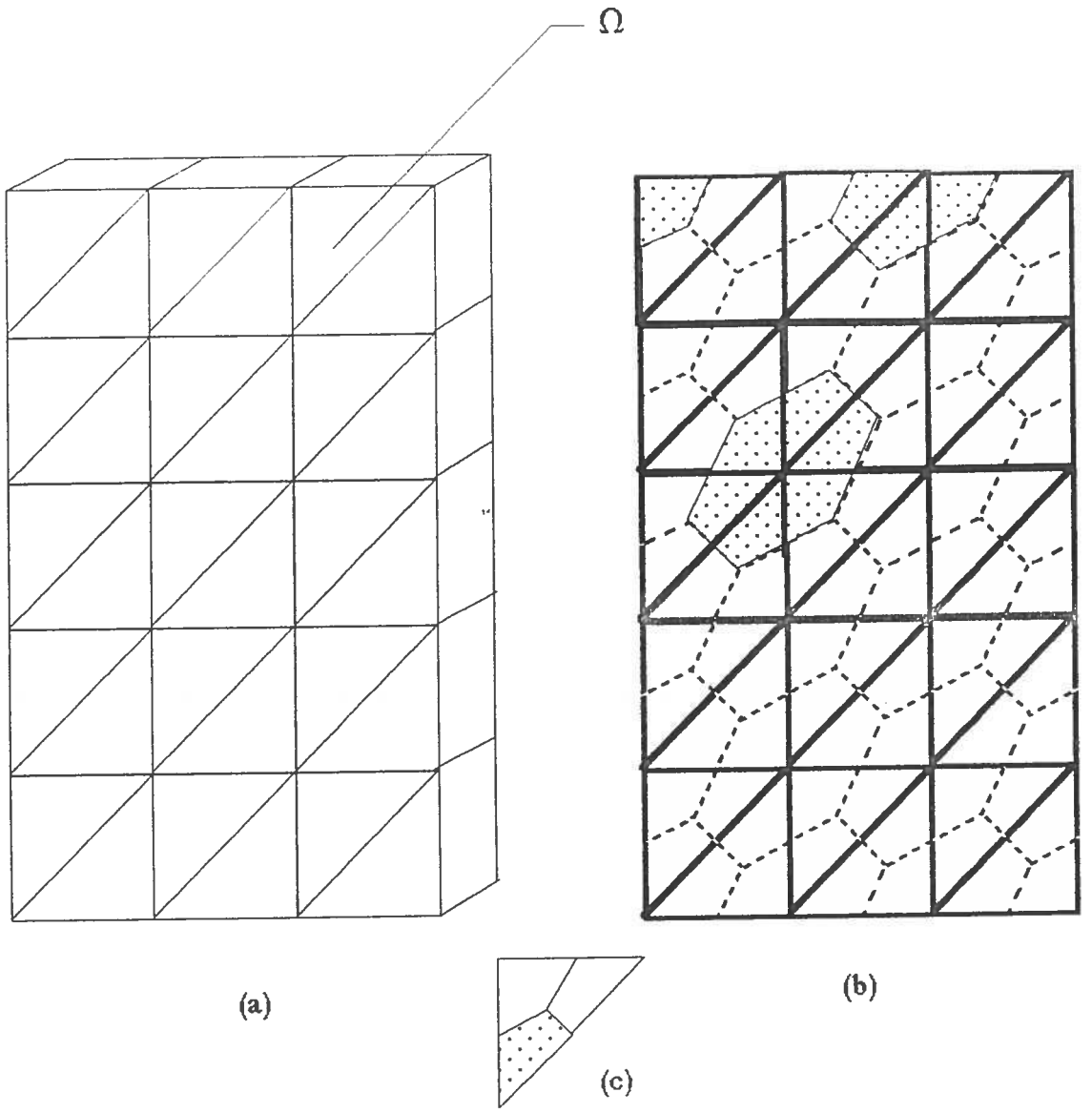


Fig. 6.2 Discretization of the calculation domain

The solid lines represent the domain and three-node triangular elements, whereas the broken ones show the control-volume boundaries. The shaded areas denote the control volumes associated with one internal node.

In this report a simple control volume approach is applied only to the isothermal phase change model for freezing and thawing soils. According to the control volume and lumping theory, any

state variable of each node (i.e.,temperature, volumetric moisture content) represents the average value over the area associated with it, (Fig. 6.3), i.e., it is entirely lumped to the node.

$$T_i = \frac{\sum_{e=1}^{6} A_e T_e}{\sum_{e=1}^{6} A_e} \qquad (6 - 30)$$

where: $T_e = \frac{(T_1+T_2+T_3)}{3}$

$A_e$ = sub-area associated with node "i"

e = number of elements associated with node "i"

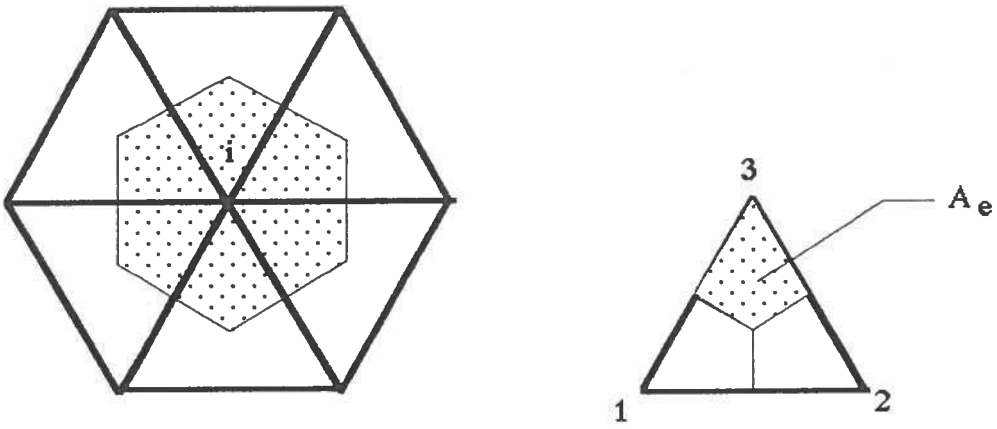


Fig. 6.3 Average state variable of the assocuated area to node "i"

The temperature at the node "i" is controlled, at the end of each calculation time step, to determine whether its temperature dropped below the freezing point. If this has happened, the amount of latent heat generated during this time step is calculated

$$Q^i_{\Delta t} = \sum_{e=1}^{n} A_e * 1 * \rho * c^* ( T_f - T_i ) \qquad (6 - 31)$$

and then compared with the total effective heat, $Q_L$, required to freeze a given control volume (associated area) assigned to node "i"

$$Q_L = \rho * L_f * \theta_i \qquad (6 - 32)$$

where: $\rho$ = density of water

$L_f$ = latent heat of fusion of water

$\theta_i$ = volumetric moisture content associated with node "i".

If $Q^i_{\Delta t} < Q_L$ then the temperature Ti is readjusted to the freezing point value, Tf , and the next time step calculations are carried out, the temperature Ti is readjusted to Tf as long as

$$\Sigma Q^i_{\Delta t} = Q_L \qquad (6 - 33)$$

When the collected amount of latent heat at the node "i" exceeds the effective heat $Q_L$ , then the node and surrounding control region are assumed to be frozen and the nodal temperature is not further readjusted to the freezing point. The thawing of soil is treated in a similar way.

To simplify the phase-change procedure, the amount of latent heat generated is usually replaced by the amount of soil water available for freezing or ice content available for thawing, in order to control isothermal phase-change model [Hromadka , 1986].

It is worthwhile pointing out that the time rate of latent heat generation is generally insensitive to large time intervals, [Hromadka and Guymon, 1981].

## 6.4 Time Integration Methods for Transient Finite Element Problems

The major field of application of the time marching procedure is to nonlinear problems, i.e. in this case, where one or more of the matrices **C**, **K**, or **f** depend on the unknown vector **a**. Here the alternatives of analytical solution present in linear situations do not exist. Therefore full integration

can only be carried out numerically and, in general, iteration within each time step appears to be necessary.

A temporal finite difference approximation must be applied to the mathematical model presented in Chapter 5, in order to obtain the numerical solution. The time derivative terms appearing in the model are thus replaced by a finite difference formula. There are numerous finite difference schemes providing varying orders of accuracy and complexity. The most common schemes for solving transient equations are listed below:

(i) explicit

(ii) implicit

(iii) three time level

Explicit schemes are relatively simple, and adaptable to a variety of heat and mass transfer problems. The time increments are restricted, however, to quite small values which may lead to excessive computer running time in the case of long simulations.

Implicit schemes are less restrictive but more complex. They may require a larger computer storage capacity. Stability is not a problem and the time increments are usually larger than those used for the explicit method. This approach, however, leads to the simultaneous solution of a large system of finite difference equations which, in our case, have a non-linear nature. The non-linearity is due to the dependence of thermo-flow characteristics of soil on moisture content and phase change phenomena associated with heat extraction and/or transfer to the ground. For that reason, the coefficients of the finite difference equations may vary from one time step to the next. Accurate solution usually requires numerous time consuming iterations.

Unnecessary iterations are eliminated in cases where a three-time-level schemes are applied. On the other hand, some problems may arrise due to oscillations of numerical results obtained. The three-time-level was first proposed by Lees (1966) for the numerical solution of quasilinear parabolic differential equations such as, for example, the heat conduction equation in the matrix form.

$$C\,\dot{a} + K\,a + f = 0 \qquad (6-34)$$

Proceding in the usual manner for discretization, with time as the independent variable, we can write

$$a \approx \hat{a} = \sum N_i\, a_i \qquad (6-35)$$

where: $a_i$ = stands for a nodal set of $a$ at time $i = n$ and $n+1$.

$N_i(t)$ = shape functions taken to be the same for each component of the vector.

A general method of formulating multi-time-level marching methods was published first by Zienkiewicz (1971). According to Wood (1978) the Zienkiewicz's three-time-level scheme had the following general form:

$$\frac{1}{2\Delta t} C\,[\,\beta_1\, a_{n+1} + \beta_2\, a_n + \beta_3\, a_{n-1}\,] + K\,[\,\beta_4\, a_{n+1} + \beta_5\, a_n + \beta_6\, a_{n-1}\,] + \bar{f} = 0 \qquad (6-36)$$

where: $\bar{f} = \beta_4\, f_{n+1} + \beta_5\, f_n + \beta_6\, f_{n-1}$

$n$ = time level

The values of coefficients $\beta_i$ for various three time level schemes are listed below:

| | | | | | | |
|---|---|---|---|---|---|---|
| Lees (1966) | $\beta_1 = 1$ | $\beta_2 = 0$ | $\beta_3 = -1$ | $\beta_4 = \frac{1}{3}$ | $\beta_5 = \frac{1}{3}$ | $\beta_6 = \frac{1}{3}$ |
| Liniger (1969) | $\beta_1 = 4.5$ | $\beta_2 = -7$ | $\beta_3 = 2.5$ | $\beta_4 = \frac{20}{12}$ | $\beta_5 = -\frac{7}{12}$ | $\beta_6 = -\frac{1}{12}$ |
| Zlámal (1975) | $\beta_1 = 5$ | $\beta_2 = -4$ | $\beta_3 = -1$ | $\beta_4 = \frac{4}{3}$ | $\beta_5 = \frac{4}{3}$ | $\beta_6 = \frac{1}{3}$ |
| Goodrich (1980) | $\beta_1 = 3$ | $\beta_2 = -4$ | $\beta_3 = 1$ | $\beta_4 = \frac{4}{5}$ | $\beta_5 = \frac{2}{5}$ | $\beta_6 = -\frac{1}{5}$ |

According to Goodrich (1980) his scheme is superior to the standard three-time-level one, as regards both oscillation and truncation error. Computations performed by Tarnawski (1982), for a one dimensional model of heat and moisture flow in ground heat storage, showed that schemes

developed by Zlamal (1975) and Goodrich (1980) produced almost identical results, but that the freezing of soil was better modelled by Goodrich's scheme.

A comparison of Goodrich's scheme vs. Crank-Nicolson, carried out by the authors of this project, has shown a superiority of the three-time-level method which produced numerical results closer to experimental data. For this reason the Goodrich scheme was selected as a time integration method in this report.

The form of Eq. (6 - 36) is very suitable for numerical modelling and details of a three-point method and the derived forms for the simultaneous equations, (6 - 22) and (6 - 23), can be found in the Appendix E.

## 6.5 The Two Dimensional Problem versus the Three Dimensional One

Knowledge of the variation of fluid temperature in the GHE is of major importance in the design and operation of ground heat pump systems. The analytical solution of this transient problem does not exist due to extremely high complexity of the problem. Therefore, in the majority of cases, fluid temperature distribution along the pipe is obtained from steady state models. To simulate a ground heat pump coupled with a horizontal ground heat exchanger, two or three dimensional mathematical models could be considered.

For the direct expansion system the fluid (refrigerant) temperature in the ground heat exchanger remains constant and the problem becomes a two-dimensional one.

As far as computer simulation of the closed loop ground heat pump system is concerned, the temperature of secondary fluid undergoes changes due to ground surface effects and the thermal properties of the ground. Therefore, in this case, the problem is a three dimensional one.

It is worth noting that the analytical solution of the simultaneous heat and mass transfer problem in soils does not exist even for the one-dimensional case. For ground heat storage, the problem becomes even more complex because of the presence of a ground heat exchanger with variable

heat flux, and soil moisture phase change phenomena. In addition, the change of fluid temperature with respect to length and time can be obtained from the following set of equations:

Fluid temperature

$$v_f \frac{\partial T_f}{\partial z} + a_f \frac{\partial^2 T_f}{\partial z^2} + \frac{2 * K_p}{r_1 \rho_f c_f} \frac{\partial T_p}{\partial r} = \frac{\partial T_f}{\partial t} \qquad (6\text{-}37)$$

Pipe wall

$$\frac{\partial^2 T_p}{\partial r^2} + \frac{1}{r} \frac{\partial T_p}{\partial r} = \frac{1}{a_p} \frac{\partial T_p}{\partial t} \qquad (6 - 38)$$

Boundary conditions :

at $r = r_1$

$$h_f (T_p - T_f) = K_p \frac{\partial T_p}{\partial r}\Big|_{r_1} \qquad (6 - 39)$$

at $r = r_2$

$$K_p \frac{\partial T_p}{\partial r}\Big|_{r_2} = K_s \frac{\partial T_s}{\partial r}\Big|_{r_2} \qquad (6 - 40)$$

where:

$a_f$ = fluid thermal diffusivity

$h_f$ = convective heat transfer coefficient

$v_f$ = fluid velocity

$T_f$ = fluid temperature

$T_p$ = pipe wall temperature

$K_p$ = pipe wall thermal conductivity

$a_p$ = pipe thermal diffusivity

$r_1$ = inner pipe diameter

$r_2$ = outer pipe diameter

$T_s$ = temperature of soil adjacent to the coil

$K_s$ = soil thermal conductivity

t = time

z = distance along the ground coil

It is obvious that the solution of the 3-D model could be obtained only by using numerical methods. There are, however, serious limitations which make this attempt not feasible for the present time.

Firstly, in the present 2-D model, the finite element domain consists of 143 elements whereas for the 3-D model this number had to be increased by factor of at least 100 in order obtain reliable and accurate results. This would lead to an extremely large computer program which could be run only on large mainframe computers. Even the present 2-D version of the program had to be modified to be run on the IBM PC since available Fortran compilers impose limits on the size of the executable version of the program.

Secondly, the computation time of the present version takes more than 2 hours on the IBM PC and it is very hard to predict what would be the time for the 3-D problem due to the difficulties described above. This problem could be solved only on powerful super-computers.

Thirdly, the output data generated by the present 2-D program requires much larger memory storage than the executable program, and therefore, there is a necessity to have a hard disk. This problem becomes much more difficult for the 3-D problem. Again this problem could be worked out on large super-computers.

Fourthly, the cost of generating software for the 3-D problem and running the program would be very high. This would reduce the number of potential users to a few who would have financial resources and easy access to the super-computer.

Due to the above reasons, the authors of this report use a steady state model describing the ground coil fluid temperature change along the GHE (see Section 2.7). It is worth mentioning that a similar approach is used successfully in buried gas pipe lines.

## 7. SAMPLES OF SIMULATION RUNS

The purpose of this chapter is to evaluate the performance of the model and the numerical procedure developed. Due to a lack of experimental data, the model evaluation was made only for natural site conditions i.e. without ground heat pump operation.

To verify the model, the numerical results were compared with the experimental data of soil temperatures recorded during the year 1987 at the site of the Agrometeorological Station in Ottawa. Comparisons were made for four randomly selected days i.e. September 13th (720 hrs from August 15th), January 21st (3840 hrs), February 14th (4416 hrs), and July 10th (7920 hrs). Climatological conditions, for the period of 140hrs prior to the selected days are shown in Figures 7.1 to 7.4.

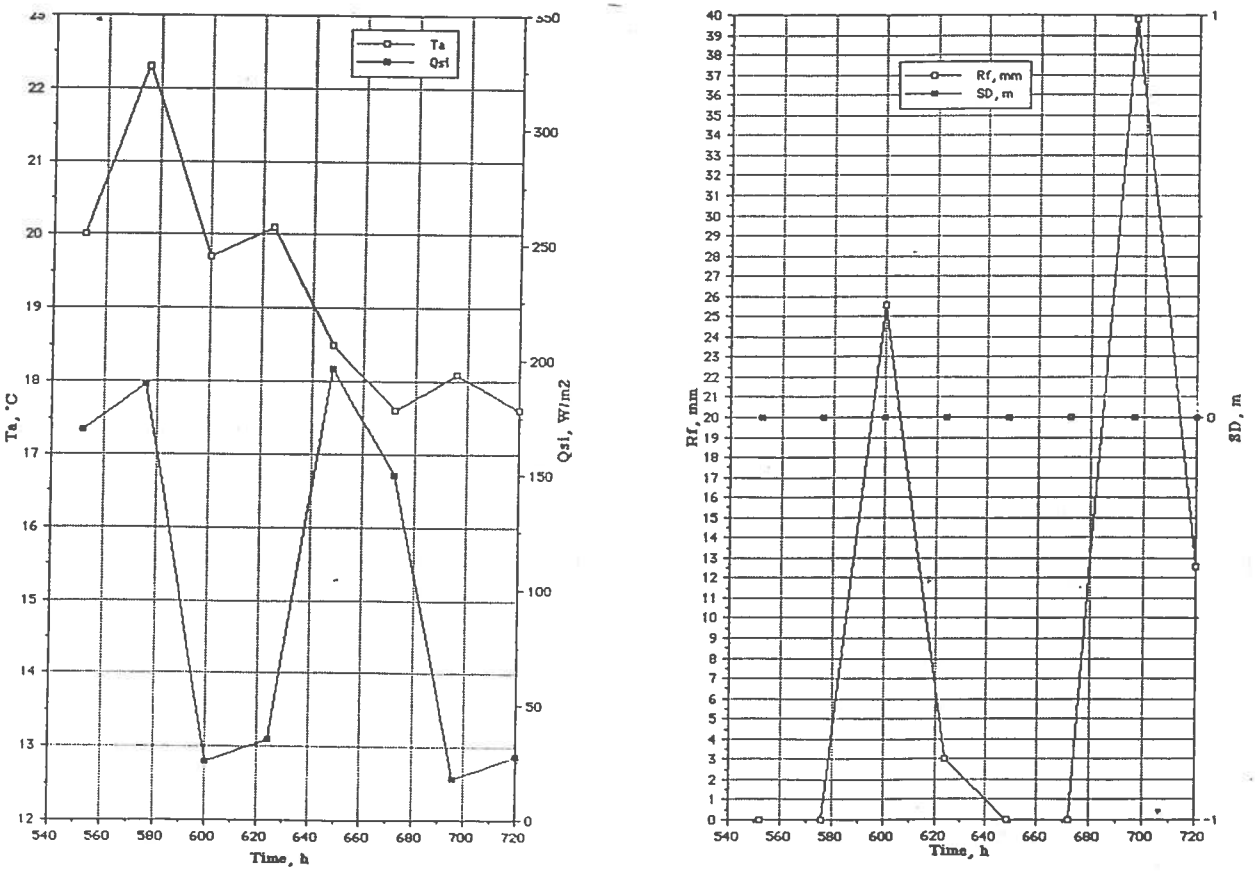


Fig. 7.1 Ambient temperature (Ta) and incoming shortwave radiation (Qsi) vs. time & Rainfall and snow depth vs. time (540 - 720 hrs)

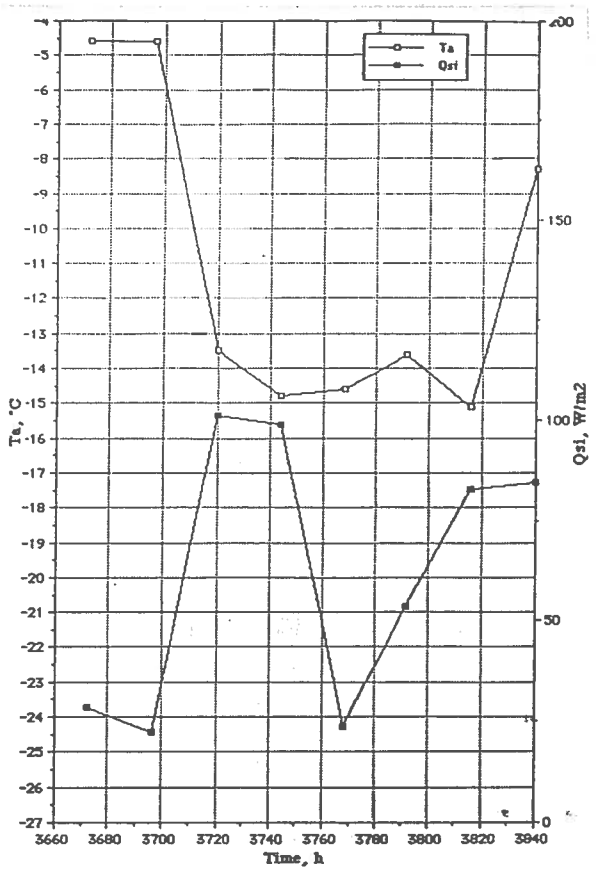


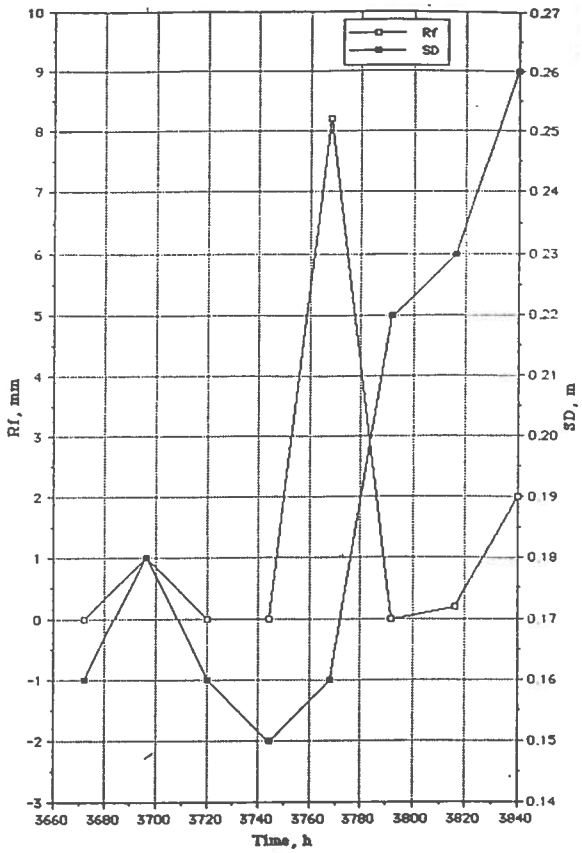


Fig. 7.2 Ambient temperature (Ta) and incoming shortwave radiation (Qsi) vs. time & Rainfall and snow depth vs. time (3660 - 3840 hrs)

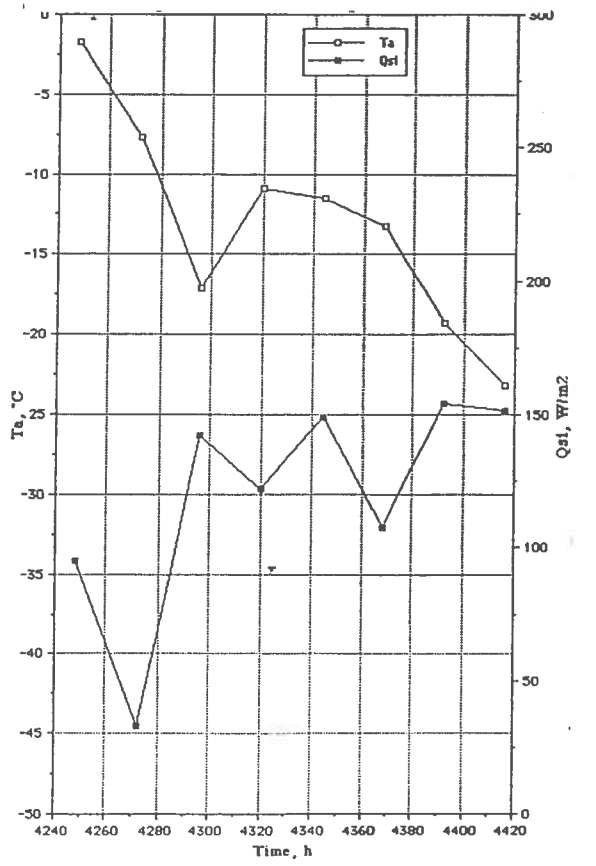


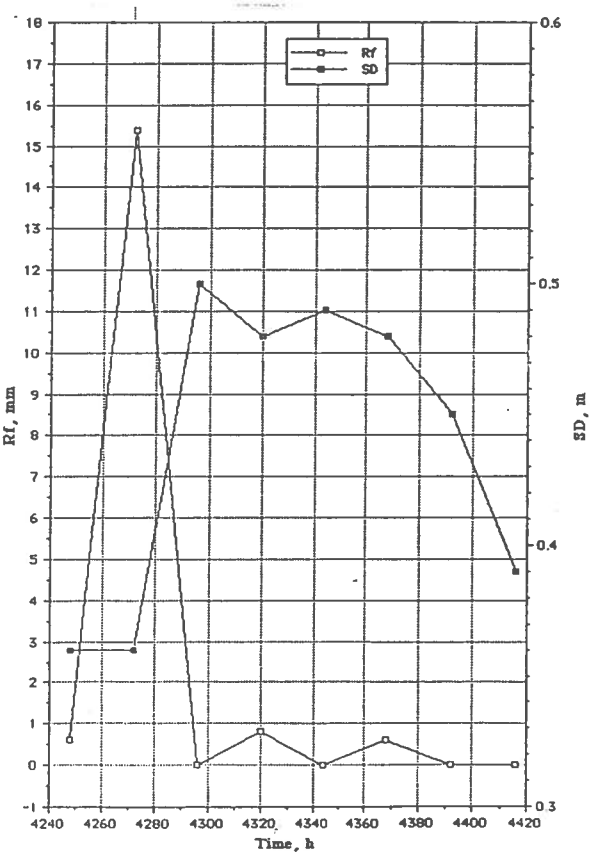


Fig. 7.3 Ambient temperature (Ta) and incoming shortwave radiation (Qsi) vs. time & Rainfall and snow depth vs. time (4240 - 4420 hrs)

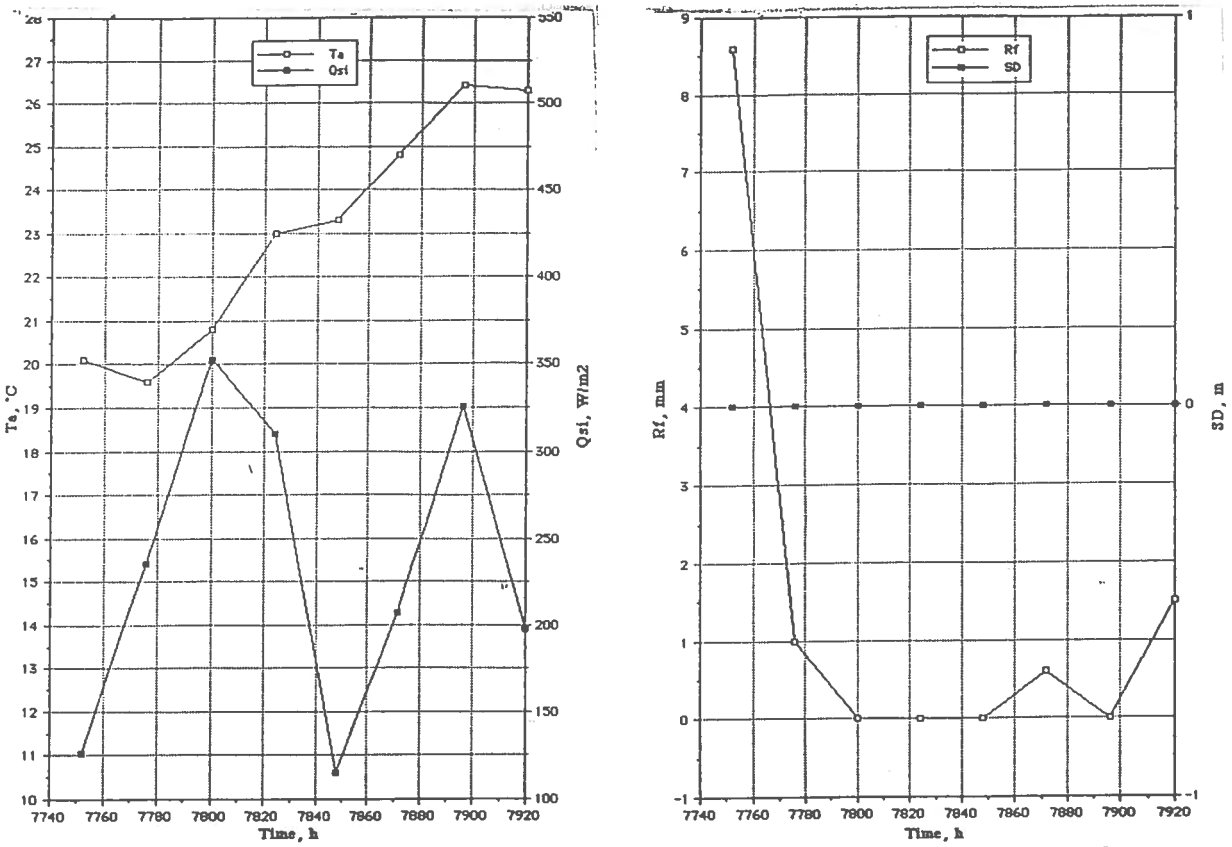


Fig. 7.4 Ambient temperature (Ta) and incoming shortwave radiation (Qsi) vs. time & Rainfall and snow depth vs. time (7740 - 7920 hrs)

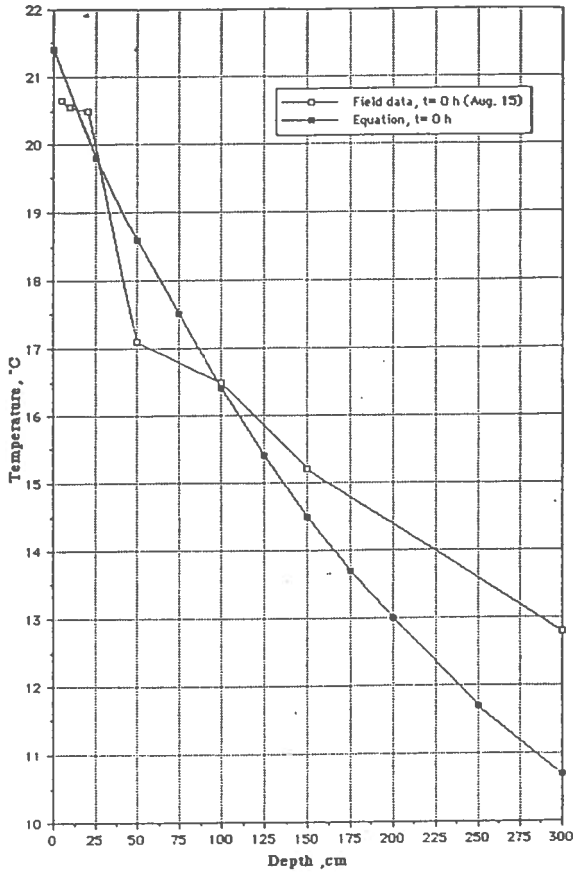


Fig. 7.5 Initial ground temperature profiles

The initial soil temperature and moisture profiles, for August 15th, were obtained from the Eqs.(4 - 61) and (4 - 62) respectively. The soil temperature distribution estimated according to Eq. (4 - 61) did not adequately correspond to experimental data. To remedy this situation, the number of days counted from January 1st to August 15th had to be reduced from 227 to 200. Figure 7.5 shows experimental data vs. estimated data for the reduced number of days.

As one can see the results obtained have a growing divergency below a ground depth of 1.0 m. Therefore, in the future the use of Eq. (4 - 61) shall be restricted to the cases where there is no experimental data available regarding ground temperature.

The computer runs were carried out for the simulation time increments of 24hrs, and for two different modes of the model:

(i) Constant thermal and mass transport properties of soil (PHCM)

(ii) Variable thermal and mass transport properties of soil (CHMM)

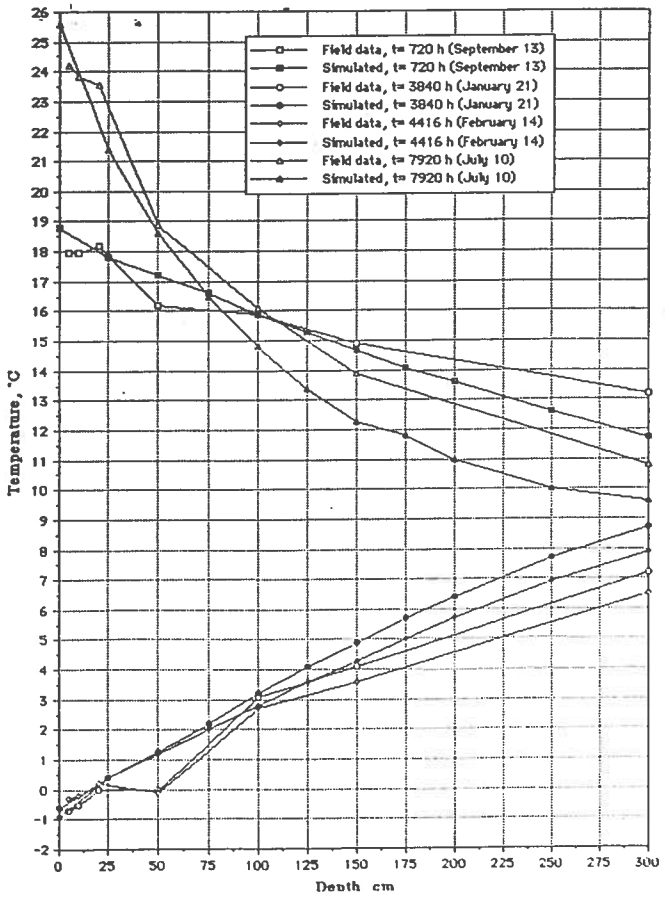


Fig. 7.6 Field and simulated ground temperatures vs. depth of the ground

A uniform soil domain filled with silty clay loam was selected as a representative soil for the site under consideration. Results of the experimental soil temperature vs. those obtained from numerical simulation of the CHMM are shown in Fig. 7.6.

For summer, simulation results closely follow the experimental data within the top layer of soil of 1.0 m depth. Below that level there is a growing divergency due to the inappropriate selection of an initial soil temperature profile.

For winter, the simulated results are even closer to the field data. This can be explained by more stable weather conditions on the soil surface, i.e. a continuous snow cover over the entire winter period. The initial volumetric soil water content profile, obtained from Eq. (4 - 62) is very difficult to verify since no experimental data is available. As one can see from Fig.7.7 , the shape of the profile obtained is very close to being linear. Its value is affected over the entire year by rainfall, snowmelt, and evapotranspiration.

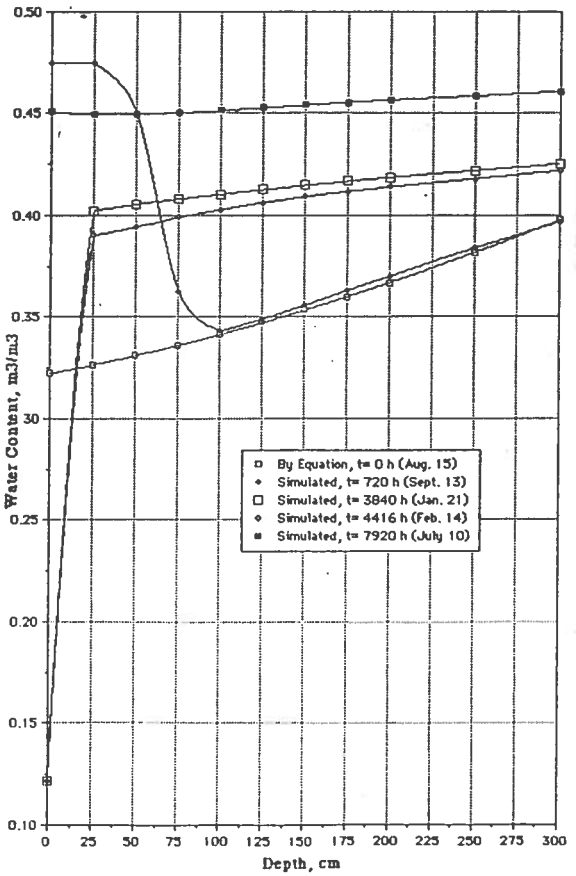


Fig. 7.7 Soil moisture profiles at various time of simulation

In general, after almost one year (7920 out of 8760 hrs) the moisture level is much higher than at the initial time 0 hrs). This means that the initial moisture content obtained from Eq. (4 - 62) does not represent the natural moisture profile. Therefore, it is suggested that, in cases were there is a lack of experimental data regarding soil temperature and moisture content, the model shall be run for natural conditions in the first year in order to obtain real initial profiles. Figure 7.7 also shows soil moisture freezing, which takes place at the top surface layer (0.25m) in winter months (January 21st, and February 14th).

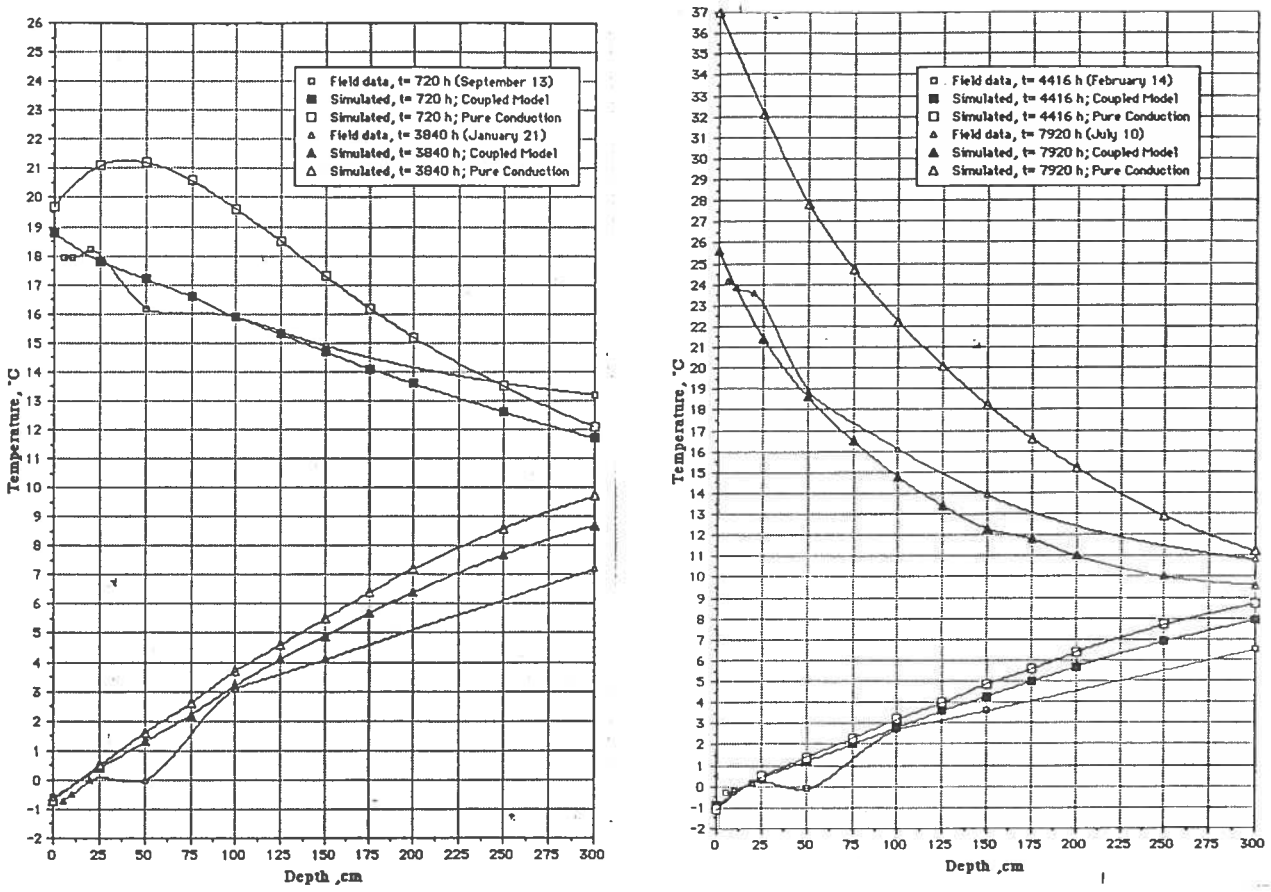


Fig. 7.8 Soil temperature profiles as predicted by CHMM and PHCM

Figure 7.8 contains the comparison made between results obtained from the PHCM and CHMM version of the model. For summer months, results obtained from the CHMM follow very closely the field data what does not happen in the case of the PHCM. The temperature difference between

these two modes can be as high as 13 °C on the surface and about 0.5 °C at depth of 3.0 m. This can be explained by the relatively small volumetric moisture content at the ground surface which is kept for the entire year as a constant by PHCM simulation. The volumetric heat capacity of soil is in this case smaller thus leading to the rapid temperature increase at the surface.

## 8. CONCLUSIONS

The two dimensional mathematical model was developed to predict soil moisture and temperature profiles in ground heat storage. The simulation model was compared to experimental undisturbed soil data recorded by the agrometeorological stations in Canada and good convergent results regarding soil temperatures were obtained. This means that the model is able to simulate the temperature regime in an actual field situation. The model however, was not verified with respect to ground heat storage operation due to a lack of a complete set of experimental data. On the basis of the preliminary results obtained from computer simulation for natural conditions, the following remarks can be made:

(i) The mathematical model developed can be applied to any climate and soil conditions.

(ii) The computer package , G-HEADS, is able to simulate the influence of a large number of design parameters on the thermal performance of the entire ground coupled heat pump system.

(iii) The results of soil temperatures obtained from the G-HEADS are in very good agreement with those recorded by agrometeorological stations in Canada for undisturbed soil conditions.

(iv) Preliminary runs for the natural conditions show that:

- initial soil temperature and moisture profile is very important for accuracy of numerical simulation
- the combined heat and mass flow model shows a superiority over the pure heat conduction model.

(v) A full year simulation of a ground heat pump system for a horizontal pipe spacing of 2m requires about 150 minutes of real time on the IBM or Mackintosh personal computer with math-coprocessor and approximately 16 minutes of CPU time.

# 9. FUTURE RESEARCH AND DEVELOPMENT CONSIDERATIONS

The authors of this report have encountered serious problems in finding a complet set of experimental data in order to verify the simulation model developed. Therefore the following steps are suggested for further reseach :

Step I

(i) Verification of the G-HEADS computer package by comparing simulated and actual results obtained from a model house. The following information shall be collected:

Site

- types of soils and strata (soil sampling)
- ground water conditions (depth variation, water velocity)
- site topography
- laboratory testing of soil samples (grain size, soil density, water content)
- soil temperature and moisture profiles over at least one year of the GHE operation.

Ground Coupled Heat Pump

- heat pump model, size, and a complete data on the thermal performance of the unit.

Ground Heat Storage

- size of ground heat storage
- ground heat exchanger arrangement (series-parallel, single, multiple-layer)
- vertical and horizontal spacing between pipes
- ground heat exchanger material, diameter, length, and circulating fluid
- backfill material in the trench.

Building

- area to be heated or/and cooled
- hourly and/or daily heating and cooling loads and their designed values.

(ii) Model calibration

(iii) Contact resistance model development and implementation

(iv) Upgrading the model by considering the vertical configuration of the GHE

(v) Climatological files development for places in Canada having a good potential for ground heat pump technology

(vi) Expanding Heat Pump file by adding larger models and including desuperheater version as well as models from various manufacturers

(vii) Fully computerized selection of ground coil - circulating fluid - flow rate data

(viii) Preliminary calculations for air distribution system

(ix) Implementing suggestions from ground heat pump industry.

(xii) Package with a choice of I-P or SI units

Step II

(i) Dynamic model of a heat pump unit

(ii) Dynamic model of a direct expansion ground heat pump system

(iii) Upgrading the computer program for hourly simulation

(iv) Dynamic simulation of the entire system.

Step III

(i) Exergy analysis of ground coupled heat pump systems

(ii) Economical analysis of the entire system

(iii) Coupled model of heat and moisture flow for saturated-unsaturated conditions and a multiple-layer soil system.

REFERENCES

ASHRAE Handbook .Fundamentals.(1989). American Society of Heating, Refrigerating and Air Conditioning Engineers, Inc. Atlanta, GA 30329.

Ahmed, A.E., Hamdy, M.Y., Roller, W.L., and Elwell, D.L. (1983). "Technical Feasibility of Utilizing Reject Heat from Power Stations in Greenhouses." Trans., ASAE , 26 (1), 200-206,210.

Bafus, G.R.and G.L. Guymon (1976). Thermal Analysis of Frozen Embankment Islands. Journal for Waterways, Harbors and Coastal Engineering ASCE, Vol. 102, pp. 123-139.

Baladi, J.Y. (1975). Transient Heat and Mass Transfer in Soils. Ph. D. Thesis, Purdue University, West Lafayette.

Baliga, B.R. and S.V. Patankar. (1980). A New Finite Element Formulation for Convection-Diffusion Problems. Numerical Heat Transfer, Vol. 3, pp. 393-409.

Berntsson, T. et al. (1980). "The use of the ground as a heat source for heat pumps in urban areas." Swedish Council for Building Research, Stockholm, Sweden.

Boltz, H. M., and Falkenberg, G., (1949). Neubestimmung der Konstanten der Ångströmschen Stralungsformel. Zeitschrift für Meteorologie Heft 4, s. 97-100.

Bose, J.E. et al. (1985). Design/Data Manual for Closed-Loop Ground-Coupled Heat Pump Systems. ASHRAE, Atlanta.

Bose, J.E., and Parker, J.D. (1983). Ground Coupled Heat Pump Research. ASHRAE Transactions, Vol. 89, Part 1, pp. 375-390.

Budyko, M.I. (1958). The Heat Balance of the Earth Surface. Translated by N.A. Stepanova, U.S. Weather Bureau, Washington.

Burt, T.P., and Williams, P.J., (1976). Hydraulic Conductivity in Frozen Soils. Earth Surface Processes, Vol. 1, pp.349-360.

Campbell, G.S. (1985). Soil Physics with Basic. Elsevier - New York.

Campbell, G.S. (1974). A Simple Method for Determining Unsaturated Conductivity from Moisture Retention Data. Soil Science, Vol. 117, No. 6, pp. 311-314.

Carry,J.W., and S.A. Taylor (1962). Thermally Driven Liquid and Vapor Phase Transfer of Water and Energy in Soil. Soil Sci. Soc. Am. Proc. Vol. 26, pp. 417-420.

Cassel, D.K., Nielsen, D.R., and Biggar, J.W. (1969). Soil Water Movement in Response to Imposed Temperature Gradients. Soil Sci. Soc. Amer. Proc. Vol. 33, pp. 493-500.

Clapp, R.B., and G.M. Hornberger. (1978). Empirical Equations for some Hydraulic Properties. Water Resources Research, Vol. 14, pp.601-604

Dahlquist, G. (1963). A Special Stability Problem for Linear Multistep Methods. B.I.T., Vol. 3, pp. 27-43.

Dakshanamurthy, V. and D.G. Fredlund. (1981). A Mathematical Model for Predicting Moisture Flow in an Unsaturated Soil under Hydraulic and Temperature Gradients. Water Resources Research, Vol. 17, No. 3, pp. 714-722.

Dempsey, B.J., (1978). Mathematical Model for Predicting Coupled Heat and Water Movement in Unsaturated Soils. International Journal of Numerical and Analytical Methods in Geomechanics, Vol. 2, No. 1, pp. 19-34.

Dirksen, C., (1964). Water Movement and Frost Heaving in Unsaturated Soil without External Source of Water, Ph.D. thesis, Cornel University.

Dirksen, C., and R.D. Miller (1966). Closed-System Freezing of Unsaturated Soil. Soil Sci. Soc. Am. Proc, Vol. 130, pp.168-173.

Eagleson, P.S. (1970). Dynamic Hydrology. McGraw-Hill Book Company.

Edwards, J.A. and P.K. Vitta (1985). Heat Transfer from Earth-Coupled Heat Exchangers. Experimental and Analytical Results. ASHRAE Transactions, HI-85-02, pp.70-80.

Edey, S.N, and Joynt, M.J. (1975). Mechanical and Thermal Characteristics of the Soil at Selected Agrometeorological Stations. Agriculture Canada, Tech. Bull. 84, pp. 1 - 40.

Eisenberg, Martin A., and Lawrence E. Malvern, 1973. "On Finite Element Integration in Natural Coordinates," Int. Journal for Numerical Methods in Engineering, Vol. 7, pp.574-575.

Evgin, E., and O.J. Svec (1988). Heat and Moisture Transfer Characteristics of Compacted Mackenzie Silt. Geotechnical Testing Journal, Vol. 11, No. 2, pp. 92-99.

Fisher, R.D. (1983). Models of Simultaneous Heat and Moisture Transfer in Soils. Battele, Columbus Laboratories, ORNL/Sub/88-7800/1806.

Flerchinger,G.N. and K.E. Saxton (1989). Simultaneous Heat and Water Model of a Freezing Snow-Residue-Soil System I. Theory and Development. Transactions of the ASAE, Vol. 32, No. 2, pp. 565-571.

Fordsmand, M. and Eggers-Lura, A. (1981). Analysis of the Factors which Determine the COP of a Heat Pump and a Feasibility Study on Ways and Means of Increasing Same, Commission of European Communities, Contract No. 370-78-EEDK, Final Report, pp.1-124.

Franck, P-A. (1986). A Study of Heat Pump Systems with Low-Temperature Seasonal Heat Storage in Clay., pp.1-226, Chalmers University of Technology, Goteborg, Sweden.

Fuch, M., Campbell, G.S., and Papendick, R.I. (1978). An Analysis of Sensible and Latent Heat Flow in Partially Frozen Unsaturated Soil. Soil Sci. Soc. Am. Journal, Vol. 42, pp.379-385.

Gee, G.W. 1966. Water Movement in Soils as Temperature Gradient. Ph. D. Dissertation, Washington State University, Pullman, WA.

Geiger, R. (1965). The Climate near the Ground. Harvard University Press, Cambridge.

Geraminegad, M. and S.K. Saxena. (1986). A Coupled Thermoelastic Model for Saturated - Unsaturated Porous Media. Géotechnique, Vol. 36, No. $, pp. 539-550.

Gnielinski, V. (1976). New Equations for Heat and Mass Transfer in Turbulent Pipe and Channel Flow. Int.Chem. Eng., Vol. 16, pp. 359-368.

Golub, G.H. and Van Loan, C.F. (1983). Matrix Computations. The Johns Hopkins University Press, Baltimore.

Goodrich, L.E. (1980). Three-Time-Level Methods for the Numerical Solution of Freezing Problems. Cold Regions Science and Technology Vol. 3, pp. 237-242.

Guymon, G.L., Hromadka II, T.V., and R.L. Berg. (1980). A one Dimensional Frost Heave Model Based Upon Simulation of Simultaneous Heat and Water Flux. Cold Regions Science and Technology, Vol. 3, pp. 253-262.

Guymon, G.L., Hromadka II, T.V., and R.L. Berg. (1984). Two-Dimensional Model of Coupled Heat and Moisture Transport in Frost-Heaving Soils. Journal of Energy Resources Technology, Vol. 106, pp. 336-343.

Harlan, R.L. (1971). Water Transport in Frozen and Partially Frozen Porous Media. Proc. Can. Hydrol. Symp. Vol. 1, No. 8, pp. 109-129.

Harlan, R.L., (1973). Analysis of Coupled Heat - Fluid Transport in Partially Frozen Soils. Water Resources Research, Vol. 9, No. 5, pp. 1314-1323.

Hartley, J.G. and W.Z. Black.(1981). Transient Simultaneous Heat and Moisture Transfer in Moist, Unsaturated Soils. Transactions of the ASME, Vol. 103, No. 5, pp. 376-382.

Haverkamp, R., Vauclin, M., Touma, J., Wierenga, P.J., and G. Vachaud., (1977). A Comparison of Numerical Simulation Models for One - Dimensional Infiltration. Soil Sci. Soc. Am. Proc., Vol, 41, No. 2, pp. 285-294.

Haynes, C.D. (1974). Calculating Temperature Profile along a Buried Gas Pipeline. Pipeline and Gas Journal, pp. 48-56.

Hillel, D. (1971). Soil and Water : Physical Principles and Processes. Academic Press, New York.

Hoekstra, P., (1966). Moisture Movement in Soils under Temperature Gradients with the Cold Side Temperature Below Freezing. Water Resources Research, Vol. 2, pp. 241-250.

Holtan, H. N., England, C. B., Lawless, G.P., and G. A. Schumaker. (1968). Moisture Tension Data for Selected Soils on Experimental Watersheds. ARS41-144. Agic. Res. Ser. Beltsville, Md.

Hookey, N.A. (1986). Evaluation and Enhancement of Control-Volume Finite Element Methods for Two-Dimensional Fluid Flow and Heat Transfer. M. Eng. thesis, Department of Mechanical Engineering, McGill University, Montreal, Canada.

Hromadka, II, T.V., Guymon, G.L., and R.L. Berg. (1981). Some Approaches to Modeling Phase Change in Freezing Soils. Cold Regions Science and Technology Vol. 4, pp. 137-145.

Hromadka, II, T.V.and Guymon, G.L.(1982). A Note on Approximation of One-Dimensional Heat Transfer With and Without Phase Change. Numerical Heat Transfer, Vol. 5, pp. 223-232.

Hwang, C.T. (1976). Predictions and Observations on the Behavior of a warm Gas Pipeline on Permafrost. Can. Geotech. Journal Vol. 13, pp. 452-480.

Incropera, F.P. and de Witt , D.P. (1985). Introduction to Heat Transfer. John Wiley $ Sons, Inc., New York.

Jame, Y.W., (1978). Heat and Mass Transfer in Freezing Unsaturated Soil. Ph.D. Thesis University of Saskatchewan.

Johnson, W.S., R.N. Baugh, W.A. Griffith and B.A. McGraw. 1987. Seasonal Performance Evaluation of Two Horizontal-coil Ground-coupled Heat Pump Systems. ASHRAE Transactions, Vol. 93, part 2b, pp. 1875-1885.

de Jong, R. (1982). Assessment of Empirical Parameters that Describe Soil Water Characteristics. Canadian Agricultural Engineering, Vol. 24, No. 2, pp. 65-70.

Jumikis, A.R. (1977). Thermal Geotechnics. Rutgers University Press, New Brunswick.

Jury, W. A. and E.E. Miller. (1974). Measurement of the Transport Coefficients for Coupled Flow of Heat and Moisture in a Medium Sand. Soil Sci. Soc. Amer. Proc., Vol. 38, pp. 551-557.

Karvonen, T., (1988). A Model for Predicting the Effect of Drainage on Soil Moisture, Soil Temperature and Crop Yield. Ph.D. Thesis. University of Technology, Helsinki.

Kay, B.D.,Sheppard, M.I., and J.P.G. Loch.(1978). A Preliminary Comparison of Simulated and Observed Water Redisribution in Soils Freezing under Laboratory and Field Conditions. 3rd Int'l Conf. Permafrost, op.cit.., Vol.1, pp. 30 - 41.

Kay, B.D., and P.H. Groenevelt. (1974). On the Interaction of Water and Heat Transfer in Frozen and Unfrozen Soils. Soil Sci. Soc. Am. Proc., Vol. 38, pp. 395-404.

Kersten, M.S. (1949). Laboratory research for the determination of the thermal properties of soil. Engineering Experiment Station, University of Minnesota.

Koopmans, R.W.R. and R.D. Miller .(1966). Soil Freezing and Soil Water Characteristic Curves. Soil Sci. Soc. Amer. Proc., Vol. 30, pp. 680-685.

Kung, S.K.J., and T.S. Steenhuis. (1986). Heat and Moisture Transfer in a Partly Frozen Nonheaving Soil. Soil Sci. Soc. Am. J., Vol. 50, pp. 1114- 1122.

Lettau, H. H. (1962). A Theoretical Model of Thermal Diffusion in Nonhomogeneous Conductors. Gerlands. Beitr. Geophys. Vol. 71, pp. 257-271.

Lees, M. (1966). A Linear Three Level Difference Scheme for Quasilinear Parabolic Equations. Maths. Comp., Vol. 20, pp. 516-622.

Luikov, A.V. (1966). Heat and Mass Transfer in Capillary Porous Bodies. Pergamon Press, Oxford, U.K.

Lund and Östman (1985). A Numerical Model for Seasonal Storage of Solar Heat in the Ground by Vertical Pipes. Solar Energy, Vol. 34, No. 3/4, pp. 351-366.

McQuiston, F.C., and J.D. Parker. (1988). Heating, Ventilating, and Air Conditioning. Analysis and Design. John Wiley & Sons.

Mei, V.C.(1986). Horizontal Ground-Coil Heat Exchanger. Theoretical and Experimental Analysis. ORNL/CON-193, pp. 119.

Mei, V.C. and Fischer. S.K. (1983). Vertical Concentric Tube Ground Coupled Heat Exchangers. ASHRAE Transactions, Vol. 89, Pt. 2B, DC-83-08..

Milly, P.C.D. (1982). Moisture and Heat Transport in Hysteretic, Inhomogeneous Porous Media: A Matric Head-Based Formulation and a Numerical Model. Water Resources Research, Vol. 18, No. 3, pp. 489-498.

Monteith, J.L.(1973). Principles of Environmental Physics. Edward Arnold Pub.

Nakshabandi, G.A. and H. Kohnke.(1965). Thermal Conductivity and Diffusivity of Soils as Related to Moisture Tension and other Physical Properties. Agricultural Meteorology, Vol.2, pp. 271-279.

Narasimhan, T.N. and P.A. Witherspoon. (1976). An Integrated Finite Difference Method for Analyzing Fluid Flow in Porous Media. Water Resources Research, Vol. 12, No. 1, pp. 57-64.

Newmark, N.M. (1959). A Method for Computation of Structural Dynamics. Proc. Am. Soc. Civ. Eng., Vol. 85, EM3, pp. 67-94.

Oklahoma State University. (1988). Closed - Loop/Ground Source Heat Pump System. Installation Guide.

Outcalt, S.I. 1976). A Numerical Model of Ice Lensing in Freezing Soils. Proc. Second Conf. on Soil-Water Problems in Cold Regions. Edmonton, Alberta, Canada, pp.63-74.

Partin, J.R. 1985. Sizing the Closed-loop Earth Coupling for Heat Pumps. ASHRAE Transactions, Vol. 91, Pt.1, pp. 61-69.

Passerat de Silans, A., Bruckler, L., Thony, J.L., and M.Vauclin. (1989). Numerical Modeling of Coupled Heat and Water Flows during Drying in a saturated Bare Soil- Comparison with Field Observations. Journal of Hydrology, Vol. 105, pp. 109-138.

Penman, H.L. (1948). Natural Evaporation from Open Water, Bare soil and Grass. Proc. Roy. Soc. (London), pp. 120-145.

Pepper, D.W. and A.J. Baker (1988). Finite Differences Versus Finite Elements. In "Handbook of Numerical Heat Transfer" by Minkowycz, W.J., Sparrow, E.M., Schneider, G.E.and R.H.Pletcher. (Eds). John Wiley & Sons, Inc., New York.

Petukhov, B.S. (1970). Heat Transfer and Friction in Turbulent Pipe Flow with Variable Physical Properties. In " Advances in Heat Transfer", Eds. Irvine, T.F. and J.P. Hartnett, Vol. 6, pp. 503-564.

Philip, J.R. (1975). Water Movement in Soil. In "Heat and Mass Transfer in the Biosphere." by de Vries, D.A., and N.H. Afgan (Eds.), pp. 29-47, John Wiley & Sons, Inc., New York.

Philip, J.R. and de Vries D.A. (1957). Moisture Movement in Porous Materials under temperature gradients, Transaction America Geophysical Union, Vol. 38, pp. 222-232.

Pitman,D., and Zuckerman, B. (1967). Effective thermal conductivity of Snow at -88°, -27° and -5°C. Journal of Applied Physics, Vol. 38, No. 6, pp. 2698-2699.

Prakash, C. (1986). An Improved Control Volume Finite Element Method for Heat and Mass Transfer, and for Fluid Flow Using Equal-Order Velocity-Pressure Interpolation. Numerical Heat Transfer, Vol. 9, pp. 259-280.

Puri, V.M. (1986). Feasibility and Performance Curves for Intermittent Earth Tube Heat Exchange, Transactions of ASAE, Vol. 29, pp. 526-532.

Radhakrishina, H.S, Lau, K-C, and A.M.Crawford .(1984). Coupled Heat and Moisture Flow Through Soils. Journal of Geotechnical Engineering, Vol. 110, No. 12, 1766-1784.

Raudkivi, A.J., (1979). Hydrology. Pergamon Press.

Schieldge, J.P., Kahle, A.B. and Alley, R.E. (1982). A Numerical Simulation of Soil Temperature and Moisture Variations for a Bare Field. Soil Science, Vol. 133. pp. 197-207.

Schroeder, C.N. (1974). The Development of an optimized Computer Simulation Model for Heat and Moisture Transfer in Soils. Ph.D. Thesis, Texas A&M University.

Schulz, H., Reuβ, M. and B. Wagner. (1988). Untersuchungen zur saisonalen Speicherung von Niedertemperaturwäme im Erdboden "Erd-Wärmespeicher'. Zwischenbericht zu 032-8616 A3. Landtechnischer Verein in Bayern E.V. Weihenstephan, 8050 Freising, West Germany.

Segerlind, L.J.(1984). Applied Finite Element Analysis, 2nd Edition, John Wiley and Sons,Inc., New York.

Sepaskhah, L.L., Boersma, L.R., Davis, L.R. and D.L. Slegel. (1973). Experimental Analysis of Subsurface Soil Warming and Irrigation System Utilizing Waste Heat. 73-WA/HT-11, pp.1-12, Winter Annual Meeting of the ASME, Detroit, Michigan

Shamsundar, N. and E. Rooz (1988). Numerical Methods for Moving Boundary Problems. In "Handbook of Numerical Heat Transfer" by Minkowycz, W.J., Sparrow, E.M., Schneider, G.E.and R.H.Pletcher. (Eds). John Wiley & Sons, Inc., New York.

Shapiro, H.N. and Moran, M.J. (1978). Simultaneous Heat and Mass Transfer in Soils with Application to Waste Heat Utilization. Proceedings, Six International Heat Transfer Conference, Toronto , Canada, Vol. 3, pp. 19-24.

Shen, S.L. and Ramsey, J.W. (1986). An Investigation of Transient, Two-Dimensional Coupled Heat and Moisture Flow in the Soil Surrounding a Basement Wall. International Journal of Heat and Mass Transfer, Vol. 31, No. 7, pp. 1517-1527.

Sheppard, M.I., Kay, B.D. and J.P.G. Loch.(1978). Development and Testing of a Computer Model of Heat and Mass Flow in Freezing Soils. 3rd Int'l Conf. Permafrost, op.cit.., Vol.1, pp. 75-81.

Slegel, D.L. (1975). Transient Heat and Mass Transfer in Soils in the vicinity of Heated Porous Pipes. Ph.D. Thesis, Oregon State University.

Snow Hydrology. (1956). North Pacific Division, U.S. Army Corps of Engineers. Portland , Orc.

Sophocleous, M. (1979). Analysis of Water and Heat Flow in Unsaturated - Saturated Porous Media. Water Resources Research, Vol.15, No. 5, pp.1195-1206.
Spangler, M.G., and Handy, R.L. 1982. Soil Engineering, Fourth Edition. Harper & Row, New York.

Staple, W.J. and J.J. Lehane. (1954). Movement of Moisture in Unsaturated Soils. Canadian Journal of Agricultural Science. Vol. 34, No.4, pp.329-342.

Stasa, F.L. (1985). Applied Finite Element Analysis For Engineers. CBS College Publishing, Holt, Rinehart and Winston, The Dryden Press, Saunders College Publishing, New York.

Svec, O.J. (1983). Heat Transfer in Ground. In " Annex II - Vertical Earth Heat Pump Systems. (Final Report), pp. 75-104. International Energy Agency

Svec, O.J. (1987). Potential of Ground Heat Source Systems. International Journal of Energy Research, Vol. 11, pp. 573-581.

Svec, O.J. and Palmer J.H.L. (1989). Performance of a Spiral Ground Heat Exchanger for Heat Pump Application. International Journal of Energy Research, Vol. 13, pp. 503-510.

Tarnawski, W. (1982). An analysis of heat and moisture movement in soils in the vicinity of ground heat collectors for use in heat pump systems. Acta Polytechnica Scandinavica, Mechanical Engineering Series No. 82, Helsinki 1982.

Taylor, G.S. and Luthin, J.N. (1978). A Model for Coupled Heat and Moisture Transfer during Freezing. Canadian Geotechnical Journal, Vol. 15, pp. 548-555.

Taylor, S. A. and J. W. Curry (1964). Linear Equations for the Simultaneous Flow of Matter and Energy in Continuous Soil System. Soil Sci. Soc. Am. Proc., Vol. 28, pp. 167-172.

Thomas, H.R, Morgan, K. and R.W. Lewis (1980). A Fully Nonlinear Analysis of Heat and Mass Transfer Problems in Porous Bodies. International Journal for Numerical Methods in Engineering, Vol. 15, pp. 1381-1393.

Thomas, H.R. (1985). Modelling Two-dimensional Heat and Moisture Transfer in Unsaturated Soils, including Gravity Effect, International Journal for Numerical And Analytical Methods in Geomechanics, Vol. 9, pp. 573-588.

Thomas, H.R. (1987). Non-linear Analysis of Heat and Moisture Transfer in Unsaturated Soil, Journal of Engineering Mechanics, Vol. 113, No. 8, pp. 1163-1180.

Thomas, H.R. and R.C. Owen. (1989). A Simulation of Seasonal Temperature and Moisture Content Changes in the Ground. Communications in Applied Numerical Methods, Vol. 5. pp. 171-179.

Tomthwaite, C.W. (1948). An Approach Toward a National Classification of Climate. Geogr. Rev. Vol. 38, pp. 55-94.

van Bavel, C.H.M. (1966). Potential Evaporation : The Combination Concept and Its Experimental Verification. Water Resources Research. Vol. 2. pp. 455-467.

van Wijk, W.R., and de Vries, D.A. (1963). Periodic Temperature Variations in Homogeneous Soil. In "Physics of the plant environment" by Van Wiik, W.E.,North-Holland Publishing Company, Amsterdam.

de Vries, D.A. (1975). Heat Transfer in Soils. In "Heat and Mass Transfer in the Biosphere." by de Vries, D.A., and N.H. Afgan (Eds.), pp. 5-28, John Wiley & Sons, Inc., New York.

de Vries, D.A. (1987). The Theory of Heat and Moisture Transfer in Porous Media Revisited. International Journal of Heat and Mass Transfer, Vol. 30, No. 7, pp. 1343-1350.

de Vries, D.A. (1958). "Simultaneous Transfer of Heat and Moisture in Porous Media, "Transaction of the America Geophysical Union, Vol. 39, No. 5, pp. 909-916.

de Vries, D.A. (1963). Thermal properties of soils. In "Physics of the plant environment" by Van Wiik, W.E.,North-Holland Publishing Company, Amsterdam.

Walker, W.R. and J.D. Sabey. (1981). Studies of Heat Transfer and Water Migration in Soils. DOE/CS/30139-T1 (Final Report). Colorado State University.

Water Furnace International, Inc. (1989). Liquid Source Heat Pumps.

Wilson, E.L. and R.E. Nickel.(1966). Application of the Finite Element Method to Heat Conduction Analysis. Nuclear Engineering and Design, Vol. 4, pp. 276-286.

Yen, Y.C. (1981). Review of Thermal Properties of Snow ,ice, and Sea Ice. CRREL Rep. 81-10, pp. 34, Hanover, New Hempshire, U.S.A.

Yong, R.N. and Warkentin, B.P. (1975). Soil Properties and Behaviours. Elsevier Scientific Publishing Company, New York.

Zienkiewicz, O.C. and C.J. Parekh, and A.J. Wills.(1973). The Application of Finite Elements to Heat Conduction Problems Involving Latent Heat. Rock Mechanics, Vol. 5, pp. 65-76.

Zienkiewicz, O.C. and R.L. Taylor.(1989). The Finite Element Method (Fourth Edition ). McGraw-Hill Book Company, London.

Zlámal, M. 1975. Finite Element Methods in Heat Conduction Problem. Proc. Conf. Finite Element Methods, Brunel University.

**APPENDIX A :** General Physical Relationships of Soil

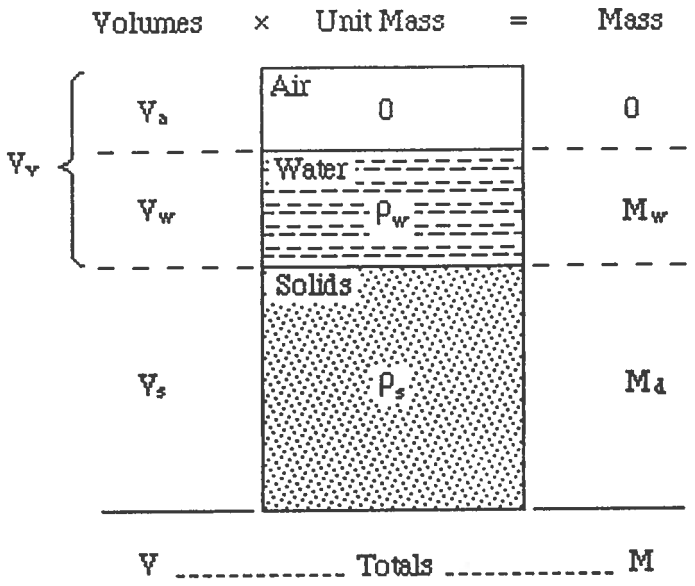


Fig. A.1. Block diagram for calculation of mass-volume relationship in soil.

$V$ = total volume of a soil mass

$V_s$ = volume of the soil particles

$V_v$ = volume of the void spaces

$V_a$ = volume of air-filled voids

$V_w$ = volume of water-filled voids

$M_w$ = mass of water in soil

$M_v$ = mass of water vapor in soil

$M_d$ = dry mass of soil

$M$ = wet mass of soil

Porosity: $$PO = \frac{V_v}{V}\ 100\% \qquad (A.1)$$

Volumetric moisture content: $$\theta = \frac{V_w}{V_s+V_v} \qquad (A.2)$$

Volumetric air content: $$\theta_a = \frac{V_a}{V_s+V_v} \qquad (A.3)$$

Dry bulk density: $$\rho_b = \frac{M_d}{V} \quad (A.4)$$

Density of solids: $$\rho_s = \frac{M_d}{V_s} \quad (A.5)$$

Mass moisture content: $$w = \frac{M_w}{M_d}\ 100\% \quad (A.6)$$

Vapor density: $$\rho_v = \frac{M_v}{V_a} \quad (A.7)$$

PO vs. $\rho_b$: $$PO = 1 - \frac{\rho_b}{\rho_s} \quad (A.8)$$

w vs. $\theta$: $$w = \theta\ \frac{\rho_w}{\rho_b} \quad (A.9)$$

**APPENDIX B :** Apparent Wind Speed Calculation

By referring to Monteith [1973], the wind speed at Z = 2 m above the ground surface with grass cover can be calculated with the following data given:

1. Wind speed at Z = 10 m
2. Thickness of grass, t = 1.5 cm = 0.015 m

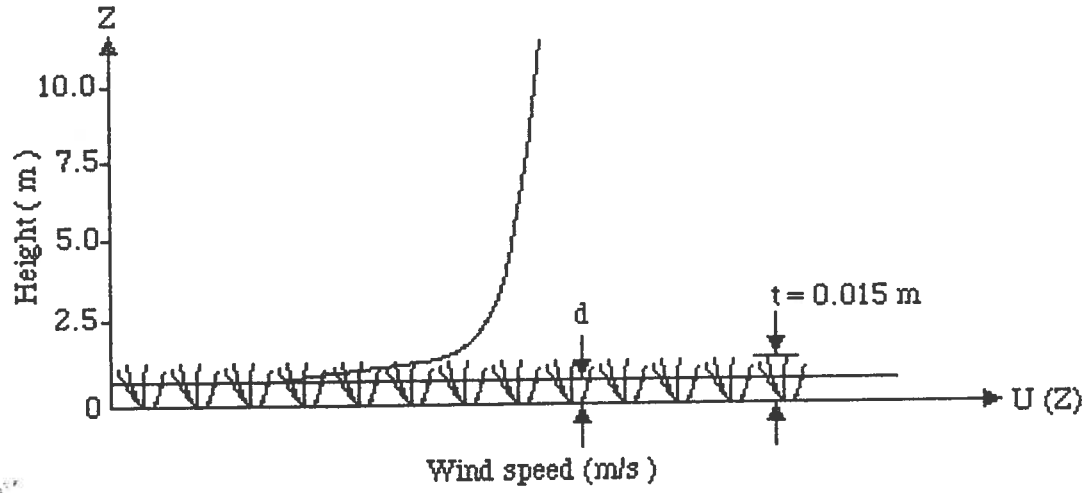


First, the zero plane displacement ( a datum level ) has to be determined, which is

$$d = 10^{(0.9793 \log t - 0.1536)} \qquad (B.1)$$

Second, the roughness length will be determined by equation shown as follow

$$Z_o = 10^{(0.997 \log t - 0.883)} \qquad (B.2)$$

Now, we can calculate the wind speed at Z = 10 m; but first, the parameter a has to be found. The relation between wind speed and height can be expressed formally by:

$$U(Z) = a\{ \ln (Z-d) - \ln Z_o \} \qquad (B.3)$$

where a, d and $Z_o$ are constants introduced before. After substitution of d and $Z_o$, and wind speed at Z = 10 m into the Eq. (B.3), we have

$$U(10) = U_{10} = a \{ \ln ( 10 - 10^{(0.9793 \log t - 0.1536)} ) - \ln ( 10^{(0.997 \log t - 0.883)} ) \}$$

thus

$$a = \frac{U_{10}}{\ln ( 10 - 10^{(0.9793 \log t - 0.1536)} ) - \ln ( 10^{(0.997 \log t - 0.883)} )}$$

Finally, the wind speed at Z = 2.0 m is calculated as follow:

$$U(2) = U_2 = \frac{U_{10}}{\ln ( 10 - 10^{(0.9793 \log t - 0.1536)} ) - \ln ( 10^{(0.997 \log t - 0.883)} )} *$$

$$\{ \ln ( 2 - 10^{(0.9793 \log t - 0.1536)} ) - \ln ( 10^{(0.997 \log t - 0.883)} ) \}$$

Finally, with t = 0.015 m

$$U_2 = 0.81 * U_{10} \qquad (B.4)$$

**APPENDIX C :** Boundary Conditions at the Ground Surface

Summer

Heat and moisture exchange with surrounding atmosphere takes place only on the boundary $\Gamma_1$ (ground surface) of the domain of interest, $\Omega$. Therefore, heat flux from underground to $\Gamma_1$, $(q_n)_{\Gamma_1}$, and moisture flux from underground to $\Gamma_1$, $(v_m)_{\Gamma_1}$, are related to ground surface temperature.

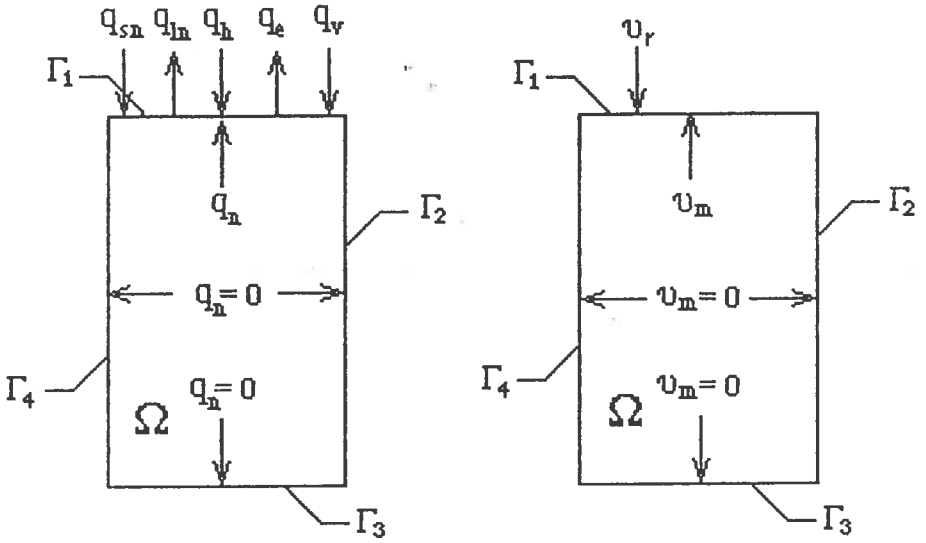


Let us perform an energy balance on the ground surface.

$$q_v + q_n + q_{sn} + q_h - q_{ln} - q_e = 0 \qquad (C.1)$$

where $q_v = q_{adv} = \frac{R_f C_w}{86400}(T_a - T)$

$$q_{sn} = q_{si}(1-a)$$

$$q_h = h(T_a - T)$$

$$q_{ln} = G_{ln} + F_{ln}$$

$$G_{ln} = \sigma T_{ka}^4 (A_1 + B_1 10^{-G_1 e_a})(1 - s_1 N^2)$$

$$F_{ln} = 4\sigma s_2 T_{ka}^3 (T - T_a)$$

$$q_e = [e_3 (q_{sn} - q_{ln}) + e_4](1 - \varepsilon)$$

$$e_3 = \frac{(\Delta/\gamma)A_eL}{(\Delta/\gamma)+1}$$

$$e_4 = \frac{B_vP_dL}{(\Delta/\gamma)+1}$$

T = ground surface temperature

Substituting all terms of the heat flux into (1), we get

$$\frac{R_f\, C_w}{86400}(T_a-T) + q_n + q_{sn} + h(T_a - T) - G_{ln}$$
$$- 4\sigma s_2 T_{ka}^3(T - T_a) - e_3\,(1- \varepsilon)\,(q_{sn} - G_{ln} - 4\sigma s_2 T_{ka}^3(T - T_a)) - e_4\,(1- \varepsilon) = 0 \qquad (C.2)$$

Combining terms and rearrangement, the equation becomes

$$(q_n)_{\Gamma_1} = -q_{sn}[1-e_3(1- \varepsilon)]+G_{ln}[1-e_3\,(1- \varepsilon)]+4\sigma s_2 T_{ka}^3(T - T_a)[1-e_3\,(1- \varepsilon)]+e_4\,(1- \varepsilon)$$
$$- h(T_a - T) - \frac{R_f\, C_w}{86400}\,(T_a-T) \qquad (C.3)$$

Grouping terms containing T, leads to the following expression

$$(q_n)_{\Gamma_1} = Q_1T + Q_2 \qquad (C.4)$$

where: $Q_1 = 4\sigma s_2 T_{ka}^3[1-e_3\,(1- \varepsilon)] + h + \frac{R_f\, C_w}{86400}$

$$Q_2 = - q_{sn}[1-e_3\,(1- \varepsilon)] + G_{ln}[1-e_3\,(1- \varepsilon)]- 4\sigma s_2 T_{ka}^3T_a[1-e_3\,(1- \varepsilon)] - hT_a$$
$$+ e_4[1-e_3\,(1- \varepsilon)] - \frac{R_f\, C_w}{86400}T_a$$

For the boundary condition at $\Gamma_1$, we have

$$(\upsilon_m)_{\Gamma_1} = - \upsilon_r$$

Winter

For winter conditions , when the soil temperature $T_s \leq 0$ and the presence of snow, the boundary conditions are altered since the snow cover is treated as an insulation layer. The electrical analogy of this problem can be represented as follows:

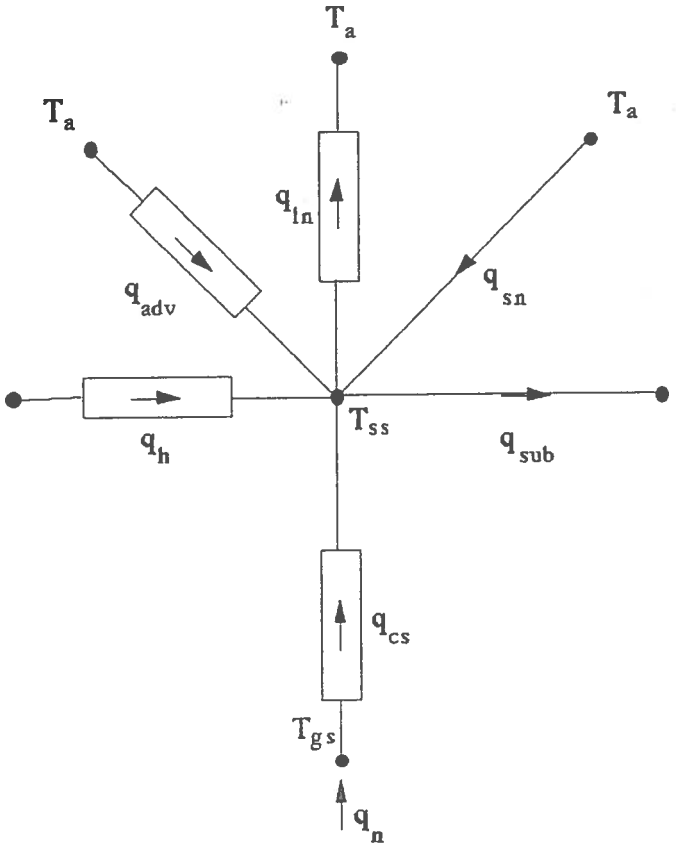


where: $q_{sub}$ = latent heat of sublimation from snow

$q_{sn}$ = net incoming short wave radiation

$q_{ln}$ = net outgoing long wave radiation

$q_h$ = convective heat transfer

$q_{adv}$ = advective energy (rain)

$q_n$ = heat flux by conduction from underground

Please notice that fluxes $q_{ln}$, $q_h$, and $q_{adv}$ are functions of snow surface temperature $T_{ss}$.

The energy balance at the node *ss* has the following form:

$$q_{sn} + q_h + q_{adv} - q_{ln} - q_{sub} + q_{cs} = 0 \qquad \text{(C.6)}$$

or

$$q_{sn} + h(T_a - T_{ss}) + \frac{R_f C_w}{86400}(T_a - T_{ss}) - G_{ln} - 4\sigma s_2 T_{ka}^3 (T_{ss} - T_a) - q_{sub} + q_{cs} = 0 \qquad \text{(C.6a)}$$

From the Fourier's law we have

$$q_{cs} = K_{sn} \frac{T_{gs} - T_{ss}}{\delta_{sn}} \qquad \text{(C.7)}$$

where: $K_{sn}$ = thermal conductivity of snow

$\delta_{sn}$ = thickness of the snow cover

$T_{gs}$ = temperature at the snow-ground interface

Substituting (7) into (6a) and after simple rearrangement the snow surface temperature is expressed as below.

$$T_{ss} = \frac{q_{sn} - G_{ln} - q_{sub} + \left(h + \frac{R_f C_w}{86400} + 4\sigma s_2 T_{ka}^3 T_a + \frac{K_{sn}}{\delta_{sn}} T_{gs}\right)}{h + \frac{R_f C_w}{86400} + 4\sigma s_2 T_{ka}^3 + \frac{K_{sn}}{\delta_{sn}}} \qquad \text{(C.8)}$$

Taking the energy balance at the node *gs* we have:

$$q_n = q_{cs} = K_{sn} \frac{T_{gs} - T_{ss}}{\delta_{sn}} \qquad \text{(C.9)}$$

Substituting (8) into (9) and rearrangement, the heat flux from underground is expressed as:

$$q_n = \frac{K_{sn}}{\delta_{sn}}\left[ T_{gs} - \frac{q_{sn} - G_{ln} - q_{sub} + \left(h + \frac{R_f C_w}{86400} + 4\sigma s_2 T_{ka}^3 T_a + \frac{K_{sn}}{\delta_{sn}} T_{gs}\right)}{h + \frac{R_f C_w}{86400} + 4\sigma s_2 T_{ka}^3 + \frac{K_{sn}}{\delta_{sn}}} \right] \qquad \text{(C.10)}$$

Grouping all terms containing $T_{gs}$, leads to the more covenient form for $q_n$.

$$q_n = \frac{K_{sn}}{\delta_{sn}}\left[ 1 - \frac{K_{sn}}{\left(h + \frac{R_f C_w}{86400} + 4\sigma s_2 T_{ka}^3 + \frac{K_{sn}}{\delta_{sn}}\right)\delta_{sn}} \right] T_{gs}$$

$$+ \frac{\left[ - q_{sn} + G_{ln} + q_{sub} - \left(h + \frac{R_f C_w}{86400} + 4\sigma s_2 T_{ka}^3\right) T_a \right] K_{sn}}{\left(h + \frac{R_f C_w}{86400} + 4\sigma s_2 T_{ka}^3 + \frac{K_{sn}}{\delta_{sn}}\right)\delta_{sn}} \qquad \text{(C.11)}$$

Hence, the heat flux from the underground toward $\Gamma_1$ can be expressed as follows:

$$(q_n)_{\Gamma_1} = Q_1 T_{gs} + Q_2 \qquad \text{(C.12)}$$

where: $$Q_1 = \frac{K_{sn}}{\delta_{sn}}\left[ 1 - \frac{K_{sn}}{\left(h + \frac{R_f C_w}{86400} + 4\sigma s_2 T_{ka}^3 + \frac{K_{sn}}{\delta_{sn}}\right)\delta_{sn}} \right]$$

$$Q_2 = \frac{\left[ - q_{sn} + G_{ln} + q_{sub} - \left(h + \frac{R_f C_w}{86400} + 4\sigma s_2 T_{ka}^3\right) T_a \right] K_{sn}}{\left(h + \frac{R_f C_w}{86400} + 4\sigma s_2 T_{ka}^3 + \frac{K_{sn}}{\delta_{sn}}\right)\delta_{sn}}$$

By implementing this flux into the finite element model and solving it numericaly, the ground surface temperature can be obtained. Then the snow temperature is computed according to equation (C.8). The snow temperature greater than zero indicates that the snow is undergoing isothermal

melting and therefore $T_{ss}$ has to be set back to 0°C and the $T_{gs}$ is recalculated again. The final step of numerical solution is screening all nodes at the ground-snow interface for values of $T_{gs} > 0°$ C. If this happens the $T_{gs}$ is set back 0°C followed by the second iteration.

**APPENDIX D :** Finite Element Matrices

By comparing Eqs.(6 - 20) and (6 - 21) to Eqs. (6 - 22) and (6 - 23), we can get element stiffness matrix of Eq. (6 - 22)

$$\mathbf{D}_K = \int_{A_s} D_K(\nabla N_r \cdot \nabla N_s)\ dA \tag{D.1}$$

element capacitance matrix of Eq. (5.22)

$$\mathbf{C}_K = \int_{A_s} C N_r N_s\ dA \tag{D.2}$$

element force vertor of Eq. (6 - 22)

$$\mathbf{F}_K = \int_{A_s} D_\varepsilon(\nabla N_r \cdot \nabla N_s)\ dA\ \theta_l + \int_{A_s} L\rho_l \varepsilon K_h \frac{\partial N_r}{\partial y}\ dA$$

$$- \int_\Gamma N_r F_K\ d\Gamma - \int_\Gamma L\rho_l \varepsilon F_\theta N_r\ d\Gamma \tag{D.3}$$

element stiffness matrix of Eq. (6 - 23)

$$\mathbf{D}_\theta = \int_{A_s} D_\theta(\nabla N_r \cdot \nabla N_s)\ dA\ \theta_l \tag{D.4}$$

element capacitance matrix of Eq. (6 - 23)

$$\mathbf{C}_\theta = \int_{A_s} N_r N_s\ dA \tag{D.4}$$

element force vector of Eq.(6 - 23)

$$\mathbf{F}_\theta = \int_{A_s} D_T(\nabla N_r \cdot \nabla N_s)\ dA + \int_{A_s} K_h \frac{\partial N_r}{\partial y}\ dA - \int_\Gamma N_r \frac{D_T}{D_K} F_K\ d\Gamma$$

$$- \int_\Gamma N_r F_\theta\ d\Gamma \tag{D.4}$$

Linear triangular element with an area $A_s$ is used in the discretization of the domain of interest, $\Omega$.

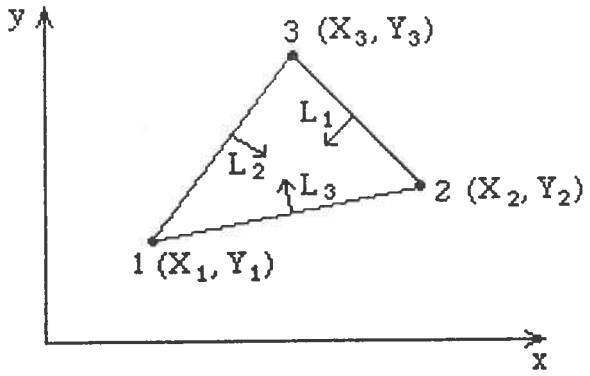


Figure D.1 Linear triangular element with area coordinates, $L_1$, $L_2$, and $L_3$.

Three nodes, one at each corner, are assigned to each $A_s$. For an element $A_s$, using xy-coordinate system, the temperature T and volumetric moisture content $\theta$ can be written as

$$T \approx N_s T_s \tag{D.5}$$

$$\theta_l \approx N_s \theta_{ls} \tag{D.6}$$

where $N_s = [\, N_1 \quad N_2 \quad N_3 \,]$

$$N_1 = \frac{1}{2A_s} [\, (X_2Y_3 - X_3Y_2) + (Y_2 - Y_3)\, x + (X_3 - X_2)\, y \,] \tag{D.7}$$

$$N_1 = \frac{1}{2A_s} [\, (X_3Y_1 - X_1Y_3) + (Y_3 - Y_1)\, x + (X_1 - X_3)\, y \,] \tag{D.8}$$

$$N_3 = \frac{1}{2A_s} [\, (X_1Y_2 - X_2Y_1) + (Y_1 - Y_2)\, x + (X_2 - X_1)\, y \,] \tag{D.9}$$

$$T_s = [\, T_1 \quad T_2 \quad T_3 \,]^T \tag{D.10}$$

$$\theta_{ls} = [\, \theta_1 \quad \theta_2 \quad \theta_3 \,]^T \tag{D.11}$$

The evaluation of integrals has some difficulties if xy-coordinate is used. The difficulties can often be decreased by changing the variables of integration. Therefore, the area coordinates is employed, and the shape functions become

$$N_s = [\, L_1 \quad L_2 \quad L_3 \,] \tag{D.12}$$

For two dimensional element, $\nabla = \mathbf{i} \frac{\partial}{\partial x} + \mathbf{j} \frac{\partial}{\partial y}$ ; therefore

$$\nabla N_r \bullet \nabla N_s = \frac{\partial N_r}{\partial x}\frac{\partial N_s}{\partial x} + \frac{\partial N_r}{\partial y}\frac{\partial N_s}{\partial y} \tag{D.13}$$

and

$$\frac{\partial N_r}{\partial x} = \frac{1}{2A_s}\begin{Bmatrix} b_1 \\ b_2 \\ b_3 \end{Bmatrix} \text{ and } \quad \frac{\partial N_s}{\partial x} = \frac{1}{2A_s}[\, b_1 \quad b_2 \quad b_3 \,] \tag{D.14}$$

$$\frac{\partial N_r}{\partial y} = \frac{1}{2A_s}\begin{Bmatrix} c_1 \\ c_2 \\ c_3 \end{Bmatrix} \text{ and } \quad \frac{\partial N_s}{\partial y} = \frac{1}{2A_s}[\, c_1 \quad c_2 \quad c_3 \,] \tag{D.15}$$

where $b_1 = Y_2 - Y_3$ ; $b_2 = Y_3 - Y_1$ ; $b_3 = Y_1 - Y_2$
$c_1 = X_3 - X_2$ ; $c_2 = X_1 - X_3$ ; $c_3 = X_2 - X_1$

Substitute of Eq. (D.13) into D.1 yields

$$\mathbf{D}_K = D_{Kx}\int_{A_s}\frac{\partial N_r}{\partial x}\frac{\partial N_s}{\partial x}\,dA + D_{Ky}\int_{A_s}\frac{\partial N_r}{\partial y}\frac{\partial N_s}{\partial y}\,dA \tag{D.16}$$

By assumption of isotropic of element, we have $D_{Kx} = D_{Ky} = D_K$. Substitution of Eqs. (D.14) and (D.15) into (D.16), finally yields the stiffness matrix (element) of Eq. (6 - 22):

$$\mathbf{D}_K = \mathbf{D}_{Kx} + \mathbf{D}_{Ky} \tag{D.17}$$

$$\mathbf{D}_{Kx} = \frac{D_K}{4A_s}\begin{bmatrix} b_1^2 & b_1b_2 & b_1b_3 \\ b_1b_2 & b_2^2 & b_2b_3 \\ b_1b_3 & b_2b_3 & b_3^2 \end{bmatrix} \tag{D.17a}$$

$$\mathbf{D}_{Ky} = \frac{D_K}{4A_s}\begin{bmatrix} c_1^2 & c_1c_2 & c_1c_3 \\ c_1c_2 & c_2^2 & c_2c_3 \\ c_1c_3 & c_2c_3 & c_3^2 \end{bmatrix} \tag{D.17b}$$

Substitution of Eqs. (D.12) and $N_r = N_s^T$ into Eq. (D.2), yields

$$\mathbf{C}_K = C\int_{A_s}\begin{bmatrix} L_1^2 & L_1L_2 & L_1L_3 \\ L_1L_2 & L_2^2 & L_2L_3 \\ L_1L_3 & L_2L_3 & L_3^2 \end{bmatrix} dA \tag{D.18}$$

The advantage of using the area coordinates system is the existence of an integration equation that simplifies the evaluation of area integrals (Eisenberg and Malvern, 1973), i.e.

$$\int_{A_s} L_1^a L_2^b L_3^c \, dA = \frac{a!\ b!\ c!}{(a+b+c+2)!} 2A_s \tag{D.19}$$

By applying Eq. (D.19) into evaluation of Eq. (D.18), finally we get the element capacitance matrix of Eq. (6 - 22):

$$\mathbf{C}_K = 2CA_s \begin{bmatrix} \frac{1}{12} & \frac{1}{24} & \frac{1}{24} \\ \frac{1}{24} & \frac{1}{12} & \frac{1}{24} \\ \frac{1}{24} & \frac{1}{24} & \frac{1}{12} \end{bmatrix} \tag{D.20}$$

Substitution of Eqs. (D.13), (D.14) and (D.15) and $N_r = N_s^T$ into Eq. (D.3) yields

$$\mathbf{F}_K = \mathbf{F}_{Kx} + \mathbf{F}_{Ky} + \mathbf{F}_{K_1} + \mathbf{F}_{K_Q} + \mathbf{F}_{K_{FK}} + \mathbf{F}_{K_{F\theta}} \tag{D.21}$$

$$\mathbf{F}_{Kx} = \frac{D\varepsilon}{4A_s} \begin{bmatrix} b_1^2 & b_1b_2 & b_1b_3 \\ b_1b_2 & b_2^2 & b_2b_3 \\ b_1b_3 & b_2b_3 & b_3^2 \end{bmatrix} \begin{Bmatrix} \theta_1 \\ \theta_2 \\ \theta_3 \end{Bmatrix} \tag{D.21a}$$

$$\mathbf{F}_{Ky} = \frac{D\varepsilon}{4A_s} \begin{bmatrix} c_1^2 & c_1c_2 & c_1c_3 \\ c_1c_2 & c_2^2 & c_2c_3 \\ c_1c_3 & c_2c_3 & c_3^2 \end{bmatrix} \begin{Bmatrix} \theta_1 \\ \theta_2 \\ \theta_3 \end{Bmatrix} \tag{D.21b}$$

where $\theta_1$, $\theta_2$, and $\theta_3$ are first approximately as the previous values, then updated during iteration.

$$\mathbf{F}_{K_1} = \frac{L\rho_l\varepsilon K_h}{2} \begin{Bmatrix} c_1 \\ c_2 \\ c_3 \end{Bmatrix} \tag{D.21c}$$

From Appendix C, one can see that $F_K$ in $\mathbf{F}_{K_{FK}}$ is a function of ground surface temperature, T, because $F_K = -\frac{D_K}{K}(Q_1T+Q_2)$ which is a substitution of Eqs. (C.4) and (C.5) into Eq. (6 - 27).

As a first approximation, the temperature T will be taken as the previous time step ground surface temperature, then it will be updated at each iteration untill a certain of accuracy.

$$\mathbf{F}_{K_{FK}} = -F_K \int_{\Gamma} \begin{Bmatrix} L_1 \\ L_2 \\ L_3 \end{Bmatrix} d\Gamma \qquad (D.22)$$

There are three possible sides of a triangular element to be boundary. With integration along one of the sides, it is similar to evaluation of integral of the type (Segerlind, 1984).

$$\int_0^S N_i^a \, N_j^b \, d\Gamma = \int_0^1 l_1^a \, l_2^b \, S \, dl_2 = S \, \frac{a! \; b!}{(a+b+1)!} \qquad (D.23)$$

where $S$ = length of the boundary side of an element

$l_1, l_2$ = natural coordinate system for the one-dimensional element

$N_i, N_j$ = shape functions of the one-dimensional element

For side 1 to be boundary,

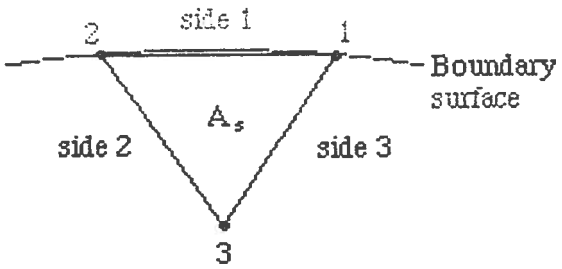


$L_3 = 0$, thus

$$\mathbf{F}_{K_{FK1}} = -F_K \int_{\Gamma_1} \begin{Bmatrix} L_1 \\ L_2 \\ 0 \end{Bmatrix} d\Gamma$$

$$= - F_K S_1 \begin{Bmatrix} \frac{1}{2} \\ \frac{1}{2} \\ 0 \end{Bmatrix} = - \frac{F_K S_1}{2} \begin{Bmatrix} 1 \\ 1 \\ 0 \end{Bmatrix} \qquad \text{(D.24)}$$

where $S_1 = \sqrt{(X_2 - X_1)^2 + (Y_2 - Y_1)^2} = \sqrt{c_3^2 + b_3^2}$

For side 2 to be boundary,

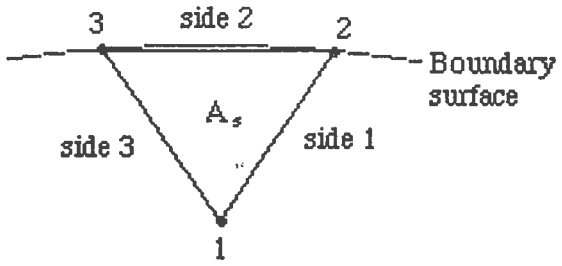


$L_1 = 0$, thus

$$\mathbf{F}_{K_{FK2}} = - F_K \int_{\Gamma_2} \begin{Bmatrix} 0 \\ L_2 \\ L_3 \end{Bmatrix} d\Gamma$$

$$= - F_K S_2 \begin{Bmatrix} 0 \\ \frac{1}{2} \\ \frac{1}{2} \end{Bmatrix} = - \frac{F_K S_2}{2} \begin{Bmatrix} 0 \\ 1 \\ 1 \end{Bmatrix} \qquad \text{(D.25)}$$

where $S_2 = \sqrt{(X_3 - X_2)^2 + (Y_3 - Y_2)^2} = \sqrt{c_1^2 + b_1^2}$

For side 3 to be boundary,

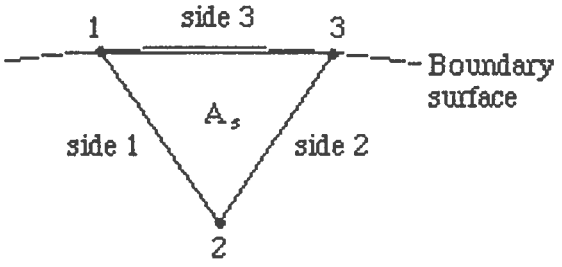


$L_2 = 0$, thus

$$\mathbf{F}_{K_{FK3}} = - F_K \int_{\Gamma_3} \begin{Bmatrix} L_1 \\ 0 \\ L_3 \end{Bmatrix} d\Gamma$$

$$= - F_K S_3 \begin{Bmatrix} \frac{1}{2} \\ 0 \\ \frac{1}{2} \end{Bmatrix} = - \frac{F_K S_3}{2} \begin{Bmatrix} 1 \\ 0 \\ 1 \end{Bmatrix} \qquad (D.26)$$

where $S_3 = \sqrt{(X_1 - X_3)^2 + (Y_1 - Y_3)^2} = \sqrt{c_2^2 + b_2^2}$

Again, $F_\theta$ in $\mathbf{F}_{K_{F\theta}}$ is a function of ground surface temperature, T. But as a first approximation, the temperature T will be taken as the previous time step ground surface temperature, then it will be updated at each iteration. Hence

$$\mathbf{F}_{K_{F\theta}} = - L\rho_l \varepsilon F_\theta \int_{\Gamma} \begin{Bmatrix} L_1 \\ L_2 \\ L_3 \end{Bmatrix} d\Gamma \qquad (D.27)$$

Similar manner as $\mathbf{F}_{K_{FK}}$,

At side 1,

$$\mathbf{F}_{K_{F\theta 1}} = - \frac{L\rho_l \varepsilon F_\theta S_1}{2} \begin{Bmatrix} 1 \\ 1 \\ 0 \end{Bmatrix} \qquad (D.28)$$

At side 2,

$$\mathbf{F}_{K_{F\theta 2}} = - \frac{L\rho_l \varepsilon F_\theta S_2}{2} \begin{Bmatrix} 0 \\ 1 \\ 1 \end{Bmatrix} \qquad (D.29)$$

At side 3,

$$\mathbf{F}_{K_{F\theta 3}} = - \frac{L\rho_l \varepsilon F_\theta S_3}{2} \begin{Bmatrix} 1 \\ 0 \\ 1 \end{Bmatrix} \qquad (D.30)$$

By the similar way, the element matrices of Eq. (6 - 23) are evaluated.

Element stiffness matrix of Eq. (6 - 23)

$$\mathbf{D}_\theta = \mathbf{D}_{\theta x} + \mathbf{D}_{\theta y} \tag{D.31}$$

$$\mathbf{D}_{\theta x} = \frac{D_\theta}{4A_s}\begin{bmatrix} b_1^2 & b_1b_2 & b_1b_3 \\ b_1b_2 & b_2^2 & b_2b_3 \\ b_1b_3 & b_2b_3 & b_3^2 \end{bmatrix} \tag{D.31a}$$

$$\mathbf{D}_{\theta y} = \frac{D_\theta}{4A_s}\begin{bmatrix} c_1^2 & c_1c_2 & c_1c_3 \\ c_1c_2 & c_2^2 & c_2c_3 \\ c_1c_3 & c_2c_3 & c_3^2 \end{bmatrix} \tag{D.31b}$$

Element capacitance matrix of Eq. (6 - 23)

$$\mathbf{C}_\theta = 2A_s\begin{bmatrix} \frac{1}{12} & \frac{1}{24} & \frac{1}{24} \\ \frac{1}{24} & \frac{1}{12} & \frac{1}{24} \\ \frac{1}{24} & \frac{1}{24} & \frac{1}{12} \end{bmatrix} \tag{D.32}$$

Element force vector of Eq. (6 - 23)

$$\mathbf{F}_\theta = \mathbf{F}_{\theta x} + \mathbf{F}_{\theta y} + \mathbf{F}_{\theta_1} + \mathbf{F}_{\theta Q} + \mathbf{F}_{\theta FK} + \mathbf{F}_{\theta F\theta} \tag{D.33}$$

$$\mathbf{F}_{\theta x} = \frac{D_T}{4A_s}\begin{bmatrix} b_1^2 & b_1b_2 & b_1b_3 \\ b_1b_2 & b_2^2 & b_2b_3 \\ b_1b_3 & b_2b_3 & b_3^2 \end{bmatrix}\begin{Bmatrix} T_1 \\ T_2 \\ T_3 \end{Bmatrix} \tag{D.33a}$$

$$\mathbf{F}_{\theta y} = \frac{D_T}{4A_s}\begin{bmatrix} c_1^2 & c_1c_2 & c_1c_3 \\ c_1c_2 & c_2^2 & c_2c_3 \\ c_1c_3 & c_2c_3 & c_3^2 \end{bmatrix}\begin{Bmatrix} T_1 \\ T_2 \\ T_3 \end{Bmatrix} \tag{D.33b}$$

where $T_1$, $T_2$, and $T_3$ are the present time step temperatures at node 1, 2, and 3 which are generated by Eq. (6 - 22).

$$\mathbf{F}_{\theta_1} = \frac{K_h}{2}\begin{Bmatrix} c_1 \\ c_2 \\ c_3 \end{Bmatrix} \tag{D.33c}$$

At side 1,

$$\mathbf{F}_{\theta FK1} = -\frac{D_T}{2D_K} F_K S_1 \begin{Bmatrix} 1 \\ 1 \\ 0 \end{Bmatrix} \tag{D.33d}$$

$$\mathbf{F}_{\theta F\theta 1} = -\frac{F_\theta S_1}{2} \begin{Bmatrix} 1 \\ 1 \\ 0 \end{Bmatrix} \tag{D.33e}$$

At side 2,

$$\mathbf{F}_{\theta FK2} = -\frac{D_T}{2D_K} F_K S_2 \begin{Bmatrix} 0 \\ 1 \\ 1 \end{Bmatrix} \tag{D.33f}$$

$$\mathbf{F}_{\theta F\theta 2} = -\frac{F_\theta S_2}{2} \begin{Bmatrix} 0 \\ 1 \\ 1 \end{Bmatrix} \tag{D.33g}$$

At side 3,

$$\mathbf{F}_{\theta FK3} = -\frac{D_T}{2D_K} F_K S_3 \begin{Bmatrix} 1 \\ 0 \\ 1 \end{Bmatrix} \tag{D.33h}$$

$$\mathbf{F}_{\theta F\theta 3} = -\frac{F_\theta S_3}{2} \begin{Bmatrix} 1 \\ 0 \\ 1 \end{Bmatrix} \tag{D.33i}$$

where $F_K$ and $F_\theta$ are evaluated based on the ground surface temperature at present time step which are generated by Eq. (6 - 22).

**APPENDIX E :** Three-Time-Step Finite Difference Model

The equation proposed by Zienkiewicz (1989) for the three-point recurence schemes has the following form:

$$[\gamma C + \beta \Delta t K] a_{n+1} + [(1 - 2\gamma) C + (\tfrac{1}{2} - 2\beta + \gamma) \Delta t K] a_n + [-(1 - \gamma) C + (\tfrac{1}{2} + \beta - \gamma) \Delta t K] a_{n-1} + \Delta t \bar{f} = 0 \qquad (E.1)$$

where

$$\bar{f} = f_{n+1}\beta + f_n(\tfrac{1}{2} - 2\beta + \gamma) + f_{n-1}(\tfrac{1}{2} + \beta - \gamma)$$

we can rearrange it to the following form:

$$\left[\frac{\gamma C}{\Delta t} + \beta K\right] a_{n+1} + \left[\frac{(1 - 2\gamma)}{\Delta t} C + (\tfrac{1}{2} - 2\beta + \gamma) K\right] a_n + \left[-\frac{(1 - \gamma)}{\Delta t} C + (\tfrac{1}{2} + \beta - \gamma) K\right] a_{n-1} + \bar{f} = 0$$

Further simplication leads to

$$\frac{C}{2\Delta t}[2\gamma a_{n+1} + 2(1 - 2\gamma) a_n + 2(1 - \gamma) a_{n-1}] + K[\beta a_{n+1} + (\tfrac{1}{2} - 2\beta + \gamma) a_n + (\tfrac{1}{2} + \beta - \gamma) a_{n-1}] + \bar{f} = 0 \qquad (E.2)$$

Let $\beta_1 = 2\gamma$ ; $\beta_2 = 2(1-\gamma)$ ; $\beta_3 = 2(\gamma - 1)$ ; $\beta_4 = \beta$ ; $\beta_5 = \tfrac{1}{2} - 2\beta - \gamma$ ; $\beta_6 = \tfrac{1}{2} + \beta - \gamma$

Hence,

$$[C]\left(\frac{\beta_1 a_{n+1} + \beta_2 a_n + \beta_3 a_{n-1}}{2\Delta t}\right) + [K](\beta_4 a_{n+1} + \beta_5 a_n + \beta_6 a_{n-1}) + \bar{f} = 0 \qquad (E.3)$$

where: $\bar{f} = \beta_4 f_{n+1} + \beta_5 f_n + \beta_6 f_{n-1}$

$2\Delta t = \Delta t_{m-1/m} + \Delta t_{m/m+1}$

$\Delta t_{m-1/m} = t_m - t_{m-1}$

$\Delta t_{m/m+1} = t_{m+1} - t_m$

Now, let us compare this equation to the first order differential equation (Eq. (6 - 34)), we get

$$\dot{a} = \frac{\beta_1 a_{n+1} + \beta_2 a_n + \beta_3 a_{n-1}}{2\Delta t} \qquad (E.4a)$$

$$a = \beta_4 a_{n+1} + \beta_5 a_n + \beta_6 a_{n-1} \qquad (E.4b)$$

$$f = \beta_4 f_{n+1} + \beta_5 f_n + \beta_6 f_{n-1} \qquad \text{(E.4c)}$$

Analogously, Eq. (E.4) is called the finite difference method.

Substitute Eq. (E.4) into Eq. (6 - 22), we get

$$\mathbf{D}_K [\beta_4 \mathbf{T}_{n+1} + \beta_5 \mathbf{T}_n + \beta_6 \mathbf{T}_{n-1}] + \mathbf{D}_\varepsilon [\beta_4 \boldsymbol{\theta}_{n+1} + \beta_5 \boldsymbol{\theta}_n + \beta_6 \boldsymbol{\theta}_{n-1}]$$

$$+ \mathbf{C}_K \left[ \frac{\beta_1 \mathbf{T}_{n+1} + \beta_2 \mathbf{T}_n + \beta_3 \mathbf{T}_{n-1}}{2\Delta t} \right] + \bar{\mathbf{F}}_K = 0 \qquad \text{(E.5)}$$

after rearranging, we have

$$\mathbf{DC41}_1\{\mathbf{T}_{n+1}\} = \mathbf{DC52}_1\{\mathbf{T}_n\} + \mathbf{DC63}_1\{\mathbf{T}_{n-1}\} + \mathbf{D456}_1 - 2\Delta t \bar{\mathbf{F}}_K \qquad \text{(E.6)}$$

where

$$\mathbf{DC41}_1 = 2\Delta t \beta_4 \mathbf{D}_K + \beta_1 \mathbf{C}_K$$
$$\mathbf{DC52}_1 = -(2\Delta t \beta_5 \mathbf{D}_K + \beta_2 \mathbf{C}_K)$$
$$\mathbf{DC63}_1 = -(2\Delta t \beta_6 \mathbf{D}_K + \beta_3 \mathbf{C}_K)$$
$$\mathbf{D456}_1 = -\mathbf{D}_\varepsilon [2\Delta t \beta_4 \boldsymbol{\theta}_{n+1} + 2\Delta t \beta_5 \boldsymbol{\theta}_n + 2\Delta t \beta_6 \boldsymbol{\theta}_{n-1}]$$
$$\bar{\mathbf{F}}_K = \beta_4 \mathbf{F}_{K_{n+1}} + \beta_5 \mathbf{F}_{K_n} + \beta_6 \mathbf{F}_{K_{n-1}}$$

Similarly, substituting Eq. (E.4) into Eq. (6 - 23),

$$\mathbf{DC41}_2\{\boldsymbol{\theta}_{n+1}\} = \mathbf{DC52}_2\{\boldsymbol{\theta}_n\} + \mathbf{DC63}_2\{\boldsymbol{\theta}_{n-1}\} + \mathbf{D456}_2 - 2\Delta t \bar{\mathbf{F}}_\theta \qquad \text{(E.7)}$$

where

$$\mathbf{DC41}_2 = 2\Delta t \beta_4 \mathbf{D}_\theta + \beta_1 \mathbf{C}_\theta$$
$$\mathbf{DC52}_2 = -(2\Delta t \beta_5 \mathbf{D}_\theta + \beta_2 \mathbf{C}_\theta)$$
$$\mathbf{DC63}_2 = -(2\Delta t \beta_6 \mathbf{D}_\theta + \beta_3 \mathbf{C}_\theta)$$
$$\mathbf{D456}_2 = -\mathbf{D}_T [2\Delta t \beta_4 \mathbf{T}_{n+1} + 2\Delta t \beta_5 \mathbf{T}_n + 2\Delta t \beta_6 \mathbf{T}_{n-1}]$$
$$\bar{\mathbf{F}}_\theta = \beta_4 \mathbf{F}_{\theta_{n+1}} + \beta_5 \mathbf{F}_{\theta_n} + \beta_6 \mathbf{F}_{\theta_{n-1}}$$

Eqs. (E.6) and (E.7) can be used to solve the temperature and liquid content in the domain of interest. First, by assuming $\boldsymbol{\theta}_{n+1} = \boldsymbol{\theta}_n$ , we solve for $\mathbf{T}_{n+1}$ by Eq. (E.6). Second, using calculated $\mathbf{T}_{n+1}$ , we can solve for $\boldsymbol{\theta}_{n+1}$ by Eq. (E.7). Then, second iteration is performed to get the corrected $\mathbf{T}_{n+1}$ by Eq. (E.6) and $\boldsymbol{\theta}_{n+1}$ by Eq. (E.7).

**APPENDIX F :** Solution of Banded Matrix System by Backward Substitution Method

A matrix **A** is said to be banded when all its nonzero elements are confined within a band form by diagonals parallel to the main diagonal. Thus, $A_{ij} = 0$ when $| i - j | > \beta$, and $A_{k,k-\beta} = 0$ or $A_{k,k+\beta} = 0$ for at least one value of k, where $\beta$ is the half-bandwidth and $2\beta+1$ is the bandwidth. The band of the matrix is a set of elements for which $| i - j | \leq \beta$. In order words, for a certain row, i, all elements having column indices in the range $i-\beta$ to $i+\beta$, a total of $2\beta+1$ elements per row, belong to the band. This can be much smaller than the order of the matrix.

When the matrix is symmetric, only a semiband needs to be represented. The upper semiband consists of all the elements in the upper portion of the band, i.e. $0 < j - i < \beta$; the lower semiband consists of all the elements in the lower portion of the band, i.e. $0 < j - i < \beta$, in both cases a total of $\beta$ elements per row. It is called semiband and define the bandwidth as equal to $\beta$ or to $\beta+1$ (Segerlind, 1984).

The diagonal storage of a symmetric band matrix **A** in an array **AN( I , J )** is illustrated by means of an example in Figure K.1. If the matrix is of order n and half-bandwidth $\beta$, the dimensions of the array are n by $\beta+1$.

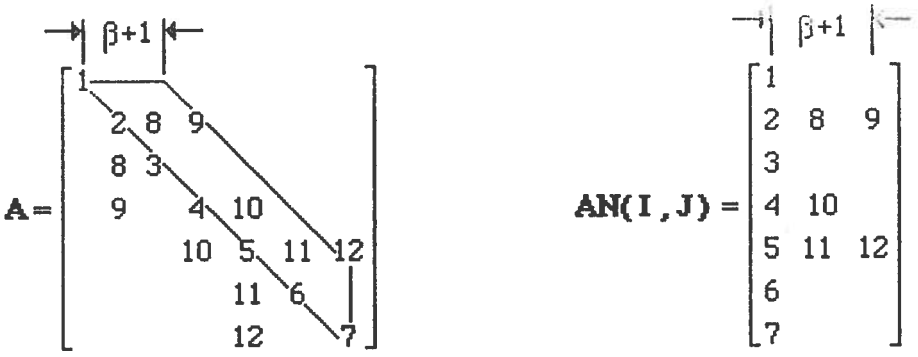


Figure K.1 A symmetric $7 \times 7$ band matrix (a) with bandwidth equal to 5, and its $7 \times 3$ diagonal storage (b) in the rectangular array **AN( I, J )**.

When a system of linear equations has a banded matrix of coefficients and the system is solved by Gauss elimination, with pivots taken from the diagonal, all arithmetic is confined to the band and no new nonzero elements are generated outside the band. Gauss elimination can be carried out in place, since a memory location was already reserved for any new nonzero that might be introduced.

Let $\mathbf{Ax} = \mathbf{b}$ be the linear system that we wish to solve by the backward substitution method [Golub and Van Loan, 1983], and $\mathbf{A} = \mathbf{U}^T\mathbf{DU}$ be the factorization of the symmetric matrix **A**. The linear system becomes $\mathbf{U}^T\mathbf{DUx} = \mathbf{b}$, which, if $\mathbf{Z} = \mathbf{DUx}$ and $\mathbf{W} = \mathbf{Ux}$, can be written :

$$\mathbf{U}^T\mathbf{Z} = \mathbf{b} \tag{F.1a}$$

$$\mathbf{DW} = \mathbf{Z} \tag{F.1b}$$

$$\mathbf{Ux} = \mathbf{W} \tag{F.1c}$$

where

**A** = the symmetric n × n matrix

**U** = the upper triangular unit diagonal matrix

D = the diagonal matrix

**b** = the right-hand side vector

**x** = the vector of unknown

**W** = the resulting vector

The system (Eqs. (F.1)) is solved, first for Z, then for W, and finally for x. Since U and $U^T$ are triangular and D is diagonal, the solution of Eqs. (F.1) is straightforward. Consider the following example :

$$A = U^T D U = \begin{bmatrix} 1 & 0 & 0 \\ d & 1 & 0 \\ e & f & 1 \end{bmatrix} \begin{bmatrix} a & 0 & 0 \\ 0 & b & 0 \\ 0 & 0 & c \end{bmatrix} \begin{bmatrix} 1 & d & e \\ 0 & 1 & f \\ 0 & 0 & 1 \end{bmatrix} \tag{F.2}$$

Then, the Eq. (F.1a) is

$$\begin{bmatrix} 1 & 0 & 0 \\ d & 1 & 0 \\ e & f & 1 \end{bmatrix} \begin{bmatrix} z_1 \\ z_2 \\ z_3 \end{bmatrix} = \begin{bmatrix} b_1 \\ b_2 \\ b_3 \end{bmatrix} \tag{F.3}$$

from which we immediately compute, by forward substitution :

$$z_1 = b_1 \tag{F.4a}$$

$$z_2 = b_2 - dz_1 \tag{F.4b}$$

$$z_3 = b_3 - ez_1 - fz_2 \tag{F.4c}$$

The second equation of the system (Eq. (F.1b)) is

$$\begin{bmatrix} a & 0 & 0 \\ 0 & b & 0 \\ 0 & 0 & c \end{bmatrix} \begin{bmatrix} w_1 \\ w_2 \\ w_3 \end{bmatrix} = \begin{bmatrix} z_1 \\ z_2 \\ z_3 \end{bmatrix} \tag{F.5}$$

so that

$$w_1 = \frac{z_1}{a} \tag{F.6a}$$

$$w_2 = \frac{z_2}{b} \tag{F.6b}$$

$$w_3 = \frac{z_3}{c} \tag{F.6c}$$

Since usually the inverse of D is stored in memory, rather D itself, Eq. (F.6) involves only multiplications, which are faster than divisions on most computers.

Finally, the Eq. (F.1c) is

$$\begin{bmatrix} 1 & d & e \\ 0 & 1 & f \\ 0 & 0 & 1 \end{bmatrix} \begin{bmatrix} x_1 \\ x_2 \\ x_3 \end{bmatrix} = \begin{bmatrix} w_1 \\ w_2 \\ w_3 \end{bmatrix} \tag{F.7}$$

The solution is easily obtained by backward substitution :

$$x_3 = w_3 \tag{F.8a}$$

$$x_2 = w_2 - fx_2 \tag{F.8b}$$

$$x_1 = w_1 - dx_2 - ex_3 \tag{F.8c}$$

Similarly, this procedure is applied to solve the unknown temperatures and water contents from the simultaneous matrix equations which are in banded form.

**APPENDIX G:** Domain of Finite Element Mesh

Given domain $\Omega$ is discretized into a large number of finite elements $A_s$ having triangular shaped

$$\Omega = \sum_{s=1}^{m} A_s$$

where $\Omega$ = total area of domain of interest

$A_s$ = area of an element

m = total number of elements

For each element at each vertex nodal points are specified i.e., this produces three nodes for each element $A_s$. Therefore any two adjoining triangular elements may have one common edge and two common nodes or just only one common node (elements connected at the vertex). A special condition must be fulfilled during the domain discretization: two adjoining elements must share the entire common border rather than a portion of it. The method of node numbering is very important since it has a strong influence on computer memory requirement and computer execution time. Therefore in this report the nodes are numbered consecutively from one to the total number. The same idea is used to define the elements. An example of nodes and elements numbering is shown in figure below.

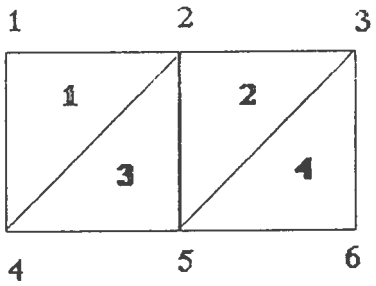


where: 1, 2, 3, 4, 5, 6 = node numbers
**1, 2, 3, 4** = element numbers

In this report the following domains $\Omega$ are considered:

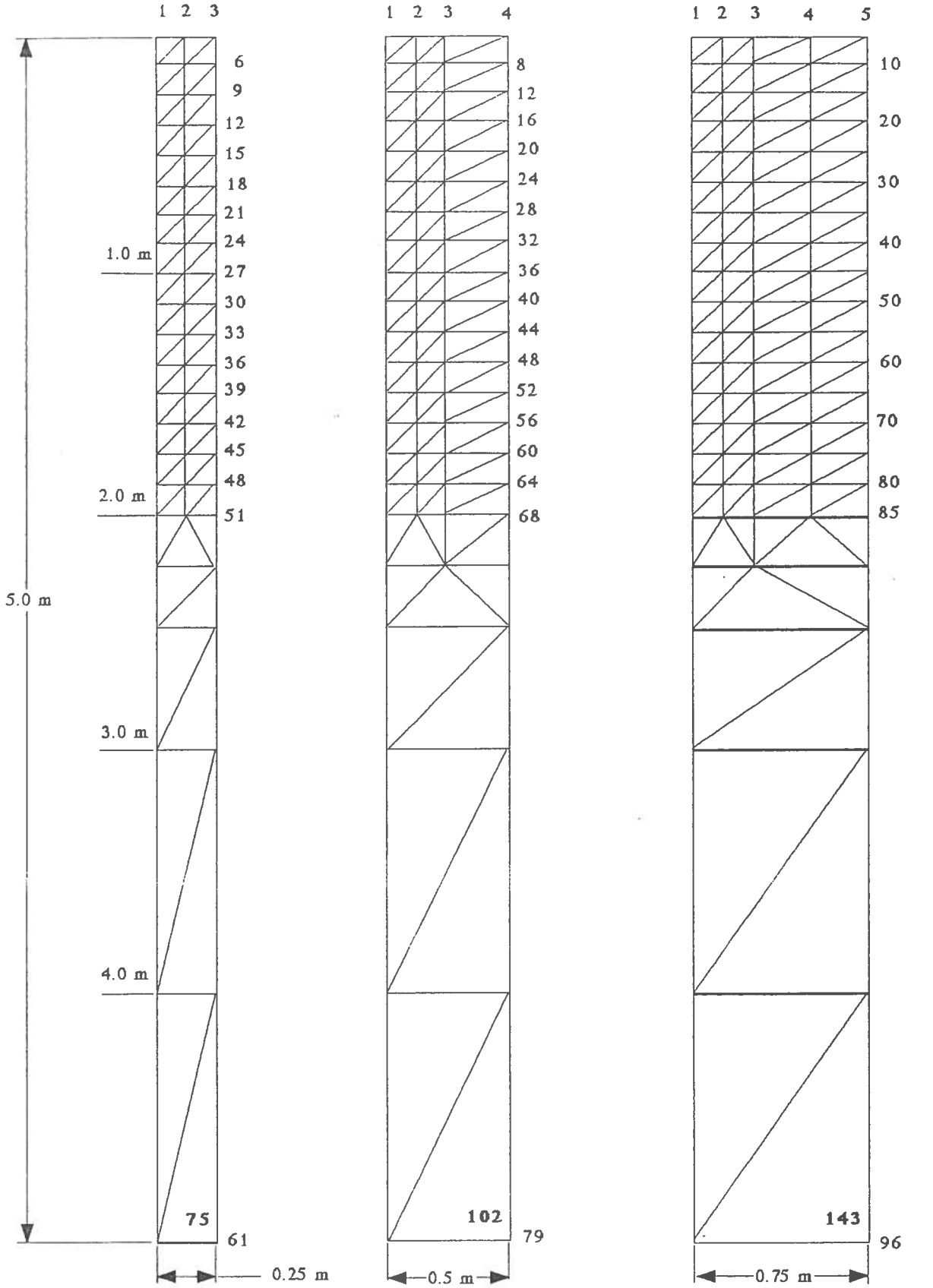


| | | | |
|---|---|---|---|
| Number of elements : | 75 | 102 | 143 |
| Number of nodes : | 61 | 79 | 96 |

The horizontal GHE can be located at any node of the left edge of the domain $\Omega$ within the depth of 2.0 m. The GHE is represented as a point since the pipe diameter is found to be small in comparison to the size of triangular element. Therefore at the GHE node the calculated temperature of the outside pipe wall is substituted. Details about temperature calculation at the pipe-soil interface can be found in Section 4.5 .

**APPENDIX H :** Model of Isothermal Phase Change

According to isothermal phase change approach, for the freezing process,the node should be kept at 0 °C as long as soil water is available for freezing. No jumping of temperature over the phase change front is allowed. For each time increment the node temperature is controlled to find out if phase change is taking place. Figures 1H, 2H and 3H show schematicaly the isothermal phase change approach used in this report.

Example: The node "i" is surrounded by four finite elements. Following the lumped matrix approach the weighted temperature is calculated as follows:

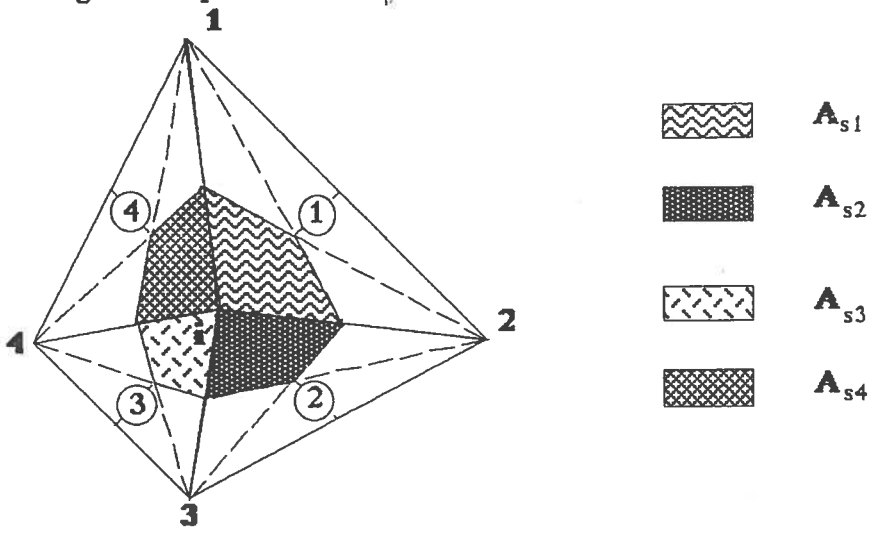


$$T_{ical} = \frac{A_{s1}\ T_{e1} + A_{s2}\ T_{e2} + A_{s3}\ T_{e3} + A_{s4}\ T_{e4}}{A_{s1} + A_{s2} + A_{s3} + A_{s4}} \qquad (H.1)$$

where: $A_{s1}, A_{s2}, A_{s3}, A_{s4}$ = subareas associated to the node "i"

$T_{e1}, T_{e2}, T_{e3}, T_{e4}$ = average temperatures of associated elements

The subareas are equal to

$$A_{s1} = \frac{1}{3} A_1 \ ; A_{s2} = \frac{1}{3} A_2 \ ; A_{s3} = \frac{1}{3} A_3 \ ; A_{s4} = \frac{1}{3} A_4 \qquad (H.2)$$

The element temperatures are taken as an arithmetic mean of three nodes, i.e.:

$$T_{e1} = \frac{1}{3} (T_1 + T_2 + T_i) \ ; \ T_{e2} = \frac{1}{3} (T_2 + T_3 + T_i)$$

$$T_{e3} = \frac{1}{3}\,(T_3 + T_4 + T_i)\;;\; T_{e4} = \frac{1}{3}\,(T_4 + T_1 + T_i) \qquad \text{(H.3)}$$

Substituting (2) and (3) to (1) we have:

$$T_{ical} = \frac{A_1\,T_{e1} + A_2\,T_{e2} + A_3\,T_{e3} + A_4\,T_{e4}}{A_1 + A_2 + A_3 + A_4} \qquad \text{(H.4)}$$

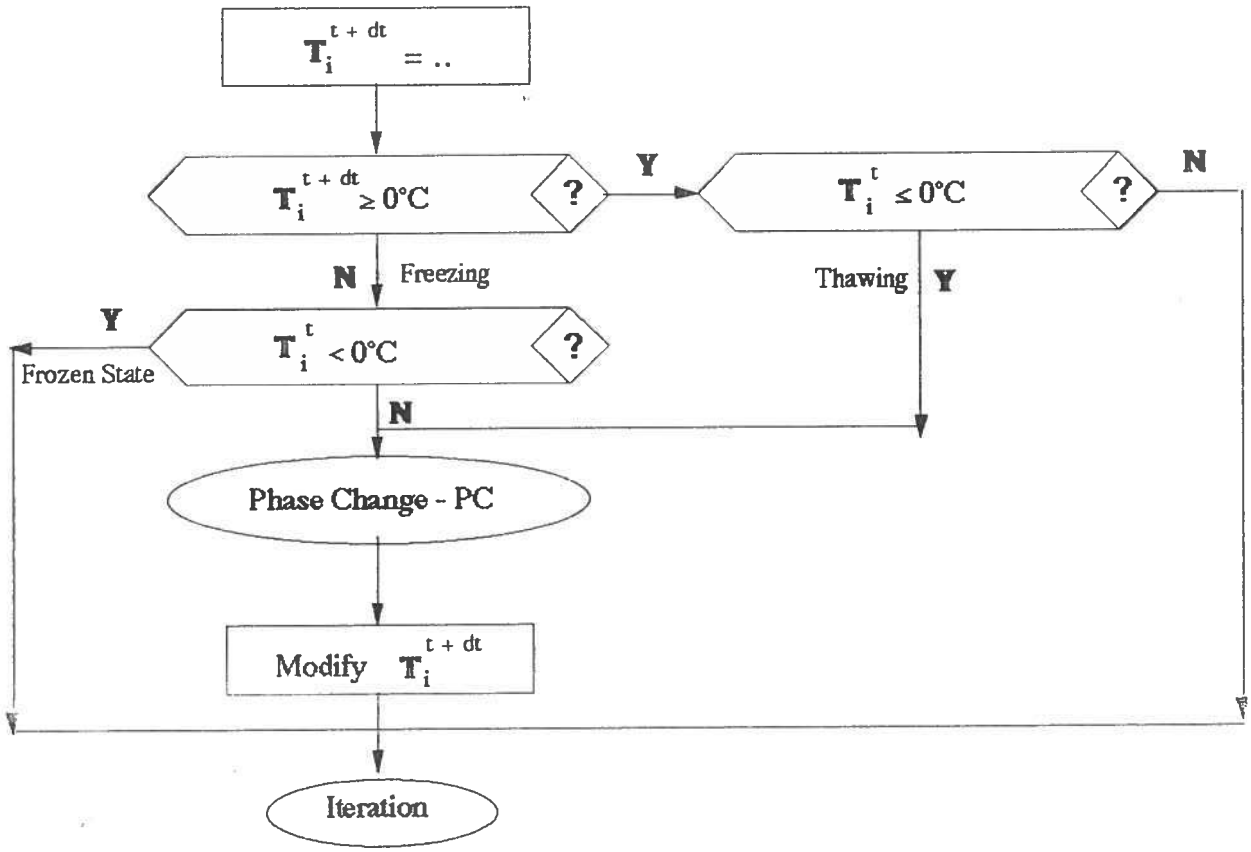


Fig. 1H. General Phase Change Approach

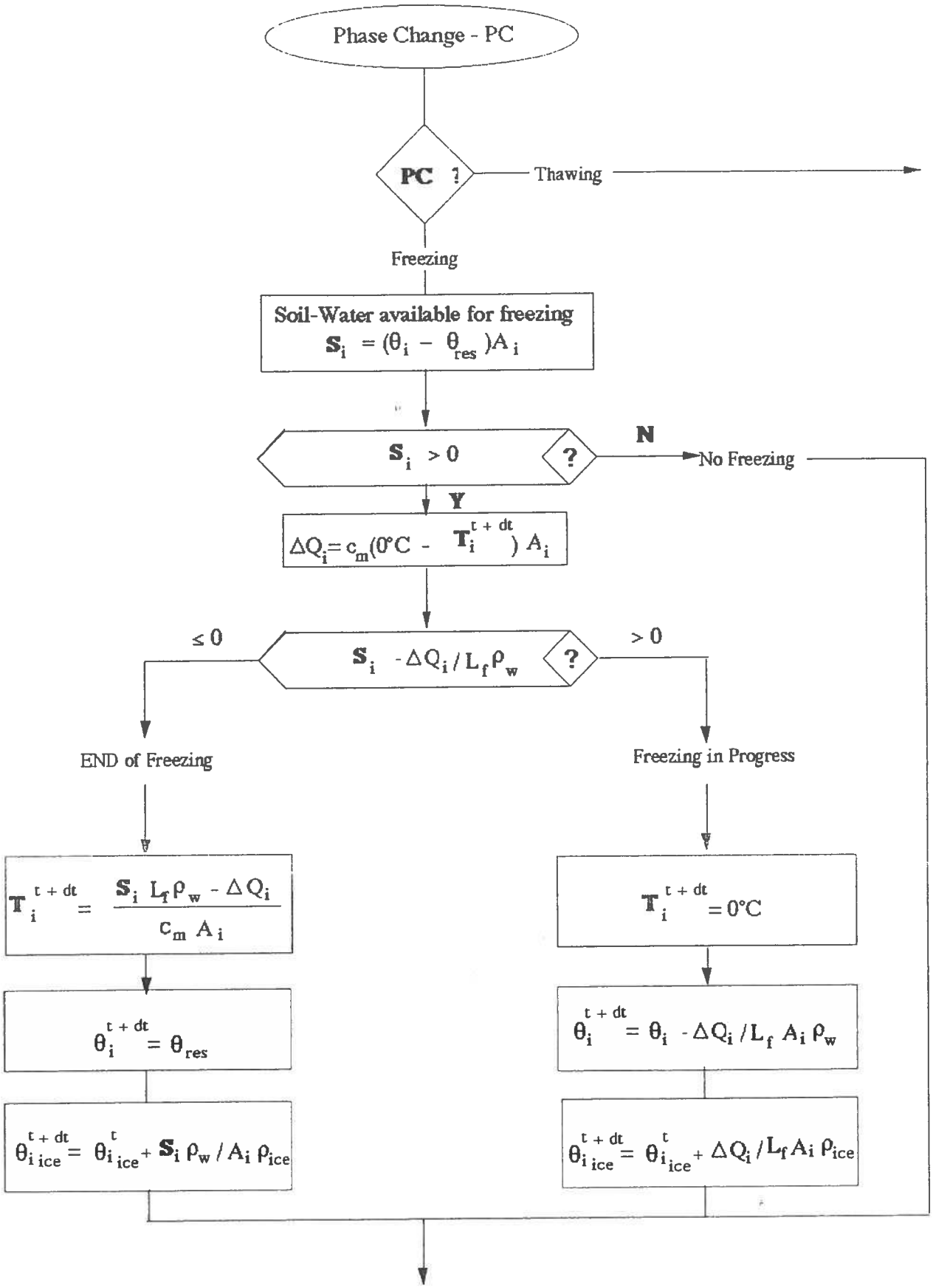


Fig. 2H. Phase Change Model of Freezing

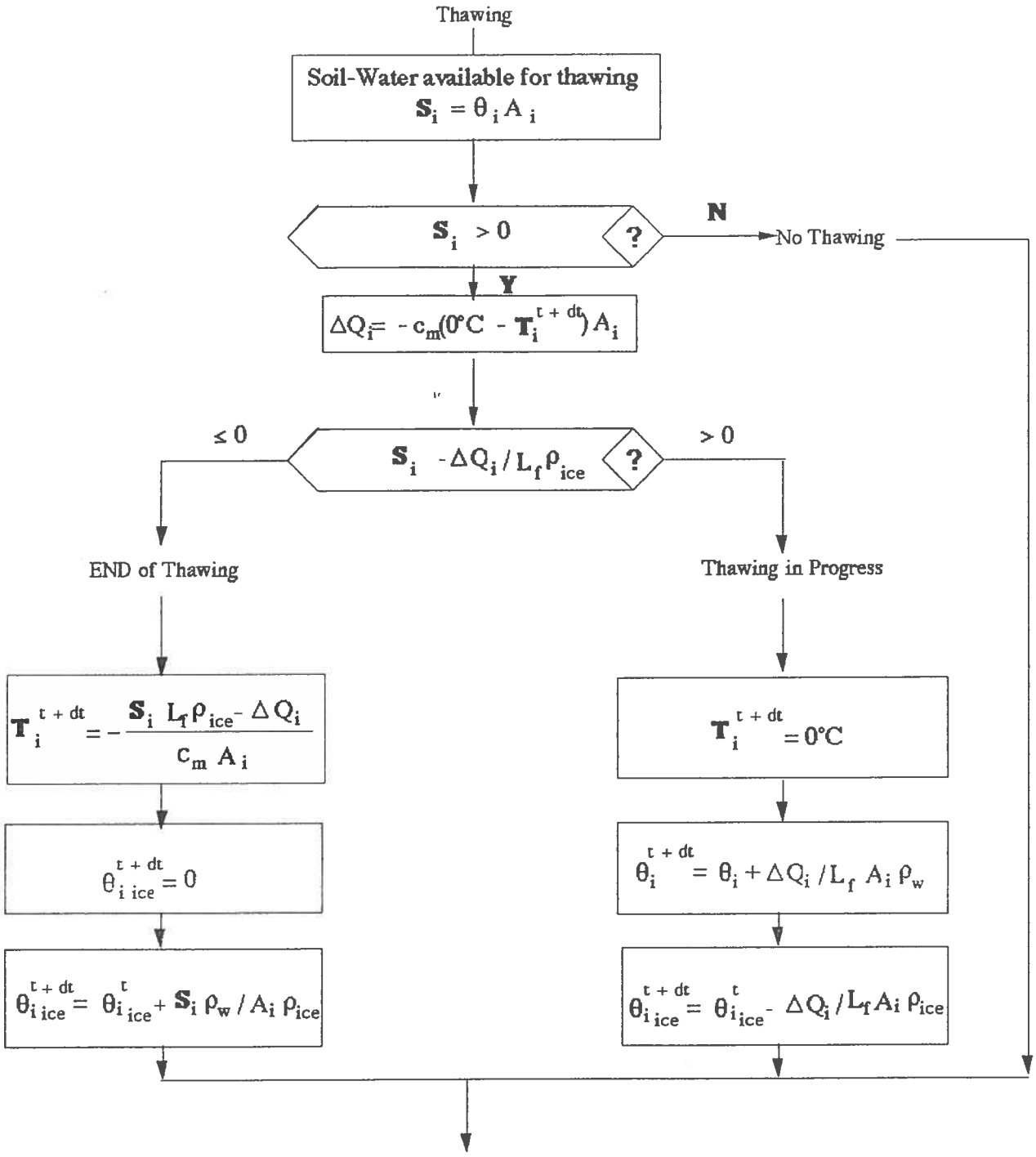


Fig. 3H. Phase Change Model of Thawing